



# Modeling the chemical trapping processes in the outer solar system

Ozge Ozgurel

## ► To cite this version:

Ozge Ozgurel. Modeling the chemical trapping processes in the outer solar system. Theoretical and/or physical chemistry. Université Pierre et Marie Curie - Paris VI, 2017. English. NNT : 2017PA066226 . tel-01687042

**HAL Id: tel-01687042**

**<https://theses.hal.science/tel-01687042>**

Submitted on 18 Jan 2018

**HAL** is a multi-disciplinary open access archive for the deposit and dissemination of scientific research documents, whether they are published or not. The documents may come from teaching and research institutions in France or abroad, or from public or private research centers.

L'archive ouverte pluridisciplinaire **HAL**, est destinée au dépôt et à la diffusion de documents scientifiques de niveau recherche, publiés ou non, émanant des établissements d'enseignement et de recherche français ou étrangers, des laboratoires publics ou privés.

# Université Pierre et Marie Curie

ED 388: Ecole Doctorale de Chimie Physique et Analytique de Paris Centre

## **Modeling the chemical trapping processes in the outer solar system**

Par Ozge Ozgurel

Thèse de doctorat de Chimie Théorique

Dirigée par Prof Alexis Markovits

Présentée et soutenue publiquement le 25 Octobre 2017

Devant un jury composé de :

Markovits Alexis	Professeur	Directeur de Thèse
Redondo Pilar	Professeur	Rapporteur
Boulet Pascal	Maître de conférences	Rapporteur
Bacchus Marie-Christine	Chargée de Recherche	Examineur
Fillion Jean-Hugues	Professeur	Examineur
Mousis Olivier	Professeur	Examineur





# Acknowledgements

I would like to thank the director of Laboratoire de Chimie Théorique Olivier Parisel to welcome me in the laboratory during my PhD studies, but also previous to that, for my master thesis.

I am grateful to my thesis advisor Alexis Markovits for his constant support and for being available in or outside of the laboratory when I needed.

I am also very grateful to Françoise Pauzat and Yves Ellinger who introduced me to computational astrochemistry five years ago when I was an Erasmus student and continued to support me afterwards with their insightful opinions.

I would like to thank Marie-Christine Bacchus who welcomed me in the Institut Lumière Matière at University Lyon 1 to study collision calculations of radiative associations and also accepted to be part of the thesis jury. I would like to thank for their participation the others members of the jury, Pilar Redondo, Pascal Boulet, Jean-Hugues Fillion and Olivier Mousis with a special mention for his helpfulness in astrophysical aspects during my PhD.

A very special gratitude to my colleagues in the laboratory for their constant support, especially Sehr, Felix and Felipe for joyful lunch hours and conversations full of laugh. I also want to thank my friends outside of the laboratory especially Ksenia for helping and pushing me all the time to do better and Onur who supported me starting from as early as my bachelor years to study in astrochemistry.

I am also very grateful to my parents who were very supportive to my choice of doing PhD from the very beginning. I also want to thank my sister for being always there to listen my problems and trying to give solutions, also my brother who probably started my interest in astronomy when I was just a kid with his science fiction stories.

# Table of contents

Acknowledgements	1
Table of contents	2
Introduction	5
I Astrophysical Context	5
I.1 Chemistry in proto-planetary disks	5
I.2 The Solar System	8
I.3 Titan	10
I.4 Europa	11
I.5 Comets	11
II Theoretical Tools	12
II.1 Quantum chemistry principle	12
II.2 Born-Oppenheimer approximation	13
II.3 Hartree Fock and Post Hartree-Fock methods	13
II.3.1 Coupled-cluster (CC) theory	14
II.4 Density Functional Theory (DFT)	14
II.4.1 Hohenberg-Kohn theorems	14
II.4.2 Kohn-Sham (KS) equations	15
II.4.3 Exchange-correlation functionals	15
II.4.4 Generalized Gradient Approximation (GGA)	16
II.4.5 Van der Waals interactions	16
III. References	18
Chapter 1: Noble gas deficiency in the atmosphere of Titan	21
I Astrophysical hypotheses	22
II Chemical trapping of noble gases by $\text{H}_3^+$ and protonated derivatives ( $\text{H}_3\text{O}^+$ , $\text{HCO}^+$ , $\text{HOC}^+$ , $\text{N}_2\text{H}^+$ ) in the proto-solar nebula	25
III Article	26
IV Conclusion and perspectives	35
V Published articles	37
VI References	44
Chapter 2: Origin of molecular oxygen and sulfur in Comet 67P/Churyumov-Gerasimenko	
I Tracking molecular oxygen in comets	49
I.1 Origin of molecular oxygen in Comet 67P/Churyumov-Gerasimenko	49
I.1.1 Reviewing the astrophysical scenarios for the origin of $\text{O}_2$	50
I.1.2 Our scenario for trapping of $\text{O}_2$ in the cometary ice	51
I.2 Modeling and computational details	53
I.2.1 Modeling the ice structure	53
I.2.2 VASP parameters	54
I.2.3 Stabilization energy	56
I.3 Tests and results	57
I.3.1 Preliminary results (primitive cell)	57
I.3.2 Improving the model	59
I.3.3 Case of $\text{O}_2$ double trapping	63
I.4 Chemical aspect: Perspective	64
II Tracking molecular sulfur in comets	65
II.1 Origin of molecular sulfur in Comet 67P/ Churyumov-Gerasimenko	65
II.1.1 Reviewing the astrophysical scenarios for the origin of $\text{S}_2$	66
II.1.2 Our scenario for trapping $\text{S}_2$ in the cometary ice	67

II.2 Tests and results	68
II.2.1 The case of S <sub>2</sub> embedded in H <sub>2</sub> O ice	68
II.2.1.2 Improving the model	70
II.2.2 The case of S <sub>2</sub> embedded in H <sub>2</sub> S ice	73
II.2.2.1 Stability of H <sub>2</sub> S in H <sub>2</sub> O ice	74
II.2.2.2 The stability of S <sub>2</sub> in H <sub>2</sub> S ice	76
Appendix A	80
III Published articles	84
IV References	94
Chapter 3: On the origin of alkali (Na, K) and alkaline earth (Mg, Ca) metals in Europa exosphere	99
I Astrophysical context	100
II Trapping of alkali and earth-alkali metals in icy crust of Europa	101
III Computational procedure	103
III.1 VASP Parameters	103
III.1.1 Preliminary results (primitive cell)	104
III.1.2 Improving the model	108
IV Conclusion and perspectives	114
V References	117
General Conclusion	120



# Introduction

## I Astrophysical Context

Astrochemistry is the study of the abundance and reactions of chemical elements and molecules in the universe, and their interaction with the radiation field. Astrochemistry is an interdisciplinary field, involving the study of physical and chemical processes, experimentally as theoretically, and the observation of molecular spectra of specific regions in space to identify the molecules present.

The field of astrochemistry started to emerge significantly with the first time detection of ammonia (Cheung et al. 1986). Since then, almost 200 different gas-phase molecules have been detected in the interstellar medium (ISM) via rotational emission spectroscopy in the millimeter and sub-millimeter regions of the spectrum. Molecules up to 13 atoms can be detected with rotational emission spectroscopy (millimeter and sub-millimeter domain) providing they have a non-zero dipole moment but, for larger molecules as polycyclic aromatic hydrocarbons (PAHs), or interstellar dusts with silicates or amorphous carbon cores and mantles of ices mainly consisting of water, CO, CO<sub>2</sub>, CH<sub>3</sub>OH, the vibrational spectra (infrared region) are used.

The interstellar spectra do not only show the presence of the molecules and allow the evaluation of their abundances, but also give information about the physical conditions of the environment in which they are formed. In astrochemical studies, these environments can be associated to two main domains: chemistry in the interstellar medium (ISM) and chemistry in the solar system (planetology). In this study, we have investigated the chemical reasons likely to account for the observations made for the different bodies in the solar system, namely Titan, the comet 67P/C-G and Europa, noting that it has also required studying the proto-planetary disk medium.

### I.1 Chemistry in proto-planetary disks

The atoms and dust particles, remnants of old stars, collect together under the influence of gravity into diffuse clouds, in which the temperature is 50-100 K and gas density  $10\text{-}10^2\text{ cm}^{-3}$ . Further gravitational contraction results in the formation of dense clouds with an average gas density of  $10^3\text{ cm}^{-3}$ . Dense clouds exist in several varieties and are quite

heterogeneous. The low-mass star formation begins in cold pre-stellar cores, where the temperature can be as low as 5-10 K and the gas density is  $10^4 \text{ cm}^{-3}$ . Under these conditions, only binary reactions without any activation barrier are possible. Such conditions are met mainly by exothermic ion-neutral reactions. The main ionization source is constituted by the collisions of atoms with cosmic rays. As a result of these reactions, relatively common terrestrial molecules are synthesized (such as CO). But, radicals (e.g.  $\text{C}_6\text{H}$ ), molecular cations (e.g.  $\text{H}_3^+$ ,  $\text{HCO}^+$ ), anions (e.g.  $\text{C}_6\text{H}^-$ ), metastable isomers (e.g. HNC,  $\text{H}_2\text{CCCC}$ ), and unsaturated long carbon chains (e.g.,  $\text{HC}_{11}\text{N}$ ), which are not stable in Earth conditions, are also formed and stay stable with a significant life time in low temperature and density environments. As a result of simple accretion from gas, cold dust grains can be formed as well.

The initial collapse of pre-stellar cores is isothermal in nature but over time, a dense central condensation occurs, out of which radiation cannot escape. Continuous central condensation and the collapse of material to the center result in forming a proto-star. When the collapsing of gas and dust reach temperatures about 100-300 K, it is called hot core and the chemistry changes significantly. This collapse of the molecular cloud cores is a process regulated by the balance of gravitational, magnetic, gas pressure, and rotational forces (Stahler & Palla 2005). Many common organic species such as alcohols, ester, acids, aldehydes, etc. are formed at that time of the evolution. Also, violent shocks eject material to the interstellar medium and disk of gas and dust begin to form and rotate around the young proto-star. In the disks, the dust particles start to collapse and agglomerated into macroscopic bodies, which eventually become comets, meteors. At the same time, much of the cloud has gone away and a young star surrounded by a dense proto-planetary disk is left. The surrounding disk continues to regulate the inward radial transport of matter and the associated angular momentum transport outward (Hartmann 2000). Then this system can eventually evolve into a planetary system.

The proto-planetary disks are characterized by strong radial and vertical temperature gradients (Henning & Semenov 2013). High-energy radiation may penetrate into the upper layers of the disks, resulting in a richer molecular chemistry whereas, in the deep interiors, temperatures become so low that the molecules freeze. The shielding of these deep interiors is due to micrometer-sized solid dust particles present in the medium. These particles first

evolve into pebbles and finally planets. This process has a strong impact on the physical structure of the disks, and therefore on the chemistry.

As the proto-planetary disks are characterized by strong vertical and radial temperature and density gradients, these locally different disk properties imply a rich and diversified chemistry, including photochemistry, molecular-ion reactions, neutral-neutral reactions, gas-grain surface interactions, and grain surface reactions. Disk chemistry can be roughly divided into two regions with respect to the radially decreasing temperature: inner disk chemistry ( $< 20$  au) and chemistry in the outer disks beyond 20 au (astronomical unit (au) is the average distance between Earth and the Sun, which is about 150 million km). The products of inner disk chemistry are best detected by infrared spectroscopy, whereas the outer disk is the domain of submillimeter-millimeter observations.

Inner disks have high temperatures (from about 100 to 5000 K) and high densities up to  $10^{12} \text{ cm}^{-3}$ . At such temperatures and densities in the disk, chemistry approaches quasi-equilibrium. In the absence of intense sources of ionizing radiation, neutral-neutral reactions with barriers ( $> 100$ -1000 K) start to play an important role in the densest warm regions (Harada et al. 2010). Therefore, the inner disk chemistry comes closer to the terrestrial chemistry conditions, driven by 3-body reactions. Molecules should be abundant in the gas phase until they are destroyed by thermal dissociation ( $T > 2500$ -3500 K) in the inner disk. Chemical models of the inner disk chemistry (Harada et al. 2010) predict high abundances of  $\text{H}_2\text{O}$  and  $\text{CO}$  vapor at 1 au and the presence of N-bearing molecules ( $\text{NH}_3$ ,  $\text{HCN}$ ,  $\text{HNC}$ ) and a variety of hydrocarbons (eg  $\text{CH}_4$  and  $\text{C}_2\text{H}_2$ ).

In contrast to the inner disk regions, the outer disk chemistry is driven by the radiation and cosmic rays (Harada et al. 2010). Radiation and the energetic particles lead to the formation of various ions, including  $\text{H}_3^+$ . The proton transfer processes from ions to other neutrals is dominated by rapid ion-molecule chemistry (Herbst & Klemperer 1973). The ion-molecule processes are mostly barrier-less so they can occur even at temperature below 100K, especially the reactions involving long-range Coulomb attraction between an ion and a polarizable molecule.

Another important feature of disk chemistry is the condensation of molecules at low temperatures in the outer disks. Then, these molecules are no longer available for gas-phase chemistry but the ices on dust surface may remain chemically active. These ices sublime at



high temperatures of the inner disks, where dust grains stay solid. The sublimation of water ice occurs at about 150 K and this defines the so-called water snow line, which is located at 2-3 au in the early solar nebula (Morbidelli et al. 2000). The CO snow line is located at 20 au, where the gas temperature is below 20 K. It should be noted that the positions of the snow lines evolve with evolutionary stage of the disks (Qi et al. 2013).

One of the most important molecules in proto-planetary disks is water. The chemistry of water and the conversion of water vapor into molecular ice are directly related to the origin of water on Earth and the formation of giant planets beyond the snow line. The position of the water snow line depends on the pressure and temperature in the disk. For the solar nebula, the snow line is assumed to be located between 2 and 3 au from the Sun. The gas planets Jupiter, Saturn, Uranus, and Neptune, being formed beyond the snow line, they are all enriched in volatiles relative to the Sun (Reipurth et al. 2007). The term “volatiles” indicates all material with low melting and condensation temperatures (gases or molecular ices) in contrast to “refractory” materials such as metallic iron and silicates.  $\text{H}_2\text{O}$  and CO are the most abundant “volatile” molecules, with  $\text{NH}_3$ ,  $\text{CH}_4$  and  $\text{CO}_2$  as other important ices.  $\text{H}_2\text{O}$ , CO, and  $\text{CO}_2$  are also the most abundant molecular components of ices in comets with small mixtures of methane and ammonia and other minor components (e.g.,  $\text{C}_2\text{H}_6$ ) (Henning & Semenov 2013).

To summarize, proto-planetary disks are structures of gas and dust surrounding young stars. They are heterogeneous, showing rich variety of chemical processes, ranging from high-temperature neutral-neutral reactions in the inner disk regions to ion-molecular chemistry and molecular condensation in the outer disk. Grain surface reactions, thermal and photo-driven desorption are also part of this rich chemistry. Astrochemical studies of proto-planetary disks will help improving our understanding about the origins of planets, satellites and comets. The first study presented in this thesis, i.e. the study about noble gases deficiency in Titan, is one example typically relevant of such an interaction.

## **1.2 The Solar System**

The major features of the solar system are given in Figure 1; the planets (including the dwarf planets) and some of their notable satellites, the asteroid and Kuiper belts. The bodies that are found within the inner solar system, are predominantly rocky, whereas the ones in the outer solar system, beyond the snow line contain large amounts of ice (Wolf et al. 2012). The terrestrial planets Mercury, Venus, Earth and Mars are found in the inner solar system with

their satellites. In the outer solar system, the gas giants Jupiter & Saturn and the ice giants Uranus & Neptune can be found with their moons. The gas giants are mostly composed of hydrogen and helium (90% for Jupiter, 75% for Saturn (Lissauer 2005); whereas the ice giants (Uranus and Neptune) are composed of volatiles and heavier elements (Miller & Fortney 2011). All of their satellites (except Jupiter's satellite Io and Saturn's satellite Titan) have water-ice rich surfaces. (Dalton et al. 2010).

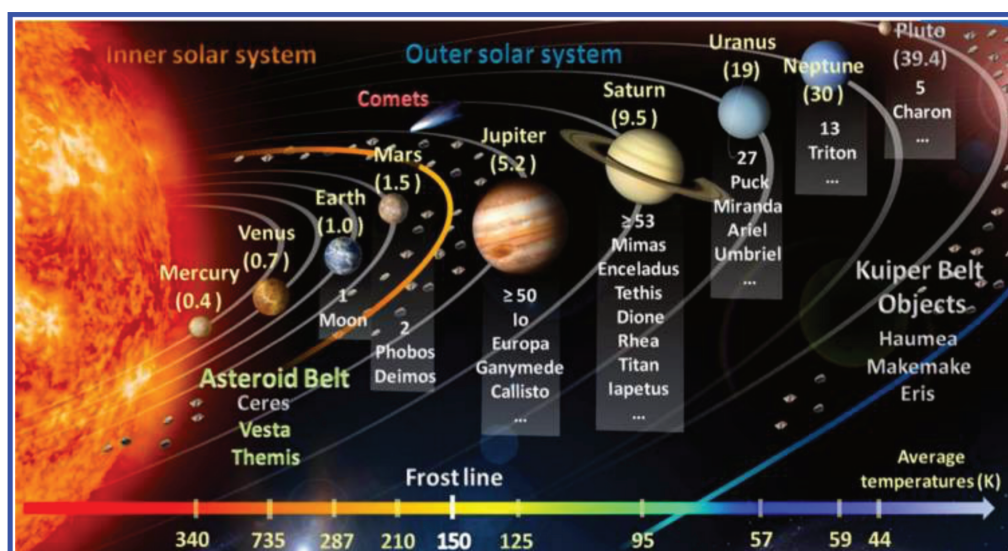


Figure 1: Solar system's planets and moons. Distances or semi-major axis from the Sun are indicated in brackets and in astronomical units (au) along with the average surface temperature (Bennett et al. 2013)

A vast reservoir of icy bodies exists in the outer solar system, which are generally referred as Trans-Neptunian Objects (TNOs). TNOs are also further classified as Kuiper Belt Objects (KBOs; 30-50 au) and Scattered-Disk Objects (SDOs; 30-100 au) and Oort cloud Objects (OCOs; 2000-50000 au). These regions are the sources of respectively, the short period comets and the long period comets.

In the past few years, several major space missions have been completed (e.g., Deep Impact, LCROSS, Chandrayaan-1, Stardust, Hayabusa), and a number of spacecrafts are currently exploring both the inner (e.g., MESSENGER, DAWN, Rosetta) and outer (Cassini, New Horizons) solar system. Recent data from these and other space missions have had a huge impact on our knowledge about the solar system bodies. In this study, we investigated chemical trapping mechanisms in gaseous and solid phase in relation to three solar system

bodies; Titan, Europa and Comets, that we present with a few more details in the following paragraphs.

### **I.3 Titan**

Titan, the biggest satellite of Saturn and the only moon of the solar system with a significant atmosphere, is considered as a possible analog of the primitive Earth; hence it has been the subject of systematic and extensive studying.

The chemistry of Titan's atmosphere is driven by the photolysis of  $\text{CH}_4$  in the thermosphere, catalytic reactions in the stratosphere and by the dissociation of  $\text{N}_2$  due to both UV photons and energetic electrons. Ethane is the most abundant gas product and HCN is the most abundant nitrile. The mixing ratios of all photochemical species, except  $\text{C}_2\text{H}_4$ , increase with altitude at equatorial and southern latitudes, indicating a transport from a high-altitude source to a condensation sink in the lower atmosphere (Strobel et al. 2009). This active atmospheric chemistry eventually produces macroscopic particles that precipitate slowly in the lower atmosphere, leading to the brownish haze permanently surrounding the satellite. These organic aerosols are important for the properties and evolution of Titan's atmosphere (Carrasco et al. 2009). However, the information on these aerosols composition is still limited in spite of extensive laboratory experiments to produce analogous materials, the so-called "tholins", to be analyzed and studied.

Earth and Titan are similar by the fact that molecular nitrogen is the major species, but the next most abundant atmospheric species on Earth is molecular oxygen, whereas it is methane in Titan. Therefore, the atmospheric and ionospheric chemistries are quite different for the two bodies. Absorption of EUV (extreme ultra-violet) radiations is a key feature of all planetary thermospheres including Titan's. In all atmospheres, at high altitudes, the neutral density is low enough such that the collisional mean free path exceeds a typical scale length. This atmospheric region is called the exosphere. EUV photons and energetic particles create ions and photoelectrons when they are absorbed and the region of an atmosphere where significant numbers of free thermal electrons and ions are present, is called ionosphere (Schunk & Nagy 2000). The specific point is that Titan's upper atmosphere and ionosphere strongly interact with Saturn's magnetospheric plasma.

## **I.4 Europa**

Europa, one of the four large Galilean satellites of Jupiter, is about the same size as the Earth's moon but it has a more dynamic surface. The surface of Europa is young, ice-covered and it is criss-crossed by a network of cracks and ridges (Greeley et al. 2004). Several scientific evidences demonstrate that Europa should have a global ocean of liquid water underneath its icy surface. This ocean maintained by tidal flexing and heating due to its eccentric orbit about Jupiter, it could be habitable by microorganisms; hence, the interest developed for Europa regarding to astrobiology.

Europa's young surface, potential subsurface ocean, and ongoing tidal flexing suggest that it is geologically active today. Europa, being located inside Jupiter's radiation belt, is bombarded by ions and electrons trapped in Jupiter's magnetic field. This satellite has a surface-bound layer atmosphere, referred as exosphere since it is collision-less gas (Johnson et al. 2004; Plainaki et al. 2010). It consists mainly of  $\text{H}_2\text{O}$ , released through surface ion sputtering by energetic bombardment, and  $\text{O}_2$  and  $\text{H}_2$ , produced through chemical reactions between different products of  $\text{H}_2\text{O}$  decomposition. However, direct measurement of these exospheric species has not been achieved; this is unfortunate because the study of the exosphere is expected to reveal the composition and features of the surface since it is mostly originated from Europa's surface.

## **I.5 Comets**

Comets are small, irregularly shaped bodies in the solar system, composed mainly of ice and dust. They travel around the sun in very elliptical orbits, which bring them very close to the Sun, then send them past Neptune. In terms of the amount of time they spend to orbit the Sun, there are two types of comets. Short-period comets orbit around 200 years around the Sun, whereas long-period returns may take over 200 years, with some taking 100000 to 1 million years. The short-period comets are thought to originate from the Kuiper Belt, an area outside of Neptune's orbit (from 30 to 50 au), containing many icy comet-like bodies. The long period comets tend to have randomly oriented orbits and not necessarily ecliptic orbits. They are thought to come from the Oort cloud, a region that has never been observed, is expected to harbour at least one thousand icy objects located between 3000 au and 100000 au. There are some other comets from the Kuiper Belt or Oort Cloud that are corraled by Jupiter's

massive gravity into its planetary family. These comets usually develop very short solar orbits from three to 20 years.

As comets come close to the Sun, the Sun's heat begins to vaporize the ices, which form an area of vaporized gas around the nucleus of the comet called as coma. Outside the coma is a layer of hydrogen gas called a hydrogen halo which diameter extends up to 1 km. The solar wind then blows these gases and dust particles away from the direction of the Sun causing the formation of two tails pointing away from the Sun as the comet travels around it. One is called the ion tail and is made of gaseous species, which have turned into charged molecules and ions by the irradiation from the Sun. Since the most abundant ion is  $\text{CO}^+$  that scatters blue light better than red light, this ion tail often appears blue to observers. The other tail is called the dust tail and normally appears white. The dust in this tail is less strongly affected by the solar wind since the particles of dust are much larger than the ions of the ion tail. The tails of the comet can be extremely large and may extend to a distance of up to 1 au.

## **II Theoretical tools**

The methods and tools proposed by computational quantum chemistry are numerous and adaptable. The choice of one or the other depends mostly of the problem to be modeled. We will do a short presentation of the basic principles of only those we have used in this specific work. Some of the practical issues as convergence and analysis of the results are discussed in the chapters where they appear relevant.

### **II.1 Quantum chemistry principle**

Quantum chemistry approaches start with the fundamental physics concepts to describe the model systems and deduce their properties. In the context of quantum chemistry, solving the time-independent Schrödinger equation allows to determine the physical properties of a quantum system.

$$H \Psi_i = E_i \Psi_i \quad (1)$$

where  $H$  is the Hamiltonian describing the system,  $\Psi_i$  the wave-functions (eigenfunctions) and  $E_i$  the corresponding state energies (eigenvalues). The solution of this equation being rapidly intractable beyond 3 interacting particles (nuclei and/or electrons) with the increasing size of the system, multiple approximations have to be done.

## II.2 Born-Oppenheimer approximation

Born-Oppenheimer approximation is currently used in most of quantum mechanics and quantum chemistry calculations. It states that the motion of electrons and nuclei may be considered independently and that the wave-function of the system can be decoupled into a nuclear wave-function and an electronic wave-function.

$$\Psi_{\text{total}} = \Psi_{\text{nuclei}} \times \Psi_{\text{electron}} \quad (2)$$

So doing, the initial problem reduces to that of finding a solution to the electronic Hamiltonian which describes the motion of the electrons and depends explicitly on the electronic coordinates, but parametrically on the nuclear coordinates.

The electronic Hamiltonian operator can be written as:

$$H = T + V + V_H + V_{XC} \quad (3)$$

where  $T$  is the kinetic energy of the electrons,  $V$  the interaction potential between electrons and nuclei,  $V_H$  the Hartree potential of the electron-electron Coulomb repulsion and  $V_{XC}$  the electron exchange and correlation potential.

At that level, two types of methods can be employed depending of the nature of the subject: wave function dependent ab-initio methods (Hartree Fock (HF) and post HF) or electronic density dependent first principles methods (Density Functional Theory (DFT)).

## II.3 Hartree Fock and Post Hartree-Fock methods

The simplest approximation to find a solution to the electronic Schrödinger equation is based on the Hartree Fock wave function theory relying mainly on the mean field approximation. The problem is then replaced by a one electron problem in which electron-electron repulsion is treated in an average way. Therefore the instantaneous interactions of electrons being neglected, the correlation energy is missing. The so-called post HF methods, (Moller-Plesset Perturbation or Configuration Interaction) can take care of it.

### II.3.1 Coupled-cluster (CC) theory

Introduced in molecular quantum chemistry by Cisek and Paldus in the late 60s, and further developed to include contributions of excited states to the correlation energy the CC theory is an efficient mathematical technique mixing a limited variational configuration interaction with perturbational treatments (for details see Bartlett 1995). The basic idea is that the exact wave function can be written as an exponential ansatz:

$$|\Psi\rangle = e^T |\Phi_0\rangle \quad (4)$$

that can be developed as Taylor power expansion

$$|\Psi\rangle = \left(1 + T + \frac{1}{2!}T^2 + \frac{1}{3!}T^3 + \dots\right) |\Phi_0\rangle \quad (5)$$

where T is an excitation operator whose power is the number of excitations.

In this study, the CCSD and CCSD(T) are used, meaning that the wave function includes single and double excitation. The term (T) indicates that the contribution of triple excitations is calculated using many-body perturbation theory.

### II.4 Density Functional Theory (DFT)

Density Functional Theory is another type of methods of quantum chemistry, modeling the electrons of a quantum-mechanical system with a density  $\rho(r)$ . It is stated that all the observable properties of the system in a ground state are determined by this density that depends on the potential  $V(r)$ .

#### II.4.1 Hohenberg-Kohn theorems

The Density Functional Theory is based on two theorems of Hohenberg and Kohn (1964):

The first theorem states that the properties of the system, including energy states, potentials and wave functions are uniquely determined by the electron density  $\rho(r)$ .

The second theorem states that the electron density  $\rho_0(r)$  for which the energy E is minimal is the true ground-state electron density.

### II.4.2 Kohn-Sham (KS) equations

A solution to determine the homogeneous electron density has been proposed by Kohn and Sham (1965). The physical system is replaced by a fictitious one constituted by the non-interacting electrons moving in effective potentials. A set of one-electron equations is solved:

$$[-T_e + V(r) + V_H(r) + V_{XC}(r)]\varphi_i(r) = \epsilon_i \varphi_i(r) \quad (6)$$

Here the first term is the kinetic energy of the electron,  $V$  the potential energy of interaction with nuclei,  $V_H(r)$  the electron-electron repulsion potential,  $V_{XC}(r)$  the exchange correlation potential. The electron density  $\rho(r)$  is determined as

$$\rho(r) = \sum_{i=1}^N \varphi_i^*(r) \varphi_i(r) \quad (7)$$

where  $N$  is the number of electrons and  $\varphi$  are one-electron wave-functions, solving the previous equation.

The potentials  $V(r)$ ,  $V_H(r)$  are known functions of the electron density, while the exact equation for  $V_{XC}(r)$  as a function of density is unknown. Finding a good approximation of the exchange-correlation functional  $V_{XC}(r)$  is one of the tasks to which the DFT developers are currently confronted.

To converge to a solution, an iterative approach is proposed by Kohn and Sham. Potentials are obtained from a trial electron density, then, the KS equations are solved to obtain the wave functions. Finally, a new electron density is constructed according to the equation (7), and the calculations cycle is repeated till convergence of the process.

### II.4.3 Exchange-correlation functionals

As mentioned in the previous section, one of the problems of the Density Functional Theory is the choice of the exchange-correlation functional  $Exc$ . Here we used a functional appropriate to the description of large variations of the density.



#### II.4.4 Generalized Gradient Approximation (GGA)

For example, geometries and ground-state energies of highly polarized molecules like H<sub>2</sub>O in water ice are better determined using Generalized Gradient Approximation (GGA) functionals. In GGA the  $E_{xc}$  is a function of both density  $\rho(r)$  and density gradient  $\Delta(\rho(r))$  so that  $E_{xc}(r) = E_{xc}(\rho(r), \Delta(\rho(r)))$ .

In this work, a GGA type functional developed by Perdew et al. (1996) is used (PBE). It gives good results for geometries and atomization energies and reproduces well the hydrogen bonds.

Other classes of functionals exist, but lack of generality since they are often tuned to solve particular problems.

#### II.4.5 Van der Waals interactions

In the systems studied in this thesis, most interactions to be taken into account are Van der Waals type of interactions, i.e. electrostatic interactions between dipoles, permanent or induced ones.

As traditional DFT functionals fail to describe such interactions correctly, in particular the ones between induced dipoles (London dispersion force), corrections had to be added as a remedy. In this work a semi-empirical approach DFT-D2 proposed by Grimme (2006) is employed. This is a computationally cheap and reasonably accurate method to take the Van der Waals interactions into account. A dispersion term is added to the total DFT energy:

$$E_{disp} = -s_6 \sum_{i \neq j}^{Nat} \frac{C_6^{ij}}{R_{ij}^6} f_{dmp}(R_{ij})$$

Here,  $Nat$  is the number of atoms in the system,

$$C_6^{ij} = \sqrt{C_6^i C_6^j}$$

denotes the dispersion coefficient for atom pair  $ij$ ,  $s_6$  is a global scaling factor that only depends on the density functional used, and  $R_{ij}$  is an inter-atomic distance. In order to avoid near-singularities for small  $R$ , a damping function  $f_{dmp}$  is used. Coefficients are determined as an empirical function of calculated atom ionization potentials and polarizabilities.

To summarize, both types of methods are designed to obtain the best energy and the best electronic description: post Hartree-Fock methods use an exact hamiltonian and work to improve the wave function whereas DFT methods postulate an exact density and work to improve the Hamiltonian.

### III. References

- Bartlett R.J. (1995) *Modern Electronic Structure Theory*, Yarkony, D. R. Ed., Part 2, Chap. 6, New York: World Scientific.
- Carrasco, N., Schmitz-Afonso, I., Bonnet, J. Y., Quirico, E., Thissen, R., Dutuit, O., ... & Adandé, G. (2009). Chemical characterization of Titan's tholins: Solubility, morphology and molecular structure revisited. *The Journal of Physical Chemistry A*, 113(42), 11195-11203.
- Cheung, A. C., Rank, D. M., Townes, C. H., Thornton, D. D., & Welch, W. J. (1968). Detection of NH<sub>3</sub> Molecules in the Interstellar Medium by Their Microwave Emission. *Physical Review Letters*, 21(25), 1701.
- Dalton, J. B., Cruikshank, D. P., Stephan, K., McCord, T. B., Coustenis, A., Carlson, R. W., & Coradini, A. (2010). Chemical composition of icy satellite surfaces. *Space science reviews*, 153(1-4), 113-154.
- Greeley, R., Chyba, C. F., Head III, J. W., McCord, T. B., McKinnon, W. B., Pappalardo, R. T., & Figueredo, P. H. (2004). *Geology of Europa Jupiter: The Planet, Satellites and Magnetosphere* ed Bagenal et al.
- Grimme, S. (2006). Semiempirical GGA-type density functional constructed with a long-range dispersion correction. *Journal of Computational Chemistry*, 27(15), 1787-1799.
- Harada, N., Herbst, E., & Wakelam, V. (2010). A new network for higher-temperature gas-phase chemistry. I. A preliminary study of accretion disks in active galactic nuclei. *The Astrophysical Journal*, 721(2), 1570.
- Hartmann, L. (2009) *Accretion Processes in Star Formation*, 2nd ed, Cambridge, U.K.: Cambridge University Press
- Henning, T., & Semenov, D. (2013). Chemistry in protoplanetary disks. *Chemical Reviews*, 113(12), 9016-9042.
- Herbst, E., & Klemperer, W. (1973). The formation and depletion of molecules in dense interstellar clouds. *The Astrophysical Journal*, 185, 505-534.

Hohenberg P. and Kohn. W. (1964). Inhomogeneous electron gas. *Physical Review* 136.3B, B864–B871.

Johnson, R.E. et al., In: Bagenal, F., Dowling, T., McKinnon, W.B. (2004), *Jupiter-The Planet, Satellites and Magnetosphere*. pp. 485–512, Cambridge, U.K.: Cambridge University Press .

Kohn W. et Sham L. J . (1965) Self-consistent equations including exchange and correlation effect. *Physical Review* 140, A1133–A1138.

Lissauer, J. J. (2005). Formation of the outer planets. *The Outer Planets and their Moons* (pp. 11-24). Netherlands: Springer.

Miller, N., & Fortney, J. J. (2011). The heavy-element masses of extrasolar giant planets, revealed. *The Astrophysical Journal Letters*, 736(2), L29.

Morbidelli, A., Chambers, J., Lunine, J. I., Petit, J. M., Robert, F., Valsecchi, G. B., & Cyr, K. E. (2000). Source regions and timescales for the delivery of water to the Earth. *Meteoritics & Planetary Science*, 35(6), 1309-1320.

Perdew, J. P., Burke, K., & Ernzerhof, M. (1996). Generalized gradient approximation made simple. *Physical Review Letters*, 77(18), 3865.

Plainaki, C., Milillo, A., Mura, A., Orsini, S., & Cassidy, T. (2010). Neutral particle release from Europa's surface. *Icarus*, 210(1), 385-395.

Qi, C., Öberg, K. I., Wilner, D. J., d'Alessio, P., Bergin, E., Andrews, S. M., ... & Van Dishoeck, E. F. (2013). Imaging of the CO snow line in a solar nebula analog. *Science*, 341(6146), 630-632.

Reipurth, B., Jewitt, D., & Keil, K. (Eds.). (2007). *Protostars and Planets V*. University of Arizona Press.

Schunk RW, Nagy AF (2000) Ionospheres: physics, plasma physics, and chemistry. *Cambridge atmospheric and space science series*, pp 104–147, Cambridge, UK: Cambridge University Press.

Stahler, S., & Palla, F. (2005). *The Formation of Stars* Weinheim : Wiley-VCH Verlag GmbH

Strobel, D. F., Atreya, S. K., Bézard, B., Ferri, F., Flasar, F. M., Fulchignoni, M., ... & Müller-Wodarg, I. (2009). Atmospheric structure and composition. *Titan from Cassini-Huygens* (pp. 235-257). Netherlands: Springer.

Wolf, S., Malbet, F., Alexander, R., Berger, J. P., Creech-Eakman, M., Duchene, G., ... & Pott, J. U. (2012). Circumstellar disks and planets. *The Astronomy and Astrophysics Review*, 20(1), 52.

## Chapter 1: Noble gas deficiency in the atmosphere of Titan

Titan, the biggest satellite of Saturn, is the only moon in the solar system with a significant atmosphere, which is composed of at least four distinct regions: troposphere, stratosphere, mesosphere and thermosphere (Yelle 1991). Throughout the Titan's atmosphere, the far most abundant species is  $N_2$ , followed by several per cent of  $CH_4$  and several tenths of per cent of  $H_2$ . The dissociation of  $N_2$  and  $CH_4$  by solar UV photons, energetic ions and electrons from Saturn's atmosphere, as well as cosmic ray particles (Yung et al. 1989), initiates a complex photochemical network, resulting in the production of various hydrocarbons and nitrogen-bearing species, labelled by the generic name of “tholins”.

The first breakthrough about the Titan's atmosphere came with the flyby of Voyager I in 1980. In order to study the chemical composition of the atmosphere, especially looking for species like HCN,  $HC_3N$ ,  $CH_3CN$ , CO and  $H_2O$ , two spectrometers were used on the Voyager I probe: IRIS, an infrared spectrometer with a range of 180 to 2500  $cm^{-1}$  (4-55  $\mu m$ ) with a spectral resolution of 4.3  $cm^{-1}$ , and UVS, an ultraviolet spectrometer operating from 52 to 170 nm with a resolution of 1.5nm.

More detailed observations started in October 2004 with the Cassini-Huygens mission. The combined Cassini-Huygens spacecraft composed of the Cassini orbiter to study the Saturn system, including its rings and moons, with a special focus on Titan and the Huygens probe designed to make in situ observations of Titan. The Cassini orbiter's visits to the upper atmosphere of Titan down to  $\sim 950$  km, provided various data from the remote and in situ observations. The major development relative to Voyager I was the Ion Neutral Mass Spectrometer (INMS) for in situ studies of the neutral and ionic composition of the atmosphere. Also were operating, the Cassini Plasma Spectrometer (CAPS) to measure heavy positive and negative ions densities, with the Langmuir probe (LP) and the Magnetospheric Imaging Instrument (MIMI) to study the plasma environment around Titan (Krasnopolsy 2009).

The Huygens probe was the first probe to land on an object of the outer Solar System. It landed on Titan and made it possible to study the atmosphere below 150 km. It had six different instruments: Huygens Atmospheric Structure Instrument (HASI), Surface Science Package (SSP), Doppler Wind Experiment (DWE), Descent Imager/Spectral Radiometer

(DISR), Aerosol Collector Pyrolyzer (ACP) and Gas Chromatograph Mass Spectrometer (GCMS) designed to measure the chemical composition of the Titan's atmosphere and to determine the isotope ratios of the major gaseous constituents at lower altitudes.

Voyager I remote sensing instruments identified the major and several minor constituents above Titan's troposphere; however, as the measurements were made in the stratosphere, the evolution of the photo-chemically produced trace gases in the upper atmosphere remained unknown. With the Cassini orbiter instruments, several data about the composition of organic trace gases in stratosphere and the upper atmosphere were provided. In other words, they provided information on these gases in the regions where they first formed. One of the objectives of the Huygens probe was to determine to which extent the simpler trace gases can form complex molecules, condensates, or aerosols, which will eventually precipitate onto the Titan's surface.

The unexpected characteristic of the atmosphere of Titan is that no noble gas other than argon was detected by the Gas Chromatograph Mass Spectrometer (GCMS) aboard the Huygens probe during its descent to the surface of Titan in January 2005. The only isotopes of argon detected consist of primordial  $^{36}\text{Ar}$  (the main isotope) but very impoverished compared to its solar abundance and  $^{40}\text{Ar}$ , which is a decay product of  $^{40}\text{K}$  (Niemann et al. 2005). The general deficiency observed for the noble gases is surprising when taking into consideration that this satellite, in all existing scenarios, was expected to be made from the same building blocks in the feeding zone of Saturn (Mousis et al. 2002) and to share a similar composition with the noble gas-rich planetesimals from which Jupiter was formed. (Alibert et al. 2005).

## **I Astrophysical hypotheses**

The noble gas deficiency observed in Titan's atmosphere has been the subject of a number of studies. The different mechanisms proposed to explain such a deficiency can be divided into two types: one can be referred as the "external" type, depending on the chemical and physical conditions of the proto-solar nebula during the formation of Titan, the other one as the "internal" type related to the conditions in the present atmosphere of Titan.

### **i) Internal mechanisms**

This category includes mainly the five mechanisms detailed below.

i. Osegovic & Max (2005) proposed that the noble gases could have been stocked in ices (clathrates) supposed to be present on Titan's surface and they showed that Xe could be efficiently trapped in this way. However the CSHMYD code used for the demonstration was developed by Sloan (1998) for industrial applications and is not supposed to function for temperatures lower than 140 K, whereas the surface temperature of Titan is about 90-95 K. Moreover, at the time, Ar and Kr could not be treated with this code. This point was solved later on by Thomas et al. (2008) who found that Kr as Xe could be efficiently trapped by clathrates whatever their initial abundance within the condition that there is sufficient amount of clathrates present on the surface. More recently, the same team (Mousis et al. 2011), using a new set of potential interaction parameters showed that Ar could also be trapped by this mechanism. However, it has to be reminded that the existence of such mechanism entirely relies on the abundance of clathrates on Titan's surface, which is still highly controversial.

ii. In another study, Cordier et al. (2010) suggested the dissolution of atmospheric compounds in the liquid hydrocarbons on Titan's surface as a possible reason to the observed noble gas deficiency. They assumed thermodynamic equilibrium between the liquid and the atmosphere and calculated abundances of the different constituents of liquid on the surface accordingly. They showed that the lakes on the Titan's surface could trap atmospheric Xenon efficiently. However, the estimated amount of liquid hydrocarbons on Titan is not sufficient enough to explain the observed deficiency in Ar and Kr.

iii. Another mechanism was suggested by Jacovi & Baar-Nun (2008), based on laboratory experiments. According to this experimental study, noble gases could be trapped by atmospheric aerosols, which are the products of a complex chemistry based on the photolysis of methane rejected by cryo-volcanos in the atmosphere of Titan, implying that these aerosols could have been present in the atmosphere of Titan for millions of years. In such a mechanism, the open structure of aerosols would let the noble gases fill their pores. However, this type of physical trapping is very dependent on the structure of the aerosols considered and the structures of the materials in suspension present in the experiment may be quite different from those present in Titan atmosphere. A reliable and extensive modeling of this mechanism is still missing and remains to be done.



iv. A fourth mechanism has been proposed, appealing to chemical trapping. Lundel et al. (2002), Lignell et al. (2006) showed that the insertion of Xenon into hydrocarbons may lead to stable compounds. However, the direct insertion mechanism of Xe into the CH bond of hydrocarbons is an endothermic process with a high activation energy. In the absence of other effective chemical mechanism, this reaction is not likely to occur in the Titan's atmosphere.

v. Noble gases might also be trapped chemically by the most abundant ions present in Titan's upper atmosphere and ionosphere. Noble gases can form stable structures with ions driven by ion-dipole interactions and contrary to their direct insertion into the hydrocarbons, these complexes may be obtained via radiative associations without an energy barrier.

## **ii) External mechanisms**

Two mechanisms can be related to the second category:

i. The first argument for such a mechanism was proposed in an interdisciplinary study chemistry-planetology by Mousis et al. (2008). Based on the complete theoretical study of the interaction of molecular ion  $\text{H}_3^+$  with noble gases Ar, Kr and Xe (Pauzat & Ellinger 2007; Pauzat et al. 2009), this chemical trapping mechanism is assumed to occur during the formation of the satellite's constructive planetesimals in the proto-solar nebula and it depends mostly on the abundance of  $\text{H}_3^+$  molecule in that medium. Therefore, the modeling of the  $\text{H}_3^+$  abundance profile is crucial. The abundance of  $\text{H}_3^+$  depends not only on its production but also on its destruction, its main destruction agents being  $\text{H}_2\text{O}$ ,  $\text{CO}$ ,  $\text{N}_2$ . These destructive reactions may form protonated ions, which may be capable of trapping also the noble gases. In this study, the efficiency of such a trapping mechanism has been fully investigated.

ii. Other trapping mechanisms, not necessarily chemical, might be at work in the nebula. It can be quoted that the adsorption on the solid surfaces available in the primitive nebula, among which the refractory solids of the primitive grains, or the integration into the holes of the icy mantles irradiated and pierced by cosmic rays. The impact of such mechanisms on the noble gases abundances has yet to be investigated.

## II Chemical trapping of noble gases by $\text{H}_3^+$ and protonated derivatives ( $\text{H}_3\text{O}^+$ , $\text{HCO}^+$ , $\text{HOC}^+$ , $\text{N}_2\text{H}^+$ ) in the proto-solar nebula

The hypothesis at the basis of the model is that Titan, as other interstellar objects, has been formed from icy planetesimals already noble-gas impoverished in the proto-planetary nebula and that this impoverishment could be due to the sequestration of noble gases by  $\text{H}_3^+$  during the early stages of the formation of the solar system. Depending on the region where the constitutive planetesimals were formed, the abundance in  $\text{H}_3^+$  was different and the trapping more or less efficient. In such a scenario, it is obvious that the abundance profile of  $\text{H}_3^+$  is the main concern.

In the previous article promoting the model (Mousis et al. 2008), the abundance profile of  $\text{H}_3^+$  was calculated and it was found that its abundance increases with the heliocentric distance.  $\text{H}_3^+$  is formed following the ionization of the molecule  $\text{H}_2$  by energetic particles, X-rays or cosmic rays and is destroyed by the reactions with the most abundant molecules in the surrounding gas phase, namely  $\text{H}_2\text{O}$ ,  $\text{CO}$  and  $\text{N}_2$ . Within a steady state description, the formation and destruction rates balance each other, giving the following relationship:

$$x_{\text{H}_3^+} = \frac{\zeta}{n_{\text{H}_2} (K_{d\text{H}_2\text{O}} x_{d\text{H}_2\text{O}} + K_{d\text{CO}} x_{\text{CO}} + K_{d\text{N}_2} x_{d\text{N}_2})}$$

where  $x$  is the abundance,  $n$  is the density and  $\zeta$  is the ionization rate.

The  $\text{H}_3^+$  abundance profile was evaluated with different ionization sources, assuming the usual increase for further heliocentric distances (Figure 1). When it is compared with the calculated proto-solar abundances of noble gases (Table 1), it is seen that with the addition of other energetic particle sources to the cosmic rays, the amount of  $\text{H}_3^+$  may be sufficient enough to trap the noble gases except Ar whose abundances are much higher than the other noble gases.

If in the steady state conditions, the formation and destruction rates balance each other, it is no longer the case when the solar nebula cools down; then, the destructive molecules, namely  $\text{H}_2\text{O}$ ,  $\text{CO}$  and  $\text{N}_2$ , do not remain in the gas phase (local temperature lower than 150K), being trapped themselves as clathrates or simply condensing, and the balance has to be adjusted, taking care of the consequences of the cooling.

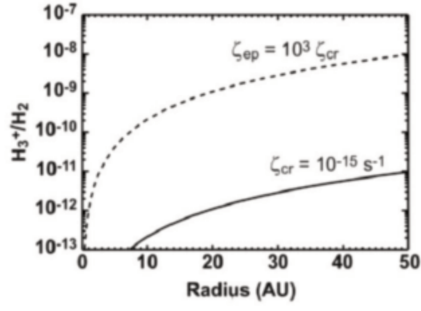
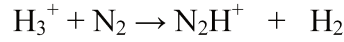
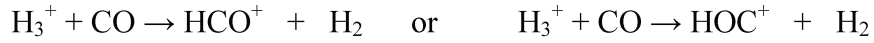
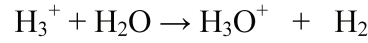


Figure 1:  $\text{H}_3^+$  abundance in the disk plane as a function of the distance from the center of noble gases (Mousis et al. 2008).

Species	Abundance
Ar	$3.02 \times 10^{-6}$
Kr	$3.82 \times 10^{-9}$
Xe	$3.72 \times 10^{-10}$

Table 1: Proto-solar abundances (molar ratio with respect to  $\text{H}_2$ ) (Alecian et al. 2005)

However, if the destructive reactions of  $\text{H}_3^+$  also produce ions capable of trapping noble gases with an analogous efficiency, most of adjustments for the  $\text{H}_3^+$  density profile could be avoided, since each  $\text{H}_3^+$  destroyed is replaced by another trapping agent through the following reactions:



At that point, it has to be stressed that all the preceding reactions have been verified to be thermodynamically (exothermic) and dynamically (no barrier) possible and that all the ions obtained are well-known and ubiquitous in astrophysical objects. And it has to be reminded of the preceding study I was in charge of during my internship in the same team (see paper at the end of the chapter, Pauzat et al. 2013), where  $\text{H}_3\text{O}^+$  was found to form thermodynamically stable complexes with all noble gases; this led us to pursue and study the other ions as well, looking for a systemic behaviour of protonated ions.

### III Article:

Protonated ions as systemic trapping agents for noble gases: from electronic structure to radiative association (accepted JCP)

# Protonated ions as systemic trapping agents for noble gases: from electronic structure to radiative association

O. Ozgurel,<sup>1</sup> F. Pauzat,<sup>1, a)</sup> J. Pilmé,<sup>1</sup> Y. Ellinger,<sup>1</sup> M-C. Bacchus-Montabonel,<sup>2</sup> and O. Mousis<sup>3</sup>

<sup>1)</sup>*Sorbonne Universités, UPMC Univ. Paris 06, UMR - CNRS 7616, Laboratoire de Chimie Théorique, F-75005 Paris, France*

<sup>2)</sup>*Institut Lumière Matière, UMR5306 Université Lyon1-CNRS, Université de Lyon, F-69622 Villeurbanne, France*

<sup>3)</sup>*Aix Marseille Université, CNRS, LAM (Laboratoire d'Astrophysique de Marseille) UMR 7326, 13388 Marseille, France*

(Dated: 22 September 2017)

The deficiencies of argon, krypton and xenon observed in the atmosphere of Titan as well as anticipated in some comets, might be related to a scenario of sequestration by  $\text{H}_3^+$  in the gas phase at the early evolution of the solar nebula. The chemical process implied is a radiative association, evaluated as rather efficient in the case of  $\text{H}_3^+$ , especially for krypton and xenon. This mechanism of chemical trapping might not be limited to  $\text{H}_3^+$  only, considering that the protonated ions produced in the destruction of  $\text{H}_3^+$  by its main competitors present in the primitive nebula, i.e.  $\text{H}_2\text{O}$ ,  $\text{CO}$  and  $\text{N}_2$ , might also give stable complexes with the noble gases. However the effective efficiency of such processes is still to be proven. Here, the reactivity of the noble gases Ar, Kr, Xe, with all protonated ions issued from  $\text{H}_2\text{O}$ ,  $\text{CO}$  and  $\text{N}_2$ , expected to be present in the nebula with reasonably high abundances, has been studied with quantum simulation methods, dynamics included. All of them give stable complexes and the rate coefficients of their radiative associations range from  $10^{-16}$  to  $10^{-19} \text{ cm}^3 \text{ s}^{-1}$ , which is reasonable for such reactions and has to be compared to the rates of  $10^{-16}$  to  $10^{-18} \text{ cm}^3 \text{ s}^{-1}$ , obtained with  $\text{H}_3^+$ . We can consider this process as universal for all protonated ions which, if present in the primitive nebula as astrophysical models predict, should act as sequestration agents for all three noble gases with increasing efficiency from Ar to Xe.

Keywords: astrochemistry - protoplanetary disks - comets - molecular processes - radiative association

## I. INTRODUCTION

The problem of the noble gases deficiency observed in Titan's atmosphere<sup>1</sup> has led to tentative explanations through several models, none of them fully satisfactory. Theoretical quantum chemistry, with high level ab initio simulations, demonstrated that, at least from a thermodynamic point of view,  $\text{H}_3^+$  is able to act as a trap for noble gases by forming complexes in the gas phase.<sup>2,3</sup> The coupling of these results with those of an elaborate model giving the abundance profile of  $\text{H}_3^+$  in the conditions of the cooling proto-planetary disks,<sup>4-6</sup> led to the conclusion that  $\text{H}_3^+$  might be abundant enough in the outer protosolar nebula to trap, at least Xe and Kr, prior to their condensation epochs, implying that their abundances should be solar in Saturn's current atmosphere and below the observational limit in Titan. The same scenario predicts that comets agglomerated from ices formed at high heliocentric distances might also be depleted in Kr and Xe.

In the astrophysical models, the crucial point is the accurate determination of the abundance of  $\text{H}_3^+$  which implies evaluating not only its production but also its destruction along the cooling evolution of the proto-planetary disk. That is why, a complete modeling should take into account the molecules able to react with  $\text{H}_3^+$

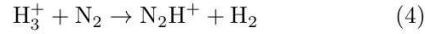
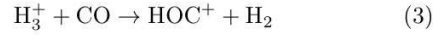
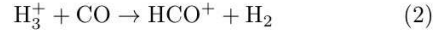
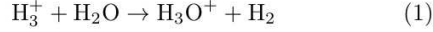
during this period and the evolution of their abundances with time.

From a chemical point of view, when we looked at the main destructive agent for  $\text{H}_3^+$ , i.e.  $\text{H}_2\text{O}$ , we found that the result of the destructive reaction, i.e.  $\text{H}_3\text{O}^+$ , could also act as a trapping agent for the noble gases, leading to chemically stable complexes<sup>6</sup> via radiative associations with the noble gases. Then we have to consider the possibility of a similar behavior for all protonated ions, among which those issued from the other main destructors of  $\text{H}_3^+$  present in the environment. Nevertheless, to be conclusive it implies performing a complete quantitative study of these radiative associations and in particular to evaluate reliable rate constants of these reactions which belong to a category usually considered not to be very efficient.

In the solar nebula, the  $\text{H}_3^+$  formed can be destroyed by the reactions with the most abundant molecules of the gas phase, namely  $\text{H}_2\text{O}$ ,  $\text{CO}$ , and  $\text{N}_2$ .<sup>6</sup> In a steady state, formation and destruction rates balance each other, but when the solar nebula cools down, the destructive molecules do not remain in the gas phase (the upper limit being a local temperature of 150K), being trapped themselves as clathrates or simply condensing, and the balance has to be adjusted. However, if these molecules are reacting with  $\text{H}_3^+$  to give ions with a significant capability for trapping the noble gases, most adjustments of the density of  $\text{H}_3^+$  could be avoided, each  $\text{H}_3^+$  destroyed being replaced by another trapping ion. This can be argued safely as long as the trapping capabilities are more or less equivalent. In these reactions,  $\text{H}_3^+$  plays the role

<sup>a)</sup>Electronic mail: pauzat@lct.jussieu.fr.

of a universal proton donor; the reactions implied in such a scheme are:

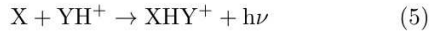


All these ions are well-known and ubiquitous in astrophysical objects. Looking at the reported original detections in the interstellar medium (ISM) and circumstellar envelopes we can cite<sup>7</sup>  $\text{HCO}^+$  first seen in 1970 and confirmed five years later,<sup>8</sup>  $\text{HN}_2^+$ ,<sup>9,10</sup>  $\text{HOC}^+$ ,<sup>11,12</sup> We can also mention further detections of  $\text{HCO}^+$ ,<sup>13</sup>  $\text{HN}_2^+$ ,<sup>14</sup> and  $\text{HOC}^+$ .<sup>15</sup> The detection of  $\text{H}_3\text{O}^+$  has also been reported in the ISM.<sup>16,17</sup> Moreover, all these reactions (Eq.1-4) are known to be thermodynamically (exothermic) and dynamically efficient (<http://www.rate99.co.uk/>).

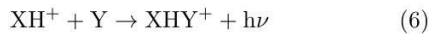
In the Solar system, the  $\text{H}_3^+$  emission has been recorded towards the auroral zone of Jupiter, soon followed by its detection in Saturn and Uranus giant planets<sup>18</sup> whereas it took ten more years to succeed in the detection of  $\text{H}_3^+$  and its isotopologs<sup>19,20</sup> in the ISM.

The role of  $\text{H}_3^+$  itself, as possible trapping agent for noble gases, has already been fully investigated<sup>21</sup> but one has to be aware that till now, this scenario has never been quantified for any other trapping agent beyond a static description of the trapping processes.

In a general way, two radiative association processes would lead to the  $\text{XHY}^+$  complex (with  $\text{X} = \text{Ar}, \text{Kr}, \text{Xe}$  and  $\text{Y} = \text{H}_2\text{O}, \text{CO}, \text{N}_2$ ), namely:



and



Because the concentrations of the  $\text{XH}^+$  species are so low (no detection has been reported apart from that of  $^{36}\text{ArH}^+$  in a supernova remnant known as the Crab nebula),<sup>22</sup> the formation of the  $\text{XHY}^+$  complexes via (Eq.6) is assumed to be negligible and therefore the only route to be considered is the radiative association (Eq.5).

## II. COMPUTATIONAL STRATEGY

To reduce the length of the story, only a brief overview of the key theoretical points of the static and dynamic aspects of this research are presented (see Appendix for more details). In the present study we employ a fully ab-initio approach, from the calculations of the reactive potential surfaces to the determination of the corresponding radiative association rate constants.

Concerning the thermodynamic part, all treatments belong to the ab initio coupled cluster area, i.e. CCSD and CCSDT associated with a correlation consistent basis set cc-pVQZ and its augmented versions (aug-) of increasing flexibility in the valence shell. The calculations were performed with the G09 version of the Gaussian package.<sup>23</sup>

i) The first task is to determine the structure of the complexes. All stationary points were optimized and the stability conditions were verified by a vibrational analysis.

ii) In order to get reliable geometries and stabilities, the potential energy surface around the minima had to be reconstructed to correct the bias introduced by the artificial stabilization of the energy of such weakly bound complexes due to the fact that the interacting fragments borrow each others basis sets to lower their energies. This artifact is known as the basis set superposition error (BSSE). It was corrected here using the counterpoise method,<sup>24</sup> for all points of the re-optimization of the geometrical parameters implied in the description of the two entities interacting in the complex. The difficulty is to determine the fragments to be considered when several separations are possible, a situation we have already faced with the complexes between  $\text{H}_3^+$  and the noble gases. Usually we can refer to those of lowest energy dissociation. However, when it was unclear which separation to use, we relied on a topological analysis (see Section IV and Appendix A) of the complex to get the partitioning of the physical space into well defined interacting fragments.

For the dynamic part, the radiative association calculations are done in a pseudo-diatom approximation. (see Appendix B). We relied on the previous computational experiments<sup>21</sup> performed for the rate constants of the radiative associations of argon with  $\text{H}_3^+$ .

## III. STRUCTURE AND STABILITY OF THE PROTONATED IONS

Taking  $\text{H}_3^+$  as a reference for the capture of noble gases X, we report some preceding results for the structure (Figure 1) and binding energies (Table I) of the  $\text{X-H}_3^+$  complexes.<sup>2</sup>



FIG. 1: The stable structure of  $(\text{X} \cdots \text{H}_3^+)$  for  $\text{X} = \text{Ar}, \text{Kr}, \text{and Xe}$

For all  $\text{X-H}_3^+$  complexes, the most stable geometry is that of  $\text{C}_{2v}$  symmetry in which X points to an apex of the  $\text{H}_3^+$  triangle (Figure 1), this at all levels of theory.

The convergence of the computational methods used allows to consider the energetic calculations reliable by

TABLE I: Stabilities of the  $X \cdots H_3^+$  complexes (kcal/mole), including harmonic zero point energies\* and BSSE correction, related to reactions R1 and R2†

Complex	Ar $\cdots H_3^+$		Kr $\cdots H_3^+$		Xe $\cdots H_3^+$	
Reactions	R1	R2	R1	R2	R1	R2
CCSD(T)/Q	7.27	16.01	13.03	8.60	23.22	2.93
CCSD(T)/aug-Q	7.35	16.16	13.50	8.54	23.64	2.78

Basis sets: /Q = cc-pVQZ ; /aug-Q = aug-cc-pVQZ  
 \*calculated at level CCSD(T)/Q  
 †R1= $X \cdots H_3^+ \rightarrow X + H_3^+$  and R2= $X \cdots H_3^+ \rightarrow XH^+ + H_2$

1-2% when reaching the CCSDT/aug-cc-pVQZ level.

#### A. The structures of protonated ions with noble gases [X-ion-H]<sup>+</sup> (X=Ar, Kr, Xe)

All complexes, whatever the noble gas, are structurally similar (Figure 2). The geometries presented in Table II show that the BSSE corrections, that could lead to changes of 1-2% in the most influenced bond lengths, cannot be escaped. This is especially true if spectroscopic data are to be calculated in order to help with the detection of such species. It should be emphasized that contrary to a posteriori corrections of the energy of the equilibrium structures, the optimization procedure reported here are carried out including an a priori correction of the BSSE artifact for all the geometrical parameters defining the molecular structures.

#### B. The binding energies of protonated ions with noble gases [X-ion-H]<sup>+</sup> (X=Ar, Kr, Xe)

The evolutions of the complexes stabilities within the series Ar  $\rightarrow$  Kr  $\rightarrow$  Xe present the same trend: as for the  $XH_3^+$  complexes, the stability decreases in the R1 fragmentation from Ar to Xe whereas it increases for R2 (see Table III).

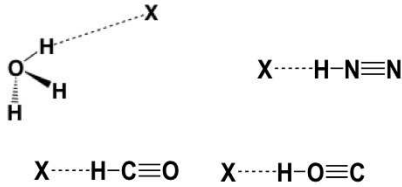


FIG. 2: Equilibrium structures of the [X-protonated ions] with X = Ar, Kr, and Xe.

Looking at the energetic balance, one has:

- i) For  $X-H_3O^+$ , we found that, contrary to the reference  $XH_3^+$ , all complexes prefer a common dissociative process

leading to  $X + H_3O^+$  whatever the noble gas. The point to be noted, is that, when comparing the stabilities values in Table III and Table I, it is obvious that each  $H_3O^+$  ion issued from the destruction of a  $H_3^+$  by  $H_2O$  in the gas phase should be able to play an almost equivalent role in the capture process of noble gases.

ii) For  $X-HCO^+$  and  $X-HOC^+$ , one has two different situations although they are isomers whose difference is only due to the attachment of the proton to one or the other extremity of the CO diatomic species. The case of  $XHCO^+$  is very close to  $X-H_3O^+$ : for all X, R1 is the preferred dissociative channel with similar energies increasing from Ar to Xe. The case of  $XHOC^+$  is different and closer to  $XH_3^+$ . If the R1 dissociation is favored for Ar, it is the R2 dissociation that is favored for Xe. The case of Kr is very sensitive to the method used. Indeed,  $X-HOC^+$  dissociates following the R1 route for DFT but following the R2 route for MP2 (not shown here). However, higher levels of theory, as CCSD and CCSDT, agree on this complex being intermediate between two cluster structures as shown below in the topological analysis of the electronic structure of this complex. Finally, confronting the values obtained for both complex families shows that their stabilities are equivalent  $XH_3^+$  reported in Table I (7.3, 8.5, 2.8 kcal), indicating that the trapping power of  $HCO^+$  and  $HOC^+$  could be at least as efficient as the one of  $XH_3^+$ .

iii) For  $HNN^+$  the situation is closer to that of  $HOC^+$  but with an inversion of the preference for the dissociative reaction only for xenon: Ar and Kr preferring to dissociate through the R1 mechanism whereas xenon dissociates through the R2 route. The trend is the same, that is an increase of the binding energies relative to R1 dissociation and a decrease for those relative to R2 when going from Ar to Xe, with a crossing of the values for Xe (although the energy difference between two routes is much smaller than for  $HOC^+$ ). According to the DFT method (not shown),  $XeHNN^+$  dissociates through R1 whereas for all the other post HF methods, it prefers R2. Similar to the  $KrHOC^+$ , this shows that high level methods are needed to describe these rather weakly bonded complexes.

#### IV. BONDING PICTURES IN THE NOBLE GAS COMPLEXES

Even though, most of the time, the fragments interacting in the complexes can be identified from their preferred dissociation mechanism, a better understanding of bonding pictures can be obtained using both, the topological analysis of the electron localization function (ELF)<sup>25-27</sup> and the *Atoms in Molecular Theory* (QTAIM)<sup>28,29</sup>. As these methodologies have been widely discussed in the literature, they are only recalled in Annex A. Introduced<sup>30</sup> by Bader and Stephens and later revisited<sup>31</sup> by Fradera et al., the delocalization index (DI) is a measure of the electron-sharing between two

TABLE II: Raw and BSSE-optimized equilibrium geometries\* of the  $X \cdots \text{Ion}^+$  complexes ( $X=\text{Ar}, \text{Kr}, \text{Xe}$ ) and rotational constants in GHz at the CCSD(T)/cc-pVQZ level of theory and dipole moments in Debye at CCSD.

Complex	Raw-optimized geometry				BSSE-optimized geometry				A	B	C	$\mu$
	X-H <sub>X</sub>	H <sub>X</sub> -O	H <sub>O</sub> -O	H <sub>O</sub> -O-H <sub>O</sub>	X-H <sub>X</sub>	H <sub>X</sub> -O	H <sub>O</sub> -O	H <sub>O</sub> -O-H <sub>O</sub>				
Ar $\cdots\text{H}_3\text{O}^+$	2.053	0.991	0.974	111.21	2.068	0.990	0.974	111.29	319.6	4.175	4.140	8.3
Kr $\cdots\text{H}_3\text{O}^+$	2.151	0.997	0.974	111.16	2.187	0.995	0.974	111.22	318.2	3.215	3.195	10.2
Xe $\cdots\text{H}_3\text{O}^+$	2.293	1.005	0.974	110.87	2.340	1.002	0.974	110.95	318.3	2.721	2.706	10.9
	X-H <sub>X</sub>	H <sub>X</sub> -C	C-O		X-H <sub>X</sub>	H <sub>X</sub> -C	C-O					
Ar $\cdots\text{HCO}^+$	2.110	1.112	1.110		2.133	1.111	1.110			1.973	1.973	5.3
Kr $\cdots\text{HCO}^+$	2.199	1.120	1.110		2.239	1.118	1.110			1.468	1.468	8.0
Xe $\cdots\text{HCO}^+$	2.316	1.135	1.111		2.372	1.130	1.110			1.244	1.244	9.2
	X-H <sub>X</sub>	H <sub>X</sub> -O	O-C		X-H <sub>X</sub>	H <sub>X</sub> -O	O-C					
Ar $\cdots\text{HOC}^+$	1.695	1.073	1.153		1.707	1.071	1.153			2.724	2.724	3.3
Kr $\cdots\text{HOC}^+$	1.737	1.135	1.146		1.739	1.139	1.151			2.035	2.035	4.8
Xe $\cdots\text{HOC}^+$	1.648	1.579	1.142		1.642	1.611	1.142			1.516	1.516	5.0
	X-H <sub>X</sub>	H <sub>X</sub> -N	N-N		X-H <sub>X</sub>	H <sub>X</sub> -N	N-N					
Ar $\cdots\text{HNN}^+$	1.881	1.076	1.096		1.893	1.075	1.096			2.383	2.383	4.2
Kr $\cdots\text{HNN}^+$	1.950	1.099	1.096		1.991	1.092	1.096			1.764	1.764	6.4
Xe $\cdots\text{HNN}^+$	2.049	1.142	1.097		2.057	1.145	1.097			1.508	1.508	7.1

\*Bond lengths in Å; angles in deg.

TABLE III: Stabilities of the  $X \cdots \text{H}_3^+$  complexes (kcal/mole), including harmonic zero point energies\* and BSSE correction, related to reactions R1 and R2†

Complex	[Ar-ion-H] <sup>+</sup>		[Kr-ion-H] <sup>+</sup>		[Xe-ion-H] <sup>+</sup>	
Reactions	R1	R2	R1	R2	R1	R2
[ion-H] <sup>+</sup> = H <sub>3</sub> O <sup>+</sup>						
CCSD(T)/Q	4.24	78.47	5.80	67.19	7.85	52.53
CCSD(T)/aug-Q	4.43	77.55	6.00	65.84	8.12	50.76
[ion-H] <sup>+</sup> = HCO <sup>+</sup>						
CCSD(T)/Q	4.31	54.54	5.81	43.21	7.99	28.66
CCSD(T)/aug-Q	4.53	54.78	5.73	42.71	8.26	28.04
[ion-H] <sup>+</sup> = HOC <sup>+</sup>						
CCSD(T)/Q	10.82	23.70	15.16	15.21	23.60	6.92
CCSD(T)/aug-Q	10.90	23.86	15.47	15.16	24.59	7.07
[ion-H] <sup>+</sup> = HNN <sup>+</sup>						
CCSD(T)/Q	7.74	34.37	10.32	24.11	14.26	11.33
CCSD(T)/aug-Q	7.92	34.27	10.27	23.35	15.47	11.34

Basis sets: /Q = cc-pVQZ ; /aug-Q = aug-cc-pVQZ

\*calculated at level CCSD(T)/Q

†R1= $X \cdots \text{H}_3^+ \rightarrow X + \text{H}_3^+$  and R2= $X \cdots \text{H}_3^+ \rightarrow \text{XH}^+ + \text{H}_2$

atoms and can be compared to other bond order indices. The relative percentage of the two resonance structures Ia and Ib, respectively  $[X + \text{ion}^+]$  and  $[X\text{-H}^+ + \text{neutral}]$ , has been evaluated using the DI of protonated bonds. For example in the case of  $X\text{-H}_3\text{O}^+$  complexes, Ia and Ib are calculated as follows:

$$I_a = 100 \left( \frac{DI_{OH_x}}{DI_{OH_x} + DI_{XH_x}} \right) \text{ and } I_b = 100 - I_a$$

H<sub>X</sub> is here the hydrogen located in front of the noble

TABLE IV: ELF population analysis of  $X\text{-H}_3\text{O}^+$  ( $X=\text{Ar}, \text{Kr}, \text{Xe}$ ). Populations of basins and QTAIM charges are in electrons.\*

$X\text{-H}_3\text{O}^+$	C(X)+V(X)	V(H <sub>X</sub> , O)	q(X)	Ia	Ib
Ar-H <sub>3</sub> O <sup>+</sup>	17.96	0.93	0.04	80	20
Kr-H <sub>3</sub> O <sup>+</sup>	35.94	1.29	0.06	76	24
Xe-H <sub>3</sub> O <sup>+</sup>	25.91	1.23	0.09	74	26
H <sub>3</sub> O <sup>+</sup>	-	1.86			

\*The 28 innermost electrons of Xe are not treated explicitly but through an effective core potential

gas. In this work, these results have also provided a rationale about the choice of the partition of the systems into fragments to be used for BSSE corrections, especially when there is no straightforward clue, such as for KrHOC<sup>+</sup>.

The ELF topological analysis applied previously to  $X_n(\text{H}_3^+)$  ( $X=\text{Ne}, \text{Ar}, \text{Kr}, ; n=1,3$ ) complexes has shown the crucial role of the charge transfer from the noble gases toward the  $\text{H}_3^+$  cation as a driving force in the bonding along the series. It was also consistent with the increase in the atomic polarizabilities from neon to krypton.<sup>3</sup> In this work, a net positive charge  $q(X)$  discloses also a charge transfer from the noble gas towards the cation ( $\text{H}_3\text{O}^+$ ,  $\text{HCO}^+$  or  $\text{HNN}^+$ ). However, the magnitude of  $q(X)$  remains small ( $<0.2$  e) except for XeOC<sup>+</sup> (0.45 e).

The ELF localization domains are displayed in Figure 3. The ELF populations analysis for all  $X\text{-H}_3\text{O}^+$ ,  $X\text{-HCO}^+$ ,  $X\text{-HOC}^+$  and  $X\text{-HNN}^+$  complexes are reported in Tables IV, V, VI and VII, respectively.

As observed in Figure 3 and Table IV, the ELF topology of  $X\text{-H}_3\text{O}^+$  complexes shows two well-separated domains. The first one corresponds to the neutral X noble



gas ( $q(X)$  remaining always lower than 0.1 electron); it splits into a core basin  $C(X)$  and valence basins  $V(X)$ . The second domain corresponds to  $H_3O^+$  where one O-H bond viewed as the protonated  $V(H_X, O)$  topological basin, is stretched toward the noble gas. The population of this latter basin was found lower than 1.5 electrons whereas the other  $V(O, H)$  populations remain close to 2 electrons. It should be noted that no covalent character was identified for the  $X-H_3O^+$  interaction since there are no disynaptic basins located between  $X$  and  $H$ . It is fully consistent with a large weight of around 75% for  $I_a$  in all these complexes. Thus, it gives a better understanding of the fragmentation used for the BSSE corrections for which the R2 route is energetically preferred.

The topological analysis of  $XHCO^+$  complexes (Table V) shows a very similar pattern to that of  $H_3O^+$  complexes, i.e., two well-separated domains around the noble gas and the  $HCO^+$  ion. As previously, the population of the protonated  $V(H_X, C)$  bonding basin remains lower than 2 electrons for all noble gases. The  $I_a$  and  $I_b$  weights have been found quite similar for both  $XH_3O^+$  and  $XHCO^+$  complexes. This confirms again the validity of the fragmentation into the noble gas and  $HCO^+$  moieties used for the BSSE corrections.

Except for  $ArHOC^+$  showing a very similar topology to other Ar species ( $I_a > I_b$ ), the bonding picture of  $XHOC^+$  complexes differs from previous compounds (see Table VI). First, the charge  $q(X)$  increases drastically from 0.1 e (Ar) to 0.45 e (Xe). This is in agreement with the increase of the weight of  $[X-H]^+$  ( $I_b$ ) in Kr- and Xe- complexes (see Tables V-VI). The ELF topology of  $KrHOC^+$  undergoes a clear modification since the  $V(H_X, O)$  basin splits into non-bonding basins  $V(H)$  and  $V(O)$ . Thus, the weights of  $I_a$  and  $I_b$  configurations become very similar in agreement with the practically equal binding energies of 15.5 and 15.2 kcal/mol respectively obtained from the dissociation R1 and R2 routes. For  $XeHOC^+$ , the  $V(H_X, O)$  basin disappears in favor of a new disynaptic protonated  $V(H, X)$  basin. Consequently, the weight of  $I_b$  becomes larger than  $I_a$  in agreement with the binding energies respectively obtained from R1 (24.6 kcal/mol) and R2 (7.1 kcal/mol) routes.

Protonated  $N_2$ , though soelectronic with protonated CO isomers, offers another situation. For  $XHN_2^+$  complexes (see Table VII), two well-separated domains are observed for Ar and Kr. The first domains contain the noble gas basins whereas the others are distributed over the  $HN_2^+$  cation. Thus, the weight  $I_a$  remains larger than  $I_b$ . By contrast, the  $XeHN_2^+$  bonding picture looks like  $KrHOC^+$  since the protonated  $V(H_X, N)$  basin splits into  $V(H_X)$  and  $V(N)$  valence basins. The weight  $I_a$  (35%) remains smaller than  $I_b$  (65%), again in accordance with the preferred dissociation mechanism (see Table III).

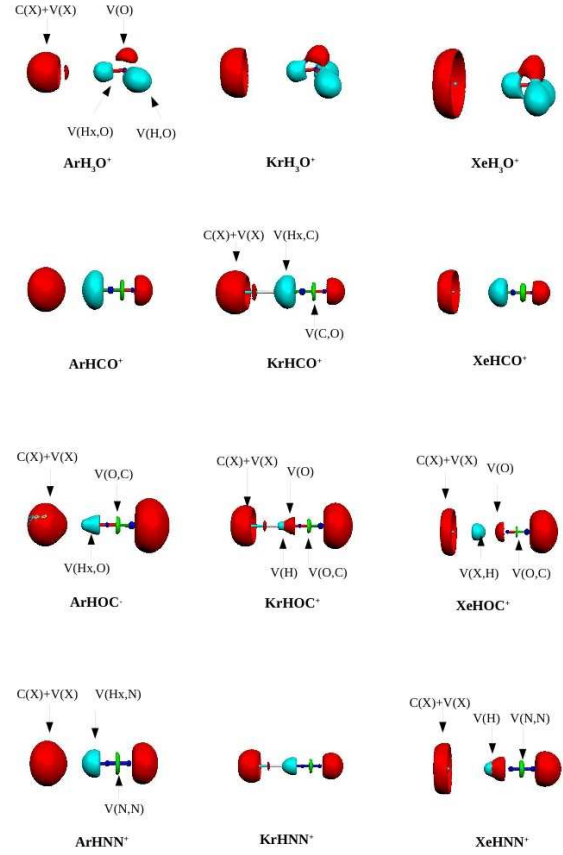


FIG. 3: View of the electron localization function (ELF=0.85) isosurfaces (top to bottom) for  $X-H_3O^+$ ,  $X-HCO^+$ ,  $X-HOC^+$ ,  $X-HNN^+$ . Color code: magenta: core basins, red: non-bonding basins, green: bonding basins, light blue: protonated basins.

## V. RATE CONSTANTS OF THE RADIATIVE ASSOCIATIONS

The formation of all complexes occurs without an activation barrier. The rate constants of these radiative associations are reported in Tables VIII, IX, X (for Ar, Kr, Xe, respectively) for temperatures in the range of 10-100 K, which includes typical temperature interval (30-100K) in proto solar nebula.<sup>32</sup> All rates present similar variations with the temperature i.e. a maximum around 60K.

Regarding Ar complexes with the four different ions, the rates stay close to the value  $0.5 \times 10^{-18} \text{ cm}^3 \text{ s}^{-1}$  obtained for  $H_3^+$ , within one order of magnitude, with a small advantage to  $ArHOC^+$  whose higher binding energy gives a formation rate going up to  $1 \times 10^{-18} \text{ cm}^3 \text{ s}^{-1}$ . Likewise, the maximum rate constants of Kr complexes



TABLE V: ELF population analysis of X-HCO<sup>+</sup> (X= Ar, Kr, Xe). Populations of basins and QTAIM charges are in electrons.\*

X-HCO <sup>+</sup>	C(X)+V(X)	V(H <sub>X</sub> , C)	q(X)	I <sub>a</sub>	I <sub>b</sub>
Ar-HCO <sup>+</sup>	17.96	2.36	0.04	86	14
Kr-HCO <sup>+</sup>	35.93	2.38	0.07	82	18
Xe-HCO <sup>+</sup>	25.90	2.39	0.10	79	21
HCO <sup>+</sup>		2.21			

\*The 28 innermost electrons of Xe are not treated explicitly but through an effective core potential

TABLE VI: ELF population analysis of X-HOC<sup>+</sup> (X= Ar, Kr, Xe). Populations of basins and QTAIM charges are in electrons.\*

X-HOC <sup>+</sup>	C(X)+V(X)	V(H <sub>X</sub> , O)	V(H <sub>X</sub> )	V(O)	V(H <sub>X</sub> , X)	q(X)	I <sub>a</sub>	I <sub>b</sub>
Ar-HOC <sup>+</sup>	17.90	2.42	-	-	-	0.10	61	39
Kr-HOC <sup>+</sup>	35.85	-	0.25	4.86	-	0.15	52	48
Xe-HOC <sup>+</sup>	24.27	-	-	4.52	1.81	0.45	24	76
HOC <sup>+</sup>		2.32						

\*The 28 innermost electrons of Xe are not treated explicitly but through an effective core potential

are in between  $0.4 \times 10^{-18}$  and  $5 \times 10^{-18}$  cm<sup>3</sup>s<sup>-1</sup> in agreement with their relative binding energies. The efficiency of the reactions for Xe complexes increases again with the binding energy, starting from  $0.6 \times 10^{-18}$  up to almost  $10 \times 10^{-18}$  cm<sup>3</sup>s<sup>-1</sup>.

Comparing these results with the rate constants of the H<sub>3</sub><sup>+</sup> complexes, we observe that those of Ar complexes are in the same order of magnitude as ArH<sub>3</sub><sup>+</sup>, whereas the rates of Kr complexes are lower than KrH<sub>3</sub><sup>+</sup>, by almost one order of magnitude for KrN<sub>2</sub>H<sup>+</sup> and KrHOC<sup>+</sup> and even two for KrH<sub>3</sub>O<sup>+</sup> and KrHCO<sup>+</sup>; the same behavior is observed for Xe complexes. However, it has to be noted that all the rates concerning Kr and Xe complexes are higher than those of Ar complexes and that even the smallest rates of Kr and Xe complexes can compare with those of ArH<sub>3</sub><sup>+</sup>. Thus, they all can be considered as quite efficient in terms of radiative association reactions.

It has also to be reminded that, since the approach applied treats the complexes as pseudo-diatomic systems, the accuracy of the rate constant calculations is lesser for the ions having linear geometry than for H<sub>3</sub><sup>+</sup> that has a more sphere like symmetry.

## VI. CONCLUDING REMARKS

An extensive study of the complexes issued from the trapping of the noble gases by the H<sub>3</sub><sup>+</sup> ion had indicated that such complexes were far more stable than expected. The important result of the present study is that this property appears to generalize to other protonated ions, in particular ions issued from common in-

TABLE VII: ELF population analysis of X-HNN<sup>+</sup> (X= Ar, Kr, Xe). Populations of basins and QTAIM charges are in electrons.\*

X-HNN <sup>+</sup>	C(X)+V(X)	V(H <sub>X</sub> , N)	V(H <sub>X</sub> )	V(N)	q(X)	I <sub>a</sub>	I <sub>b</sub>
Ar-X-HNN <sup>+</sup>	17.93	2.74	-	-	0.07	73	27
Kr-X-HNN <sup>+</sup>	35.88	2.79	-	-	0.12	68	32
Xe-X-HNN <sup>+</sup>	25.82	-	0.33	2.49	0.18	35	65
HN <sub>2</sub> <sup>+</sup>		2.60					

\*The 28 innermost electrons of Xe are not treated explicitly but through an effective core potential.

TABLE VIII: Rate constants for the radiative association of Ar with protonated ions in  $10^{-18}$  cm<sup>3</sup>s<sup>-1</sup> as a function of T(K).

T(K)	ArH <sub>3</sub> <sup>+</sup>	ArH <sub>3</sub> O <sup>+</sup>	ArHCO <sup>+</sup>	ArHOC <sup>+</sup>	ArHNN <sup>+</sup>
10	0.33	0.16	0.09	0.68	0.33
20	0.43	0.22	0.11	0.94	0.45
30	0.49	0.26	0.13	1.11	0.52
40	0.52	0.28	0.14	1.21	0.57
50	0.53	0.29	0.15	1.25	0.58
60	0.53	0.29	0.14	1.25	0.58
70	0.52	0.28	0.14	1.22	0.56
80	0.50	0.27	0.13	1.18	0.54
90	0.48	0.26	0.13	1.13	0.52
100	0.47	0.25	0.12	1.08	0.49

terstellar molecules as H<sub>2</sub>O, CO, N<sub>2</sub> which, through interaction with H<sub>3</sub><sup>+</sup>, give H<sub>3</sub>O<sup>+</sup>, HCO<sup>+</sup>, HOC<sup>+</sup>, N<sub>2</sub>H<sup>+</sup>. Apart from H<sub>3</sub>O<sup>+</sup>, all of these complexes have a linear structure, the noble gas pointing to the hydrogen side. Although all these well-defined complexes are stabilized by long-range interactions, they do not belong to the same family. The topological analysis of electron localization function shows that XH<sub>3</sub>O<sup>+</sup>, XHCO<sup>+</sup> and ArHOC<sup>+</sup>, ArN<sub>2</sub>H<sup>+</sup> and KrN<sub>2</sub>H<sup>+</sup> complexes, can be described as (X...Ion) systems whereas XeHOC<sup>+</sup> and XeN<sub>2</sub>H<sup>+</sup> are better described as (XH<sup>+</sup>...Neutral) systems, the case of KrHOC<sup>+</sup> remaining unclear. The partitioning so obtained is at the basis of a reliable evaluation of the BSSE corrections necessary to determine accurate geometries and rotational constants in view of the search for these species at radio wavelengths (in the laboratory or in space). However, the trapping ability of these ions, had also to be investigated by evaluating their formation reactions rates. A fully ab initio approach has been applied in the framework of the one-dimensional reaction coordinate approximation. According to our results, the noble gas complexes with the ions obtained by the destructive reactions of H<sub>3</sub><sup>+</sup> have rate constants in the range of  $10^{-19}$  to  $10^{-17}$  cm<sup>3</sup>s<sup>-1</sup> which can be considered fairly efficient values for radiative association reactions. Therefore, the destruction of H<sub>3</sub><sup>+</sup> also forms ions which have the capacity to trap noble gases as well.

From an astrochemical point of view, these results support the hypothesis that the heavy noble gases could be sequestered by protonated species (H<sub>3</sub><sup>+</sup> or/and daugh-

TABLE IX: Rate constants for the radiative association of Kr with protonated ions in  $10^{-17} \text{ cm}^3 \text{ s}^{-1}$  as a function of  $T(\text{K})$ .

T(K)	KrH <sub>3</sub> <sup>+</sup>	KrH <sub>3</sub> O <sup>+</sup>	KrHCO <sup>+</sup>	KrHOC <sup>+</sup>	KrHNN <sup>+</sup>
10	1.75	0.019	0.010	0.26	0.12
20	2.43	0.026	0.019	0.35	0.17
30	2.91	0.031	0.021	0.42	0.20
40	3.23	0.034	0.024	0.47	0.21
50	3.42	0.035	0.026	0.50	0.22
60	3.50	0.035	0.026	0.51	0.22
70	3.50	0.034	0.024	0.52	0.21
80	3.44	0.033	0.023	0.51	0.21
90	3.35	0.021	0.021	0.51	0.20
100	3.24	0.020	0.029	0.49	0.19

TABLE X: Rate constants for the radiative association of Xe with protonated ions in  $10^{-17} \text{ cm}^3 \text{ s}^{-1}$  as a function of  $T(\text{K})$ .

T(K)	XeH <sub>3</sub> <sup>+</sup>	XeH <sub>3</sub> O <sup>+</sup>	XeHCO <sup>+</sup>	XeHOC <sup>+</sup>	XeHNN <sup>+</sup>
10	4.90	0.064	0.031	0.44	0.29
20	6.96	0.087	0.042	0.61	0.40
30	8.36	0.10	0.050	0.74	0.47
40	9.24	0.11	0.056	0.82	0.52
50	9.72	0.12	0.059	0.89	0.55
60	9.87	0.12	0.061	0.93	0.57
70	9.73	0.11	0.062	0.94	0.57
80	9.55	0.11	0.061	0.94	0.56
90	9.23	0.10	0.060	0.93	0.54
100	8.83	0.099	0.059	0.91	0.52

ter molecules) in the gas phase of the protosolar nebula. These properties would then prevent the noble gases from condensation or incorporation in the ices formed at large heliocentric distances during the cooling of the protosolar nebula. The trapping ability of the products formed by the destruction of H<sub>3</sub><sup>+</sup> ions remains preserved since this mechanism leads to the same number of protonated trapping agents at least as efficient as the parent ion H<sub>3</sub><sup>+</sup>. These processes could explain the noble gases depletion in the planetesimals which, later on, agglomerated to form Titan.<sup>4</sup>

They are also relevant to the determination of the origin of comets since a larger noble gas deficiency in a comet may imply that this body agglomerated from grains formed at larger heliocentric distances, where the trapping efficiency by protonated species increases. The in situ measurements<sup>33</sup> in comet 67P/Churyumov-Gerasimenko made by the ROSINA mass spectrometer aboard the *Rosetta* spacecraft give <sup>36</sup>Ar/H<sub>2</sub>O  $\sim 0.1$ – $2.3 \times 10^{-5}$ . This value, compared with <sup>36</sup>Ar/H<sub>2</sub>O  $\sim 5.9 \times 10^{-3}$  in the protosolar nebula,<sup>34</sup> indicates a significant though moderate depletion, as expected from our model. The future measurement of Kr and Xe abundances in long period comets, such as C/1995 O1 (Hale-Bopp), will be needed to assess the validity of our model. On the other hand, similar determinations in short period

comets, such as comet 67P/Churyumov-Gerasimenko, may not display values representative of those acquired at their formation epoch in the protosolar nebula. This alteration could result from the progressive devolatilization of these comets during their multiple orbits with perihelions close to the Sun.

Moreover, the mechanism proposed here is valid in the ISM where H<sub>3</sub><sup>+</sup> should be even more abundant than in the protosolar nebula. However, it has to be reminded that the H<sub>3</sub><sup>+</sup> abundance in ISM is poorly constrained compared to those of HCO<sup>+</sup> and the other ions; this resulting from the fact that the H<sub>3</sub><sup>+</sup> abundance must be determined at infrared wavelengths, a difficult task to perform compared to the case of the other ions whose abundances can be fairly easily quantified in the radio domain.

## ACKNOWLEDGMENTS

This work was supported by CNRS national program PCMI (Physics and Chemistry of the Interstellar Medium) and COST Action CM 1401, “Our Astrochemical History”. We acknowledge computational resources from the CCIN2P3 in Villeurbanne. O.M. acknowledges support from CNES. This work has been partly carried out thanks to the support of the A\*MIDEX project (n° ANR-11-IDEX-0001-02) funded by the “Investissements d’Avenir” French Government program, managed by the French National Research Agency (ANR).

## Appendix A: Quantum Chemical Topology

The methodology lies on the analysis of the gradient field of a scalar function by applying the theory of dynamical systems. The latter provides a partitioning of the molecular space into non-overlapping volumes (basins) localized around maxima of the scalar function and are separated by zero flux surfaces. In the *Atoms in Molecular Theory* (QTAIM), the function is the electron density. Each atom of a molecule corresponds to a basin and the integration of the electron density over the basin volume provides an atomic population. The atomic charge of a topological atom  $\Omega$ ,  $q(\Omega)$ , is calculated by subtracting the atomic population from the atomic number,  $Z(\Omega)$ . If effective core potentials (ECPs) are used for some atoms (case of Xe species), the calculation of their atomic charge involves  $Z_{\text{eff}}$ , the charge of the inner-core. If the scalar function is the electron localization function (ELF) of Becke and Edgecombe, atomic and non-atomic basins are found. The topology of the function can be related to chemical concepts issued from the Lewis theory. The core basins ( $Z > 2$ ) are located at nuclear centers whereas the valence basins are located in the remaining space: monosynaptic basins, labeled  $V(X)$ , usually correspond to the lone-pair regions of X atoms while disynaptic basins, labeled  $V(X, Y)$ , correspond to two-center

X-Y bonds. Disynaptic basins  $V(H, Y)$  are termed as protonated basins. The integration of the total electron density over the basin volume provides a covalent bond population for  $V(X, Y)$  basins while lone-pair populations can be obtained for  $V(X)$  basins.

## Appendix B: Quantum dynamic procedure

We used a complete ab initio method<sup>35–37</sup> to determine rate constants, in which they are calculated by averaging over the cross sections with a Maxwellian velocity distribution at temperature  $T$

$$k(T) = \langle v, \sigma(v) \rangle$$

as proposed<sup>38</sup> by Bacchus-Montabonel et al. The quantum expression of the cross section at a given relative collision energy  $E$  of the colliding fragments is given by:

$$\sigma(E) = \sum_J \sigma_J(E) \quad (B1)$$

with

$$\sigma_J(E) = \sum_{v'J'} \frac{64}{3} \frac{\pi^5}{c^3} \frac{g}{2\mu E} \nu_{E,v'J'}^3 S_{JJ'} M_{EJ,v'J'}^2, \quad (B2)$$

where  $\mu$  is the reduced mass,  $g$  is a parameter accounting for the degeneracy of the electronic state (here  $g=1$ ),  $S_{JJ'}$ , the Höln-London coefficients characteristic of the  $J J'$  pair of rotational levels, and  $M_{EJ,v'J'}^2$  is the free-bound transition moment matrix element of the dipole moment  $D(R)$  between the energy normalized function  $f_{EJ}$  of the continuum and the bound rovibrational function  $\phi_{v'J'}$  for the same potential. In this expression,  $\nu_{E,v'J'}$  is the emitted photon frequency corresponding to the energy difference between the continuum level of energy  $E$  and the rovibrational bound state of energy  $E_{v'J'}$  is given by:

$$\Delta E = h\nu_{v'J'} = E - E_{v'J'}$$

For diatomic molecules, the rovibrational bound states and corresponding free-bound dipole transition moments can be evaluated so that rate constants may be calculated with a quantum chemical treatment. This approach may be extended for larger molecules, in the framework of the one-dimensional reaction coordinate approximation in which the complex can be divided into two fragments and potential energy is optimized for each distance between the fragments. Therefore, in this work, we considered the formation of noble gas complexes to occur along the [ion... noble gas] reaction coordinate, in its electronic ground state potential energy curve, as no excited states could be involved in the process. Although this model cannot take into account all degrees of freedom of the complex, it is shown to give reliable results even in the case of two molecular fragments ( $CH_3^+$  and  $H_2$ ).<sup>38</sup>

<sup>1</sup>H. B. Niemann, S. K. Atreya, S. J. Bauer, *Nature*, **438**, 779 (2005).

- <sup>2</sup>F. Pauzat and Y. Ellinger, *J. Chem. Phys.*, **127**, 014308 (2007).  
<sup>3</sup>F. Pauzat, Y. Ellinger, J. Pilmé, O. Mousis, *J. Chem. Phys.*, **130**, 174313 (2009).  
<sup>4</sup>O. Mousis, F. Pauzat, Y. Ellinger, C. Ceccarelli, *Astrophys. J.* **673**, 637 (2008).  
<sup>5</sup>O. Mousis, U. Marboeuf, J. I. Lunine, et al., *Astrophys. J.* **696**, 1348 (2009).  
<sup>6</sup>F. Pauzat, Y. Ellinger, O. Mousis, M. Ali-Dib, O. Ozgurel, *Astrophys. J.* **777**, 29 (2013).  
<sup>7</sup>D. Buhl and L. E. Snyder, *Nature* **228**, 267 (1970).  
<sup>8</sup>R. C. Woods, T. A. Dixon, R. J. Saykally, and P. G. Szanto, *Phys. Rev. Lett.* **35**, 1269 (1975).  
<sup>9</sup>B. E. Turner, *Astrophys. J.* **193**, L83 (1974).  
<sup>10</sup>S. Green, J. A. Montgomery, Jr., and P. Thaddeus, *Astrophys. J.* **193**, L89 (1974).  
<sup>11</sup>R. C. Woods, C. S. Gudeman, R. L. Dickman, P. F. Goldsmith, G. R. Huguenin, W. M. Irvine, J. Hjalmarson, L.-. Nyman, and H. Olofsson, *Astrophys. J.* **270**, 583, (1983).  
<sup>12</sup>L. M. Ziurys and A. J. Apponi, *Astrophys. J.* **455**, L73 (1995).  
<sup>13</sup>A. A. Stark and R. S. Wolff, *Astrophys. J.* **229**, 118 (1979).  
<sup>14</sup>R. Mauersberger and C. Henkel, *Astron. Astrophys.* **245**, 457 (1991).  
<sup>15</sup>A. Usero, S. Garca-Burillo, A. Fuente, J. Martin-Pintado, and N. J. Rodriguez-Fernandez, *Astron. Astrophys.* **419**, 897 (2004).  
<sup>16</sup>J. M. Hollis, E. B. Churchwell, E. Herbst, and F. C. de Lucia, *Nature* **322**, 524 (1986).  
<sup>17</sup>A. Wootten, F. Boulanger, M. Bogey, F. Combes, P. J. Encrenaz, M. Gerin, and L. Ziurys, *Astron. Astrophys.* **166**, L15 (1986).  
<sup>18</sup>P. Drossart, J.-P. Maillard, J. Caldwell, et al., *Nature*, **340**, 539 (1989).  
<sup>19</sup>T. R. Geballe and T. Oka, *Nature* **384**, 334 (1996).  
<sup>20</sup>B. J. McCall, T. R. Geballe, K. H. Hinkle, and T. Oka, *Science* **279**, 1910 (1998).  
<sup>21</sup>F. Pauzat, M.-C. Bacchus-Montabonel, Y. Ellinger, O. Mousis, *Astrophys. J.* **821**, L33 (2016).  
<sup>22</sup>M. J. Barlow, B. M. Swinyard, P. J. Owen, J. Cernicharo, H. L. Gomez, R. J. Ivison, O. Krause, T. L. Lim, M. Matsuura, S. Miller, G. Olofsson, and E. T. Polehampton, *Science*, **342**, 1343 (2013).  
<sup>23</sup>M. Frisch, G. W. Trucks, H. B. Schlegel, G. E., Scuseria, et al. Gaussian 09, Inc. Wallingford, CT, **19**, 227 (2009).  
<sup>24</sup>S. F. Boys, and F. Bernardi, *Mol. Phys.*, **19**, 553 (1970).  
<sup>25</sup>B. Silvi and A. Savin, *Nature* **371** (6499), 683 (1994).  
<sup>26</sup>A. D. Becke and K. E. Edgecombe, *J. Chem. Phys.* **92**, 5397 (1990).  
<sup>27</sup>A. Savin, O. Jepsen, J. Flad, O. K. Andersen, H. Preuss and H. G. von Schnering, *Angew. Chem. Int.* **31** (2), 187 (1992).  
<sup>28</sup>R. F. W. Bader, *Chem. Rev.* **91** (5), 893 (1991).  
<sup>29</sup>R.F.W. Bader, *Atoms in Molecules: A Quantum Theory*, Oxford University Press, New York, (1994).  
<sup>30</sup>R. F. W. Bader and M. E. Stephens, *J. Am. Chem. Soc.*, **97**, 7391 (1975).  
<sup>31</sup>X. Fradera, M. A. Austen and R. F. W. Bader, *J. Phys. Chem. A*, **103**, 304 (1998).  
<sup>32</sup>O. Mousis and D. Gautier, *PSS*, **52**, 361 (2004).  
<sup>33</sup>H. Balsiger, K. Altmegg, A. Bar-Nun, et al. *Science Advances*, **1**, e1500377 (2015).  
<sup>34</sup>K. Lodders, H. Palme and H.-P. Gail, *Landolt Brnstein*, ed. J. E. Tmper (Berlin: Springer), 560 (2009).  
<sup>35</sup>B. Zygelman, and A. Dalgarno, *Astrophys. J.* **365**, 239 (1990).  
<sup>36</sup>P. C. Stancil, J. F. Babb, and A. Dalgarno, *Astrophys. J.* **414**, 672 (1993).  
<sup>37</sup>F. A. Gianturco, and P. Gori-Giorgi, *Astrophys. J.* **479**, 560 (1997).  
<sup>38</sup>M. C. Bacchus-Montabonel, D. Talbi, and M. Persico, *J. Phys. B.* **33**, 955 (2000).

#### IV Conclusion and perspectives

The main aim of this study was to comfort one specific scenario among those proposed to account for the observed noble gas deficiency in the Titan's atmosphere. Nevertheless, this specific process, being expected to develop in low density and low temperature interstellar environments, might also be available in many other cases. The scenario initially based on the chemical trapping of noble gases by  $\text{H}_3^+$  at the proto-solar nebula stage, was extended to the participation of the destructive reagents of  $\text{H}_3^+$ , present in abundance in the medium at the time. The results obtained show that even if these molecules ( $\text{N}_2$ ,  $\text{CO}$ ,  $\text{H}_2\text{O}$ ) might partially destroy  $\text{H}_3^+$  in the medium, they simultaneously form protonated daughters molecules ( $\text{N}_2\text{H}^+$ ,  $\text{HCO}^+$ ,  $\text{HOC}^+$ ,  $\text{H}_3\text{O}^+$ ) which are also capable of trapping the noble gases, and this with a similar efficiency.

This has two consequences, one obvious concerning the efficiency of the scenario for Titan, the other, more general, pointing to a systemic phenomenon of trapping by the protonated species available in the ISM.

If the trapping of noble gases by  $\text{H}_3^+$  could be the main reason for the deficiency in Titan, it may have also consequences on for the composition of bodies formed in the outer part of PSN, as giant planets and comets. For the bodies whose building blocks formed at higher heliocentric distances, noble gas enrichment should be limited. Since Saturn's building blocks were expected to form at the same location as Titan's planetesimals, the abundances of noble gases should remain solar in Saturn's atmosphere. The other implication is for comets. Since the trapping is directly related to the distance from the Sun, a comet formed at distances longer from the sun, should be impoverished in Kr and Xe. First in situ measurements in 67P released from ROSINA give  $^{36}\text{Ar}/\text{H}_2\text{O} \sim 0.1\text{-}2.3 \times 10^{-5}$  (Balsiger et al. 2015) to be compared to  $^{36}\text{Ar}/\text{O}_2 \sim 5.9 \times 10^{-3}$  in the proto-solar nebula (Lodders et al. 2009), which indicate a significant though moderate depletion as expected in our model. The release of numbers for the expected strong depletion of Kr and Xe will be critical.

However, if the deficiency of Kr and Xe in Titan can be justified by the trapping scenario in the PSN, lower binding energies and reaction rates for Ar complexes cannot fully explain the deficiency of the most abundant noble gas.

Other mechanisms of the “external” type might have also to be considered for further analysis. One possibility is the trapping of the noble gases in the ice before their incorporation into the building blocks of Titan. Solid-state calculations of this other trapping mechanism could be well adapted and might give interesting results as illustrated in the following chapters.

Alternative trapping mechanisms of “internal” type might also be considered, as the trapping by the so-called “tholins” present in the lower layers of the Titan's atmosphere. The major difficulty of such a study would be to obtain a good representation of these tholins, whose compositions are not well known. Periodic DFT methods as developed for polymer calculations would be employed to obtain a satisfactory plausible representation of such compounds, after which the step of trapping the noble gases in/by those complex structures could be studied.



## GAS-PHASE SEQUESTRATION OF NOBLE GASES IN THE PROTOSOLAR NEBULA: POSSIBLE CONSEQUENCES ON THE OUTER SOLAR SYSTEM COMPOSITION

F. PAUZAT<sup>1</sup>, Y. ELLINGER<sup>1</sup>, O. MOUSIS<sup>2</sup>, M. ALI DIB<sup>2</sup>, AND O. OZGUREL<sup>1</sup>

<sup>1</sup> Laboratoire de Chimie Théorique, UMR 7616-CNRS, UPMC Univ. Paris 06, F-75005 Paris, France;

pauzat@lct.jussieu.fr, ellinger@lct.jussieu.fr, zge.zgerel@gmail.com

<sup>2</sup> Institut UTINAM, CNRS/INSU, UMR 6213, Université de Franche-Comté, F-25030 Besançon Cedex, France;

olivier.mousis@obs-besancon.fr, mdib@obs-besancon.fr

Received 2013 April 18; accepted 2013 August 28; published 2013 October 10

### ABSTRACT

We address the problem of the sequestration of Ar, Kr, and Xe by  $H_3^+$  in the gas-phase conditions encountered during the cooling of protoplanetary disks when  $H_3^+$  is competing with other species present in the same environment. Using high-level ab initio simulations, we try to quantify other sequestration possibilities involving He,  $H_3^+$ ,  $H_2O$ , and  $H_3O^+$  present in the protosolar nebula. Apart from the fact that  $H_3^+$  complexes formed with heavy noble gases are found to be by far much more stable than those formed with He or  $H_2O$ , we show that  $H_2D^+$  and  $H_3O^+$ , both products of the reactions of  $H_3^+$  with HD and  $H_2O$ , can also be efficient trapping agents for Ar, Kr, and Xe. Meanwhile, the abundance profile of  $H_3^+$  in the outer part of the nebula is revisited with the use of an evolutionary accretion disk model that allows us to investigate the possibility that heavy noble gases can be sequestered by  $H_3^+$  at earlier epochs than those corresponding to their trapping in planetesimals. We find that  $H_3^+$  might be abundant enough in the outer protosolar nebula to trap Xe and Kr prior their condensation epochs, implying that their abundances should be solar in Saturn's current atmosphere and below the observational limit in Titan. The same scenario predicts that comets formed at high heliocentric distances should also be depleted in Kr and Xe. In situ measurements, such as those planned with the *Rosetta* mission on 67P/Churyumov–Gerasimenko, will be critical to check the validity of our hypotheses.

**Key words:** accretion, accretion disks – astrochemistry – comets: general – molecular processes – planets and satellites: formation

### 1. INTRODUCTION

The noble gas deficiency observed in Titan's atmosphere (Niemann et al. 2005), together with the non-detection of noble gases in comets (Weaver et al. 2002; Iro et al. 2003), has led to the hypothesis that these objects could have been formed from planetesimals already poor in noble gases (Pauzat et al. 2006; Mousis et al. 2008). We have proposed that the observed deficit in the aforementioned bodies could be due to the sequestration of the noble gases by  $H_3^+$  during the early stages of the solar nebula (Mousis et al. 2008). The fact that  $H_3^+$  may be a partner for accreting noble gases in the gas phase is a reasonable assumption for two reasons, at least.

First,  $H_3^+$  is known, from laboratory experiments, to produce molecular complexes with Ar whose thermodynamic stabilities have been determined by Hiraoka & Mori (1989). The structure of  $ArH_3^+$  was determined by microwave spectroscopy (Bogey et al. 1988) at about the same time. To the best of our knowledge, nothing is known experimentally for the other noble gases. Nevertheless, computational experiments performed on  $XH_3^+$  ( $X = Ar, Kr, \text{ and } Xe$ ) were able to reproduce the existing data on Ar and predict the existence of stable complexes for the other noble gases. Their structures and binding energies were determined by means of high-level ab initio calculations (Pauzat & Ellinger 2005; Pauzat et al. 2009).

Second,  $H_3^+$  is ubiquitous in space. It has been observed in star-forming regions (Geballe & Oka 1996), in diffuse interstellar media (McCall et al. 2002), as well as in the solar system at the poles of Jupiter (Maillard et al. 1990) and other giant planets (Miller et al. 2000). It has also been detected under its deuterated form  $H_2D^+$  in protoplanetary disks (Ceccarelli et al. 2004). In addition, the calculated abundance profile of  $H_3^+$

shows an important increase in the outer solar nebula. All these considerations prompted us to consider the possibility of  $H_3^+$  being a trap for noble gases in the gas phase, thus leading to impoverished planetesimals (Mousis et al. 2008).

However, other possible trapping agents are present in the gas phase whose role in noble gases trapping has not been considered in our previous studies but cannot be a priori ignored. This role may be twofold, i.e., forming complexes with  $H_3^+$  or with the noble gases themselves. In a first step, we add complementary quantum simulations, in which we try to quantify both aspects, possibly implying He (the most abundant noble gas),  $H_3^+$  (the first and most stable  $(H_2)_nH_3^+$  complex; Hiraoka 1987), and  $H_2O$  (presumed to be abundant in the protoplanetary disk). In a second step, we present a plausible determination of the abundance profile of  $H_3^+$  in the protosolar nebula by using an accretion disk model whose thermodynamic conditions evolve with time, in contrast with the model employed in Mousis et al. (2008). This model allows us to compute the condensation sequence of major volatiles in the disk and to derive the implications for the  $H_3^+$  abundance that result from their decoupling from gas. In the present approach, we also consider that the ionization of the disk's midplane is dominated by extreme ultraviolet (EUV) and X-rays (Glassgold et al. 2000, 2012), a scenario more plausible than the one considering that the ionization of the disk is mainly ruled by cosmic rays (Mousis et al. 2008). Under these circumstances, we show that the abundance of  $H_3^+$  in the outer part of the nebula might be high enough to allow the sequestration of substantial amounts of Kr and Xe in the form of  $XeH_3^+$  and  $KrH_3^+$  complexes. This allows us to investigate the role that  $H_3^+$  might have played in the shaping of the composition of bodies of the outer solar system during their formation in the nebula.



**Table 1**Binding Energies (eV), Including Harmonic Zero Point Energy Corrections, for  $\text{XH}_3^+$ ,  $\text{XH}_2\text{O}$ , and  $\text{XH}_3\text{O}^+$  ( $\text{X} = \text{Ar}, \text{Kr}, \text{and Xe}$ )

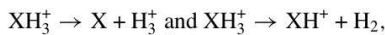
Reaction	Ar	Kr	Xe
$\text{XH}_3^+ \rightarrow \text{X} + \text{H}_3^+$	0.313	0.551	0.953
$\text{XH}_3^+ \rightarrow \text{XH}^+ + \text{H}_2$	0.739	0.413	0.153
$\text{XH}_2\text{O} \rightarrow \text{X} + \text{H}_2\text{O}$	0.016 <sup>a</sup>	0.013 <sup>b</sup>	0.024 <sup>c</sup>
$\text{XH}_3\text{O}^+ \rightarrow \text{X} + \text{H}_3\text{O}^+$	0.189	0.260	0.353
$\text{XH}_3\text{O}^+ \rightarrow \text{XH}^+ + \text{H}_2\text{O}$	3.408	2.916	2.346
$\text{XH}_5^+ \rightarrow \text{X} + \text{H}_5^+$	0.162	0.252	0.388
$\text{H}_5^+ \rightarrow \text{H}_2 + \text{H}_3^+$		0.235	

**Notes.**<sup>a</sup> Tao & Klemperer (1994).<sup>b</sup> Chalasinski et al. (1992).<sup>c</sup> Wang & Yang (2008).

## 2. COMPETITION FOR CHEMICAL TRAPPING OF NOBLE GASES

Appropriate *ab initio* quantum simulations have been employed to address this problem. The structural aspect and relative stabilities of the various complexes formed have been treated within the super-molecular approach, at different levels of theory; the convergence of the results were tested from density functional theory to coupled cluster single double and perturbative treatment of triple excitations. Large basis sets, referred to as cc-pVQZ (Woon & Dunning 1993; Peterson et al. 2003) have been used, providing a balanced description for all atoms and the remaining basis set superposition error has been corrected following the counterpoise method (Boys & Bernardi 1970). To simplify the presentation, only the numbers obtained at the MP2 level of theory have been given here. It is the first level of post Hartree–Fock theory in which the major part of the electronic correlation is taken into account via a Möller–Plesset perturbative treatment of the contribution of doubly excited configurations. A full account and comparison of the methods used, as well as the presentation of the computational details, are beyond the scope of this paper (for more information, see Pauzat & Ellinger 2007).

In a previous series of exhaustive calculations (Pauzat & Ellinger 2005, 2007; Pauzat et al. 2009), we showed that all complexes of the  $\text{XH}_3^+$  generic formula ( $\text{X} = \text{Ar}, \text{Kr}, \text{and Xe}$ ) pertinent to the present study were stable with respect to two possible dissociative channels (Table 1):



which gives a relevant clue for the trapping of the noble gas in the nebula before any possible incorporation into the forming planetesimals.

Very few experimental values are available for comparing theory to experiment. In fact, only for  $\text{ArH}_3^+$  have two different binding energies been obtained by Bogey et al. (1988) according to the shape of the potential energy surface used to analyze the spectroscopic data, namely  $\text{De} = 0.29$  or  $0.43$  eV. Using thermochemistry plots deduced from mass spectrometry experiments, Hiraoka & Mori (1989) obtained a value of  $0.29$  eV. Our theoretical value of  $\text{De} = 0.31$  eV is in remarkable agreement with those scarce experimental data, lending confidence to the energetic data reported in this work.<sup>3</sup> However, before proceeding any further, two points are still worth noting.

<sup>3</sup> The quality of the structural results may be seen in the rotational constants, i.e., 30.811 and 30.177 GHz for B and C (theory), compared with the experimental values of 30.8866 and 30.1464 GHz.

**Table 2**Enthalpies (eV), Including Harmonic Zero Point Energy Corrections, for Reactions Involving  $\text{XH}_3^+$  ( $\text{X} = \text{Ar}, \text{Kr}, \text{and Xe}$ )<sup>a</sup>

Reactions	Ar	Kr	Xe
$\text{X} + \text{H}_5^+ \rightarrow \text{XH}_3^+ + \text{H}_2$	−0.077	−0.315	−0.717
$\text{X} + \text{ArH}_3^+ \rightarrow \text{XH}_3^+ + \text{Ar}$		−0.238	−0.640
$\text{XH}_3^+ + \text{H}_2\text{O} \rightarrow \text{XH}_3\text{O}^+ + \text{H}_2$	−2.668	−2.503	−2.193
$\text{XH}_3^+ + \text{H}_2\text{O} \rightarrow \text{X} + \text{H}_3\text{O}^+ + \text{H}_2$	−2.480	−2.243	−1.840

**Note.** <sup>a</sup> A reaction is likely to occur if it has a positive exothermicity, i.e., a negative reaction enthalpy.

First, an extensive survey of the reaction path leading to the formation of the  $\text{XH}_3^+$  complexes, including a full geometry optimization and correcting for basis set superposition errors in each point along the reaction coordinate, was performed. The survey showed unambiguously that there is no activation barrier in this process regardless of the noble gas.

Second,  $\text{H}_3^+$  was found to be capable of trapping more than one noble gas (Pauzat et al. 2009), a point also supported experimentally in the case of Ar (Hiraoka & Mori 1989). The averaged binding energies, up to triple complexation, are 0.22, 0.29, and 0.44 eV for Ar, Kr, and Xe, respectively. Even if such a multiple process has a low probability of occurring, it could contribute only to more trapping by the same amount of  $\text{H}_3^+$ .

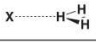
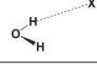
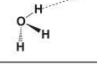
### 2.1. Comparison of the Strength of Complexation by $\text{H}_3^+$ and Other Volatiles

In the primitive nebula,  $\text{H}_3^+$  is not the only gas-phase species capable of complexing noble gases. In addition to  $\text{H}_2\text{O}$ , some other species that are also abundant in the nebular environment, such as He and  $\text{H}_2$ , could be at the origin of alternative chemical processes, that eventually interfere with the mechanism of noble gas trapping by destroying  $\text{H}_3^+$  itself.

1. Due to H/D fractionation, one may ask the question whether  $\text{H}_2\text{D}^+$ , also abundant in the gas phase, could modify the complexation energetics. Calculations of the zero point vibrational energies of  $\text{H}_2\text{D}^+$  and  $\text{XH}_2\text{D}^+$  show that the variation of the stability of the deuterated complexes with respect to the hydrogenated parents is only a few hundredths of an eV. It is much too small to alter the present trapping mechanism; in other words, the efficiency of the trapping is the same for deuterated and non-deuterated forms of the hydrogen ion.
2. Since He is the most abundant element after H, one might fear that He could interfere with the trapping of the heavier noble gases by saturating the  $\text{H}_3^+$  available in the disk. We have verified that He produces much weaker complexes: the  $\text{HeH}_3^+$  binding energy ( $\sim 0.01$  eV) is about two orders of magnitude below that of  $\text{XH}_3^+$  ( $\text{X} = \text{Ar}, \text{Kr}, \text{and Xe}$ ). With such low stability ( $\sim 50$  K), the He complex is very unlikely to form in protoplanetary environment conditions. In any case, He would never be in a position to preempt  $\text{H}_3^+$  before the heavier noble gases.
3. In the same way, if we take into account the large quantity of  $\text{H}_2$  available, one could also fear that  $\text{H}_2$  would react with  $\text{H}_3^+$  to produce the stable complex  $\text{H}_5^+$  (see line 8 in Table 1) and so doing saturate large amounts of  $\text{H}_3^+$ , which would no longer be free for the trapping of X. But, from the stabilities and enthalpies reported in Table 1 (lines 7 and 8) and Table 2 (line 1), it can be deduced that the  $\text{H}_5^+$  ion itself is able to form stable molecular complexes  $\text{XH}_5^+$  with all



**Table 3**  
XH Distances (Å) for Equilibrium Structures  
of  $\text{XH}_3^+$ ,  $\text{XH}_2\text{O}$ ,  $\text{XH}_3\text{O}^+$ , and  $\text{XH}^+$

X				$\text{XH}^+$
Ar	1.82	2.87	2.06	1.28
Kr	1.76	2.96	2.17	1.41
Xe	1.66	3.13	2.32	1.60

the noble gases. These complexes may either stay as they are or evolve into  $\text{XH}_3^+$  by returning  $\text{H}_2$  to the gas phase. In all events, the net result is that one  $\text{H}_3^+$  ion complexes one atom of noble gas, either directly or indirectly through  $\text{H}_3^+$ .

- Another matter of concern is the competition for  $\text{H}_3^+$  between the noble gas themselves. In particular, Ar is several orders of magnitudes more abundant than Kr and Xe and could be thought to preempt  $\text{H}_3^+$  and form  $\text{ArH}_3^+$  before any complexation with Kr and Xe. However, although  $\text{ArH}_3^+$  is a stable complex, the enthalpies reported in Table 2 (line 2) show that it will be destroyed in the presence of Kr and Xe to produce the more stable  $\text{KrH}_3^+$  and  $\text{XeH}_3^+$  complexes (there are no activation barriers to oppose these transformations).
- The last and most important possibility to check concerns the trapping of the noble gas by the  $\text{H}_2\text{O}$  present in the gas phase. Considering the binding energies reported in Table 1, we see that those of  $\text{XH}_2\text{O}$  (line 4) are more than one order of magnitude smaller than those of  $\text{XH}_3^+$  (lines 1 and 2). From a physical chemistry point of view, this energetic result, together with the much larger distance between X and the molecular fragment (Table 3), is the illustration of van der Waals versus ion–molecule interactions. This result rules out any possibility of direct trapping by  $\text{H}_2\text{O}$  in the gas phase.

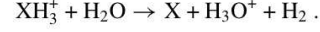
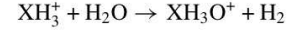
### 2.2. Possible Complexation by $\text{H}_3\text{O}^+$

The high proton affinity (PA) of  $\text{H}_2\text{O}$  compared with  $\text{H}_2$  ( $\sim 7.372$  compared with  $\sim 4.380$  eV) suggests that  $\text{H}_3^+$  and  $\text{H}_2\text{O}$  may not coexist in the gas phase. Indeed, we found that  $\text{H}_3^+ + \text{H}_2\text{O} \rightarrow \text{H}_3\text{O}^+ + \text{H}_2$  is a highly exothermic reaction (2.793 eV) with no activation barrier.

The unexpected outcome of the present study is that  $\text{H}_3\text{O}^+$ , as formed in the reaction above, may be also a noble gas trapping agent with the noble gas linked to an Hydrogen atom and binding energies in the range of 0.173–0.390 eV (Table 1, line 5). For such positively charged complexes, stabilized by ion–molecule interactions, the stability increases with the PA of the noble gas  $\text{PA}(\text{Ar}) = 3.929$  eV <  $\text{PA}(\text{Kr}) = 4.688$  eV <  $\text{PA}(\text{Xe}) = 5.412$  eV. A full account of the structures and energetics of these complexes, including multiple trapping possibilities (of no direct interest to the present discussion), will be presented in a more specialized quantum chemistry publication (O. Ozgurel et al. 2013, in preparation). The main point to be emphasized for our present purpose is that these complexes, which are formed in the gas phase, are energetically stable and should contribute, in the same way as the  $\text{XH}_3^+$  complexes, to the early trapping of the noble gases in the gas phase, keeping them away from the planetesimals.

The final question is the stability of the  $\text{XH}_3^+$  complex itself in the presence of  $\text{H}_2\text{O}$ . Our calculations (Table 2, lines 2 and 3)

of the energetics of the reactions are as follows:



These calculations show that the  $\text{XH}_3^+$  complexes should be destroyed with  $\text{H}_2$  released in the gas phase. The large exothermicity of the reaction should even lead to the release of the noble gas, allowing its recycling in any of the preceding processes.

From this theoretical survey of the chemical processes able to complex the noble gases in the gas phase, it can be stressed that  $\text{H}_3^+$  is the major agent for trapping Ar, Kr, and Xe; the role of He is completely negligible. The role of Ar, although it is also more abundant than Kr and Xe, appears secondary since most of  $\text{H}_3^+$  is taken primarily by the formation of  $\text{KrH}_3^+$  and  $\text{XeH}_3^+$ . The determination of a reliable abundance profile of  $\text{H}_3^+$  in the protosolar nebula, together with its evolution as a function of time and temperature, is therefore of utmost importance.

### 3. ABUNDANCE PROFILE OF $\text{H}_3^+$ IN THE PROTOSOLAR NEBULA

In the solar nebula,  $\text{H}_3^+$  is formed by the ionization of  $\text{H}_2$  essentially from EUV and X-rays, at a rate  $\zeta_{\text{Xr}}$  ranging between  $\sim 10^{-15}$  and  $10^{-11}$  s $^{-1}$  over a wide range of disk densities (Glassgold et al. 2000). A full penetration of the solar nebula's midplane by X-rays has been found to occur at  $\sim 5$  AU (Igea & Glassgold 1999). The X-ray ionization rate is typically equal to or larger than the rate induced by Galactic cosmic rays ( $\zeta_{\text{cr}} \sim 10^{-16}$ – $10^{-15}$  s $^{-1}$ ; Indriolo & McCall 2012) but these cosmic rays do not penetrate the inner disk due to wind modulation (Glassgold et al. 2000). In the meantime,  $\text{H}_3^+$  is destroyed by the reactions with the most abundant molecules in the gas phase, namely  $\text{H}_2\text{O}$ , CO, and  $\text{N}_2$  (see Mousis et al. 2010), at rates  $\kappa_{\text{dH}_2\text{O}}$ ,  $\kappa_{\text{dCO}}$ , and  $\kappa_{\text{dN}_2}$ , respectively. In the steady state, the formation and destruction rates balance each other, providing a relationship between the  $\text{H}_3^+$  abundance  $x_{\text{H}_3^+}$ , the  $\text{H}_2\text{O}$ , CO, and  $\text{N}_2$  abundances ( $x_{\text{H}_2\text{O}}$ ,  $x_{\text{CO}}$ , and  $x_{\text{N}_2}$ ) with respect to  $\text{H}_2$ , the  $\text{H}_2$  density  $n_{\text{H}_2}$ , and the  $\text{H}_2$  ionization rate  $\zeta_{\text{Xr}}$  (Ceccarelli & Dominik 2005; Mousis et al. 2008):

$$x_{\text{H}_3^+} = \frac{\zeta_{\text{Xr}}}{n_{\text{H}_2}(\kappa_{\text{dH}_2\text{O}}x_{\text{H}_2\text{O}} + \kappa_{\text{dCO}}x_{\text{CO}} + \kappa_{\text{dN}_2}x_{\text{N}_2})}. \quad (1)$$

Equation (1) shows that the  $\text{H}_3^+$  abundance is inversely proportional to the  $\text{H}_2$  density and linearly depends on the ionization rate  $\zeta_{\text{Xr}}$ . This relation is valid as long as  $\text{H}_2\text{O}$ , CO, and  $\text{N}_2$  remain in the gas phase (which means a local temperature of the disk higher than  $\sim 150$  K) and are not condensed or eventually trapped in clathrates in the nebula. Because the solar nebula cools down with time, the  $\text{H}_3^+$  abundance is expected to increase at a given distance when the disk's temperature decreases to values lower than those required for the condensation/trapping of  $\text{H}_2\text{O}$ , CO, and  $\text{N}_2$ . Once all of these volatiles are removed from the gas phase, the maximum  $\text{H}_3^+$  abundance should converge toward the abundance of the electrons, which, according to Fromang et al. (2002), is given by

$$x_e = \sqrt{\frac{\zeta_{\text{Xr}}}{\beta n_{\text{H}_2}}}, \quad (2)$$

where  $\beta$  is the dissociative recombination rate coefficient for molecular ions. Note that this relation is valid as long as the



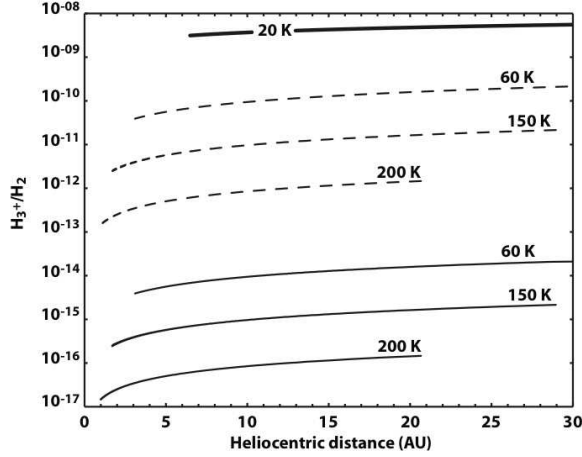


**Figure 1.**  $\text{H}_3^+$  abundance profiles in the solar nebula calculated at disk temperatures of 200, 150, and 60 K. The solid and dashed lines correspond to X-ray ionization rates of  $10^{-15} \text{ s}^{-1}$  and  $10^{-11} \text{ s}^{-1}$ , respectively (see the text). The  $\text{H}_3^+$  abundance profile calculated at 20 K corresponds to an upper limit, which is derived from the abundance of electrons.

metal atom population is negligibly small, which is a reasonable assumption at the temperatures of interest (Fromang et al. 2002).

In order to compute the time evolution of the  $\text{H}_3^+$  abundance profile in the protosolar nebula, we use a time-dependent turbulent accretion disk model based on the prescription of Shakura & Sunyaev (1973), who characterized the turbulent viscosity  $\nu_t$  as

$$\nu_t = \alpha \frac{C_s^2}{\Omega}, \quad (3)$$

where  $C_s$  is the local sound velocity,  $\Omega$  is the Keplerian rotation frequency, and  $\alpha$  is a dimensionless viscosity parameter. The physical origin of turbulence in accretion disks is still not well established, though this model is useful because it allows us to describe the qualitative influence of whichever process is responsible for the transport of angular momentum through the disk. Our model also incorporates the opacity law developed by Ruden & Pollack (1991; see, e.g., Drouart et al. 1999 for details). The temporal evolution of the disk temperature, pressure, and surface density profiles depends on the evolution of the accretion rate,  $\dot{M}$ , which we define (following Makalkin & Dorofeeva 1991) to be

$$\dot{M} = \dot{M}_0 \left(1 + \frac{t}{t_0}\right)^{-s}. \quad (4)$$

$\dot{M}$  decreases with time following a power law that is determined by the initial accretion rate  $\dot{M}_0$  and the accretion timescale  $t_0$ . In this work, we adopt  $s = 1.5$ , a value that allows our law to be consistent with that derived from the evolution of accretion rates in circumstellar disks (Hartmann et al. 1998). The accretion timescale  $t_0$  is calculated by Makalkin & Dorofeeva (1991) to be

$$t_0 = \frac{R_D^2}{3\nu_D}, \quad (5)$$

where  $\nu_D$  is the turbulent viscosity at the initial radius of the disk,  $R_D$ . Three parameters constrain  $\dot{M}_0$  and  $t_0$ : the initial mass and radius of the disk  $M_{D0}$  and  $R_{D0}$  and the coefficient of turbulent viscosity  $\alpha$ . In the present case, we utilize  $\alpha = 0.003$ ,  $R_{D0} = 30 \text{ AU}$ , and  $M_{D0} = 0.1 M_\odot$  for the parameters of the disk.

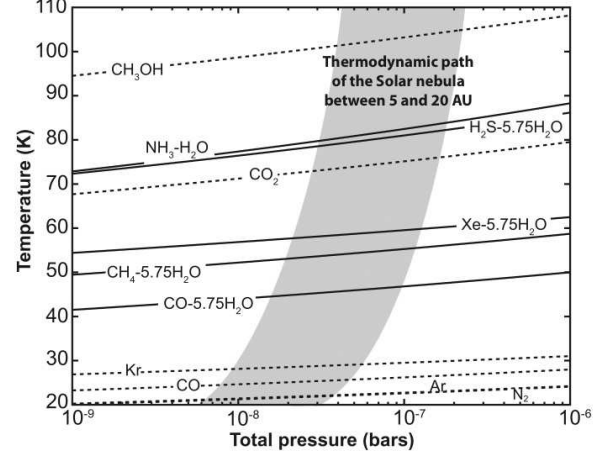


**Figure 2.** Equilibrium curves of  $\text{NH}_3\text{-H}_2\text{O}$  hydrate,  $\text{H}_2\text{S}$ , Xe,  $\text{CH}_4$ , and CO clathrates (solid lines),  $\text{CH}_3\text{OH}$ ,  $\text{CO}_2$ , Kr, CO, Ar, and  $\text{N}_2$  pure condensates (dotted lines), and the thermodynamic path followed by the solar nebula between 5 and 20 AU as a function of time, assuming a full efficiency of clathration. The abundances of various elements are solar, with  $\text{CO}:\text{CO}_2:\text{CH}_3\text{OH}:\text{CH}_4 = 70:10:2:1$  and  $\text{N}_2:\text{NH}_3 = 10:1$  in the gas phase of the disk (Mousis et al. 2010). Species remain in the gas phase above the stability curves. Below, they are trapped as clathrates or simply condense.

Figure 1 shows the  $\text{H}_3^+$  abundance profiles in the solar nebula calculated at disk temperatures of 200, 150, and 60 K for two plausible values of the X-ray ionization rate ( $\zeta_{\text{Xr}} = 10^{-15}$  and  $10^{-11} \text{ s}^{-1}$ ).

At 200 K,  $\text{H}_2\text{O}$ , CO, and  $\text{N}_2$  are all in gaseous forms in the disk with abundances of  $\sim 5.15 \times 10^{-4}$ ,  $4.91 \times 10^{-4}$ , and  $7.62 \times 10^{-5}$  relative to  $\text{H}_2$ , respectively (Mousis et al. 2010). The corresponding reaction rates for the destruction of  $\text{H}_3^+$  by these molecules ( $k_{\text{dH}_2\text{O}}$ ,  $k_{\text{dCO}}$ , and  $k_{\text{dN}_2}$ ) are  $5.9 \times 10^{-9}$ ,  $1.7 \times 10^{-9}$ , and  $1.8 \times 10^{-9} \text{ cm}^3 \text{ s}^{-1}$ , respectively (from the UMIST database for astrochemistry<sup>4</sup>). The  $\text{H}_3^+$  abundance profile calculated at 200 K must be considered to be a lower limit since our model does not take into account the fact that  $\text{H}_2\text{O}$  and  $\text{H}_3^+$  form  $\text{H}_3\text{O}^+$  when they meet, which is also an efficient trapping agent of noble gases (see Section 2.2). If one considers this effect, the  $\text{H}_3^+$  abundance profile should be very close to the one calculated at 150 K (see below).

At  $\sim 150 \text{ K}$ ,  $\text{H}_2\text{O}$  is condensed so its gas-phase abundance is set to zero. This induces an increase of the  $\text{H}_3^+$  abundance in the nebula since the ion is not destroyed anymore by encounters with  $\text{H}_2\text{O}$  molecules. Figure 2 shows that Xe is trapped in clathrates at about  $\sim 60 \text{ K}$ , so we have also computed the  $\text{H}_3^+$  abundance profile in the disk close to this temperature, which allows us to investigate the possibility of the substantial sequestration of this noble gas by  $\text{H}_3^+$  in the gas phase prior to trapping in clathrates.

Because CO and  $\text{N}_2$  both condense at  $\sim 20 \text{ K}$  in the protosolar nebula, the  $\text{H}_3^+$  abundance profile depicted by Equation (1) diverges. Hence, at this temperature, we assume that it follows the abundance profile of electrons given by Equation (2) and this profile can be compared with the nebular abundance of Kr, whose condensation is in the same temperature range as that of CO and  $\text{N}_2$ .

Figure 1 shows that, assuming an X-ray ionization rate of  $10^{-15} \text{ s}^{-1}$  in the nebula midplane, the  $\text{H}_3^+$  abundance relative to  $\text{H}_2$  ranges between  $10^{-17}$  and  $10^{-14}$  for disk temperatures

<sup>4</sup> <http://www.udfa.net/>



in the 60–200 K domain. This  $H_3^+$  abundance is at least four orders of magnitude lower than that of the most rare noble gas Xe, whose abundance is estimated to be  $\sim 10^{-10}$  relative to  $H_2$  in the nebula (Asplund et al. 2009). In this case, the noble gas sequestration by  $H_3^+$  ion is found negligible. However, the situation becomes different if a X-ray ionization rate of  $10^{-11} \text{ s}^{-1}$  is considered throughout the nebula. In this case, we note that the  $H_3^+$  abundance converges toward  $10^{-10}$  relative to  $H_2$ , a value close to the Xe abundance (Asplund et al. 2009).

The calculated  $H_3^+$  abundance at the time of Xe disappearance from the gas phase is a minimum because the efficiency of clathration is unknown in the nebula (Mousis et al. 2009c). If the clathration efficiency was indeed zero, Xe would have condensed at  $\sim 20$  K and then the  $H_3^+$  abundance would be substantially higher at this temperature. We also find that, when the disk temperature decreases to  $\sim 30$  K, i.e., slightly above the condensation temperature of Kr (see Figure 2), the  $H_3^+$  abundance also exceeds the gas-phase abundance of this noble gas in the nebula, which is  $\sim 10^{-9}$  (Asplund et al. 2009), as a result of the progressive drop of  $n_{H_2}$  due to the cooling of the disk.

Our calculations then suggest that Kr and Xe might have been efficiently trapped by  $H_3^+$  in the gas phase of the outer nebula. However, due to its higher abundance in the solar nebula gas phase (about 1000 times higher than that of Kr (Asplund et al. 2009), the trapping of Ar via this mechanism would probably be more restricted.

#### 4. IMPLICATIONS FOR THE COMPOSITION OF THE OUTER SOLAR SYSTEM

The stability of  $X_nH_3^+$  complexes in the gas phase may have important implications for the composition of bodies formed in the outer part of the protosolar nebula. Indeed, most volatile species are supposed to be trapped in the form of clathrates during the cooling of the protosolar nebula (Mousis et al. 2010); the extent of this trapping depends on the amount of  $H_2O$  available for clathration in the disk and on the fraction of the clathrate cages that are effectively filled. Once the  $H_2O$  budget has been used for clathration, the remaining volatiles form pure condensates at lower temperatures. Figure 2 shows the clathration and condensation sequences of volatiles that take place during the cooling of the protosolar nebula, assuming (1) the absence of  $H_3^+$  in the disk and (2) the formation of single guest clathrates only. In these circumstances, Xe is enclathrated in the disk at  $\sim 60$  K while Kr and Ar form pure condensates in the 20–30 K range.

Alternatively, if one assumes that substantial amounts of heavy noble gases have been sequestered by  $H_3^+$  in the form of  $X_nH_3^+$  complexes in the gas phase of the nebula prior to their subsequent clathration/condensation and agglomeration into icy planetesimals, then these solids should be particularly impoverished in Ar, Kr, and Xe, while they trapped most of the other volatiles. As discussed in Section 3, the extent of the noble gas depletion in planetesimals depends on the adopted  $H_3^+$  abundance profile in the gas phase of the disk. In any case, because the  $H_3^+$  abundance grows with increasing heliocentric distance, the formation efficiency of  $X_nH_3^+$  complexes should be higher in the outer part of the protosolar nebula.

##### 4.1. $H_3^+$ as the Cause of the Noble Gas Deficiency in Titan

The only noble gas measured in Titan's atmosphere by the mass spectrometer aboard the Huygens probe is Ar. The

gas includes primordial  $^{36}\text{Ar}$  measured in subsolar abundance ( $^{36}\text{Ar}/^{14}\text{N}$  is about six orders of magnitude lower than the solar value) and the radiogenic isotope  $^{40}\text{Ar}$ , which is a decay product of  $^{40}\text{K}$  (Niemann et al. 2005). The other primordial noble gases  $^{38}\text{Ar}$ , Kr, and Xe were not detected.

A possible interpretation of the quasi absence of noble gases on Titan is that it results from their efficient sequestration by  $H_3^+$  in the solar nebula gas phase at epochs prior to the formation of the satellite's building blocks. With respective abundances orders of  $10^{-9}$  (Kr) and  $10^{-10}$  (Xe) (Asplund et al. 2009), and considering the increase of the  $H_3^+$  abundance in the outer parts of the nebula (see Section 3), one can expect that important quantities of these noble gases were sequestered as  $X_nH_3^+$  complexes in the outer nebula. Hence, assuming that Titan accreted from planetesimals formed at these locations, the  $H_3^+$  sequestration mechanism could explain the Kr and Xe depletions inferred in the satellite's atmosphere. The case of Ar is less straightforward since this noble gas is three orders of magnitude more abundant than Kr in the nebula. It is likely that the  $H_3^+$  abundance cannot be high enough in the outer nebula to explain a high Ar impoverishment in planetesimals. As a consequence, one needs to invoke alternative mechanisms such as the partial devolatilization of Titan's building blocks when they entered Saturn's sub-nebula prior to the satellite's formation in order to account for the Ar atmospheric depletion (Mousis et al. 2009a). Interestingly, in this scenario, regular satellites such as Enceladus should share the same properties as Titan concerning Kr and Xe depletions since these bodies are expected to have accreted from similar planetesimals (Mousis et al. 2009a, 2009b).

##### 4.2. Implications for the Noble Gas Content in Giant Planets

In situ measurements by the *Galileo* probe have shown that the abundances of C, N, S, Ar, Kr, and Xe are all enriched by similar factors with respect to their solar abundances in Jupiter (Wong et al. 2004). Moreover, recent Cassini Composite Infrared Spectrometer observations confirm that C is substantially enriched in the atmosphere of Saturn (Fletcher et al. 2009). In order to interpret these measurements, it has been proposed that the main volatile compounds initially existing in the solar nebula gas phase were essentially trapped by crystalline  $H_2O$  ice in the form of clathrates or hydrates in the feeding zones of Jupiter and Saturn (Gautier et al. 2001; Alibert et al. 2005a, 2005b; Mousis et al. 2006, 2009c). These ices then agglomerated and formed planetesimals that were ultimately accreted by the forming giant planets. A fraction of these planetesimals vaporized when entering the envelopes of the growing planets and engendered the observed volatile enrichments. Figure 3 shows the observed enrichments in Jupiter plotted against those calculated by Mousis et al. (2012).

The calculated Kr and Xe enrichments are higher than the observed ones, but the presence of  $H_3^+$  ions in the primitive nebula may limit their ability to be enclathrated or condense in the outer nebula. Therefore, if the  $H_3^+$  abundance were comparable with that of Kr and Xe in Jupiter's feeding zone ( $H_3^+/H_2 \sim 10^{-9}$ – $10^{-10}$ ), which is a reasonable assumption (see Section 3), the resulting enrichments of these two noble gases in the Jovian envelope would be lower than the calculated values presented in Figure 3 and would match the observed values. In this scenario, because Saturn's planetesimals were probably formed at the same location as Titan's building blocks in the protosolar nebula (i.e., at a larger heliocentric distance than Jupiter), they should be strongly impoverished in Kr and Xe. In these



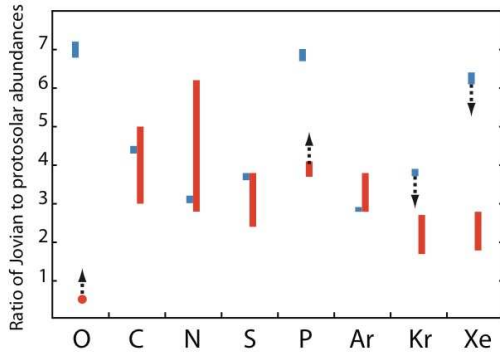


**Figure 3.** Ratio of Jovian to protosolar abundances. Red bars and the red dot correspond to *Galileo* observations (Wong et al. 2004). Blue bars correspond to calculations based on an oxygen abundance that is the protosolar value in the disk and the oxygen abundance is predicted to be 6.8–7.2 times protosolar in Jupiter (Mousis et al. 2012). Arrows pointing up correspond to the possibility that the measured oxygen and phosphorus abundances are lower than their bulk abundances and arrows pointing down correspond to the possibility that planetesimals could be impoverished in Kr and Xe due to the formation of  $X_nH_3^+$  complexes in the protosolar nebula prior to the formation of icy planetesimals (see the text).

conditions, the abundances of these two noble gases should remain solar in Saturn’s atmosphere.

#### 4.3. Predictions for Comets

The deuterium-to-hydrogen enrichment observed for  $H_2O$  in Saturn’s satellite Enceladus is remarkably similar to the values observed in Oort Cloud comets (OCCs; Waite et al. 2009). Given the predicted strong variation of D/H with heliocentric distance in the solar nebula (Mousis et al. 2000; Mousis 2004; Horner et al. 2008; Kavelaars et al. 2011), this observation links the primordial source region of these comets with the formation location of Enceladus. Because both Enceladus and Titan are expected to have formed from planetesimals sharing similar compositions (Mousis et al. 2009b), one can predict that OCCs also present important impoverishments in Kr and Xe. Short-period comets, including Jupiter family comets such as the *Rosetta* target Comet 67P/Churyumov–Gerasimenko, are expected to have formed at different locations. Dynamical and chemical models of the nebula predict the formation locations of these comets at larger heliocentric distances than OCCs (Kavelaars et al. 2011). On the other hand, recent measurement of the deuterium-to-hydrogen ratio for  $H_2O$  in the Jupiter-family comet 103P/Hartley 2, which has been found to be equal to the standard mean ocean water (SMOW) value, i.e., a value twice as low as the one systematically inferred in OCCs (Hartogh et al. 2011), suggests that this family of comets may have formed at smaller heliocentric distances. The strong variation of  $H_3^+$  abundance with heliocentric distance in the solar nebula could help to disentangle the different formation locations of these populations of comets. Comets that formed closer to the Sun than OCCs should show higher Kr and Xe abundances. In contrast, comets formed at larger heliocentric distances than OCCs should present at least similar Kr and Xe impoverishments.

## 5. CONCLUSIONS

Following previous calculations that demonstrated that the formation of complexes of the  $XH_3^+$  generic formula ( $X = Ar, Kr, \text{ and } Xe$ ) could lead to an efficient trapping of rare gases by  $H_3^+$

in the outer solar nebula, new quantum chemistry calculations show an unexpected and never-before-considered point:  $H_2O$  in the presence of  $H_3^+$  gives  $H_3O^+$ , a positive ion that is also eligible for noble gases sequestration. In addition, we have demonstrated that He, irrespective of its abundance, has no impact on the sequestration of the noble gases. These calculations show also that Ar, over a thousand times more abundant than Kr and Xe, is not able in fine to prevent the effective trapping of the latter gases. Deuteration plays no role in the process in the sense that there is no energetic difference between complexation by  $H_3^+$  or by  $H_2D^+$ . Sequestration of noble gases by neutral  $H_2O$  in the gas phase, giving very weak complexes, should be inefficient.

Coupling these results with computations showing that  $H_3^+$  might be abundant enough in the outer protosolar nebula to trap Xe and Kr prior their incorporation into planetesimals leads to a scenario in which the abundances of these two noble gases should be solar in Saturn’s current atmosphere. Our calculations are consistent with the fact that the Kr and Xe abundances measured at Jupiter are lower than those predicted from models based only on the condensation of volatiles in the protosolar nebula. The proposed  $H_3^+$  sequestration mechanism also naturally explains why Titan is impoverished in Kr and Xe. In addition, when applied to comets, this scenario predicts that those comets formed at large heliocentric distances should be depleted in Kr and Xe. In situ measurements, such as those planned with the mass spectrometer ROSINA flying aboard the *Rosetta* mission toward 67P/Churyumov–Gerasimenko, will be critical for verifying our hypotheses.

Support from the Programme National de Planétologie is acknowledged. O.M. acknowledges support from CNES. Part of the calculations were performed using HPC resources from GENCI-CINES (grant 2012-085128).

## REFERENCES

- Alibert, Y., Mousis, O., & Benz, W. 2005a, *ApJL*, 622, L145
- Alibert, Y., Mousis, O., Mordasini, C., & Benz, W. 2005b, *ApJL*, 626, L57
- Asplund, M., Grevesse, N., Sauval, A. J., & Scott, P. 2009, *ARA&A*, 47, 481
- Bogey, M., Bolvin, H., Demuynck, C., Destombes, J. L., & van Eijck, B. P. 1988, *JChPh*, 88, 4120
- Boys, S. F., & Bernardi, F. 1970, *MolPh*, 19, 553
- Ceccarelli, C., & Dominik, C. 2005, *A&A*, 440, 583
- Ceccarelli, C., Dominik, C., Lefloch, B., Caselli, P., & Caux, E. 2004, *ApJL*, 607, L51
- Chalasinski, G., Szczesniak, M. M., & Scheiner, S. 1992, *JChPh*, 97, 8181
- Drouart, A., Dubrulle, B., Gautier, D., & Robert, F. 1999, *Icar*, 140, 129
- Fletcher, L. N., Orton, G. S., Teanby, N. A., & Irwin, P. G. J. 2009, *Icar*, 202, 543
- Fromang, S., Terquem, C., & Balbus, S. A. 2002, *MNRAS*, 329, 18
- Gautier, D., Hersant, F., Mousis, O., & Lunine, J. I. 2001, *ApJL*, 550, L227
- Geballe, T. R., & Oka, T. 1996, *Natur*, 384, 334
- Glassgold, A. E., Feigelson, E. D., & Montmerle, T. 2000, in *Protostars and Planets IV*, ed. V. Mannings, A. P. Boss, & S. S. Russell (Tucson, AZ: Univ. Arizona Press), 429
- Glassgold, A. E., Galli, D., & Padovani, M. 2012, *ApJ*, 756, 157
- Hartmann, L., Calvet, N., Gullbring, E., & D’Alessio, P. 1998, *ApJ*, 495, 385
- Hartogh, P., Lis, D. C., Bockelée-Morvan, D., et al. 2011, *Natur*, 478, 218
- Hiraoka, K. 1987, *JChPh*, 87, 4048
- Hiraoka, K., & Mori, T. 1989, *JChPh*, 91, 4821
- Horner, J., Mousis, O., Alibert, Y., Lunine, J. I., & Blanc, M. 2008, *P&SS*, 56, 1585
- Igea, J., & Glassgold, A. E. 1999, *ApJ*, 518, 848
- Indriolo, N., & McCall, B. J. 2012, *ApJ*, 745, 91
- Iro, N., Gautier, D., Hersant, F., Bockelée-Morvan, D., & Lunine, J. I. 2003, *Icar*, 161, 511
- Kavelaars, J. J., Mousis, O., Petit, J.-M., & Weaver, H. A. 2011, *ApJL*, 734, L30

- Maillard, J.-P., Drossart, P., Watson, J. K. G., Kim, S. J., & Caldwell, J. 1990, *ApJL*, **363**, L37
- Makalkin, A. B., & Dorofeeva, V. A. 1991, *Prir*, **9**, 79
- McCall, B. J., Hinkle, K. H., Geballe, T. R., et al. 2002, *ApJ*, **567**, 391
- Miller, S., Achilleos, N., Ballester, G. E., et al. 2000, *RSPTA*, **358**, 2485
- Mousis, O. 2004, *A&A*, **414**, 1165
- Mousis, O., Alibert, Y., & Benz, W. 2006, *A&A*, **449**, 411
- Mousis, O., Gautier, D., Bockelée-Morvan, D., et al. 2000, *Icar*, **148**, 513
- Mousis, O., Lunine, J. I., Madhusudhan, N., & Johnson, T. V. 2012, *ApJL*, **751**, L7
- Mousis, O., Lunine, J. I., Picaud, S., & Cordier, D. 2010, *FaDi*, **147**, 509
- Mousis, O., Lunine, J. I., Thomas, C., et al. 2009a, *ApJ*, **691**, 1780
- Mousis, O., Lunine, J. I., Waite, J. H., et al. 2009b, *ApJL*, **701**, L39
- Mousis, O., Marboeuf, U., Lunine, J. I., et al. 2009c, *ApJ*, **696**, 1348
- Mousis, O., Pauzat, F., Ellinger, Y., & Ceccarelli, C. 2008, *ApJ*, **673**, 637
- Niemann, H. B., Atreya, S. K., Bauer, S. J., et al. 2005, *Natur*, **438**, 779
- Pauzat, F., & Ellinger, Y. 2005, *P&SS*, **53**, 1389
- Pauzat, F., & Ellinger, Y. 2007, *JChPh*, **127**, 014308
- Pauzat, F., Ellinger, Y., & Mousis, O. 2006, in 37th Annual Lunar and Planetary Science Conference, **37**, 1331
- Pauzat, F., Ellinger, Y., Pilmé, J., & Mousis, O. 2009, *JChPh*, **130**, 174313
- Peterson, K. A., Figgen, D., Goll, E., Stoll, H., & Dolg, M. 2003, *JChPh*, **119**, 11113
- Ruden, S. P., & Pollack, J. B. 1991, *ApJ*, **375**, 740
- Shakura, N. I., & Sunyaev, R. A. 1973, *A&A*, **24**, 337
- Tao, F.-M., & Klemperer, W. 1994, *JChPh*, **101**, 1129
- Waite, J. H., Jr., Lewis, W. S., Magee, B. A., et al. 2009, *Natur*, **460**, 487
- Wang, L., & Yang, M. 2008, *JChPh*, **129**, 174305
- Weaver, H. A., Feldman, P. D., Combi, M. R., et al. 2002, *ApJL*, **576**, L95
- Wong, M. H., Mahaffy, P. R., Atreya, S. K., Niemann, H. B., & Owen, T. C. 2004, *Icar*, **171**, 153
- Woon, D. E., & Dunning, T. H., Jr. 1993, *JChPh*, **98**, 1358

## VI References

- Abrams, M. L., Valeev, E. F., Sherrill, C. D., & Crawford, T. D. (2002). The equilibrium geometry, harmonic vibrational frequencies, and estimated ab initio limit for the barrier to planarity of the ethylene radical cation. *The Journal of Physical Chemistry A*, 106(11), 2671-2675.
- Alecian, G., Richard, O., Vauclair, S., Grevesse, N., Asplund, M., & Sauval, A. J. (2005). The new solar chemical composition. *European Astronomical Society Publications Series*, 17, 21-30.
- Alibert, Y., Mousis, O., & Benz, W. (2005). On the volatile enrichments and composition of Jupiter. *The Astrophysical Journal Letters*, 622(2), L145-L148.
- Balsiger, H., Altwegg, K., Bar-Nun, A., Berthelier, J. J., Bieler, A., Bochsler, P., ... & Eberhardt, P. (2015). Detection of argon in the coma of comet 67P/Churyumov-Gerasimenko. *Science Advances*, 1(8), e1500377.
- Cordier, D., Mousis, O., Lunine, J. I., Lebonnois, S., Lavvas, P., Lobo, L. Q., & Ferreira, A. G. M. (2010). About the possible role of hydrocarbon lakes in the origin of Titan's noble gas atmospheric depletion. *The Astrophysical Journal Letters*, 721(2), L117-L120.
- Holzmeier, F., Lang, M., Hader, K., Hemberger, P., & Fischer, I. (2013). H<sub>2</sub>CN<sup>+</sup> and H<sub>2</sub>CNH<sup>+</sup>: New insight into the structure and dynamics from mass-selected threshold photoelectron spectra. *The Journal of Chemical Physics*, 138(21), 214310.
- Jacovi, R., & Bar-Nun, A. (2008). Removal of Titan's noble gases by their trapping in its haze. *Icarus*, 196(1), 302-304.
- Krasnopolsky, V. A. (2009). A photochemical model of Titan's atmosphere and ionosphere. *Icarus*, 201(1), 226-256.
- Lignell, A., Khriachtchev, L., Lundell, J., Tanskanen, H., & Räsänen, M. (2006). On theoretical predictions of noble-gas hydrides. *The Journal of Chemical Physics*, 125(18), 184514.

Lodders, K., Palme, H., & Gail, H. P. (2009). *Abundances of the elements in the Solar System*. (pp. 712-770). Berlin Heidelberg: Springer.

Lundell, J., Cohen, A., & Gerber, R. B. (2002). Quantum chemical calculations on novel molecules from xenon insertion into hydrocarbons. *The Journal of Physical Chemistry A*, 106(49), 11950-11955.

Mandt, K. E., Gell, D. A., Perry, M., Hunter Waite, J., Crary, F. A., Young, D., ... & Miller, G. (2012). Ion densities and composition of Titan's upper atmosphere derived from the Cassini Ion Neutral Mass Spectrometer: Analysis methods and comparison of measured ion densities to photochemical model simulations. *Journal of Geophysical Research: Planets*, 117(E10), E10006.

Mousis, O., Gautier, D., & Bockelée-Morvan, D. (2002). An evolutionary turbulent model of Saturn's subnebula: implications for the origin of the atmosphere of Titan. *Icarus*, 156(1), 162-175.

Mousis, O., Pauzat, F., Ellinger, Y., & Ceccarelli, C. (2008). Sequestration of noble gases by  $H^+ 3$  in protoplanetary disks and outer solar system composition. *The Astrophysical Journal*, 673(1), 637-646.

Mousis, O., Lunine, J. I., Picaud, S., Cordier, D., Waite Jr, J. H., & Mandt, K. E. (2011). Removal of Titan's atmospheric noble gases by their sequestration in surface clathrates. *The Astrophysical Journal Letters*, 740(1), L9.

Niemann, H. B., Atreya, S. K., Bauer, S. J., Carignan, G. R., Demick, J. E., Frost, R. L., ... & Israel, G. (2005). The abundances of constituents of Titan's atmosphere from the GCMS instrument on the Huygens probe. *Nature*, 438, 779-784.

Osegovic, J. P., & Max, M. D. (2005). Compound clathrate hydrate on Titan's surface. *Journal of Geophysical Research: Planets*, 110(E8); E08004.

Pauzat, F., & Ellinger, Y. (2007).  $H_3^+$  as a trap for noble gases-2: structure and energetics of  $XH_3^+$  complexes from X= neon to xenon. *The Journal of Chemical Physics*, 127(1), 014308.

Pauzat, F., Ellinger, Y., Pilmé, J., & Mousis, O. (2009). H<sub>3</sub><sup>+</sup> as a trap for noble gases-3: Multiple trapping of neon, argon, and krypton in XnH<sub>3</sub><sup>+</sup>(n= 1–3). *The Journal of Chemical Physics*, 130(17), 174313.

Pauzat, F., Ellinger, Y., Mousis, O., Dib, M. A., & Ozgurel, O. (2013). Gas-phase sequestration of noble gases in the protosolar nebula: possible consequences on the outer solar system composition. *The Astrophysical Journal*, 777(1), 29.

Sloan Jr, E. D., & Koh, C. (2007). *Clathrate hydrates of natural gases*. CRC press.

Thomas, C., Picaud, S., Mousis, O., & Ballenegger, V. (2008). A theoretical investigation into the trapping of noble gases by clathrates on Titan. *Planetary and Space Science*, 56(12), 1607-1617.

Waite, J. H., Combi, M. R., Ip, W. H., Cravens, T. E., McNutt, R. L., Kasprzak, W., ... & Magee, B. (2006). Cassini ion and neutral mass spectrometer: Enceladus plume composition and structure. *Science*, 311(5766), 1419-1422.

Yelle, R. V. (1991). Non-LTE models of Titan's upper atmosphere. *The Astrophysical Journal*, 383, 380-400.

Yung, Y. L., Allen, M., & Pinto, J. P. (1984). Photochemistry of the atmosphere of Titan-Comparison between model and observations. *The Astrophysical Journal Supplement Series*, 55, 465-506.

## Chapter 2: Origin of molecular oxygen and sulfur in Comet 67P/Churyumov-Gerasimenko

Comets are one of the most primitive objects in the solar system. So their study may reveal the earlier composition and characteristics of the solar system, i.e. the proto solar nebula. With the groundbreaking Rosetta project, we have improved our knowledge about those particular objects. In this project, to investigate the gas and dust ejected from the nucleus of 67P/C-G (67P/Churyumov–Gerasimenko) as it approaches to the Sun, as well as the composition of the nucleus, the Rosetta spacecraft carried eleven different instruments on the comet orbiter and the associated lander Philae carried ten additional instruments performing surface measurements. The instruments in the Rosetta orbiter which addressed various spectroscopic measurements were: Alice (Ultraviolet Imaging Spectrometer), CONSERT (Comet Nucleus Sounding Experiment by Radio wave Transmission), COSIMA (Cometary Secondary Ion Mass Analyzer), GIADA (Grain Impact Analyser and Dust Accumulator), MISDAS (Micro-Imaging Dust Analysis System), MICRO Microwave Instrument for the Rosetta Orbiter, (OSIRIS) Optical, Spectroscopic, and Infrared Remote Imaging System), ROSINA (Rosetta Orbiter Spectrometer for Ion and Neutral Analysis), RPC (Rosetta Plasma Consortium), RSI (Radio Science Investigation) and finally VIRTIS (Visible and Infrared Thermal Imaging). (Figure 1)

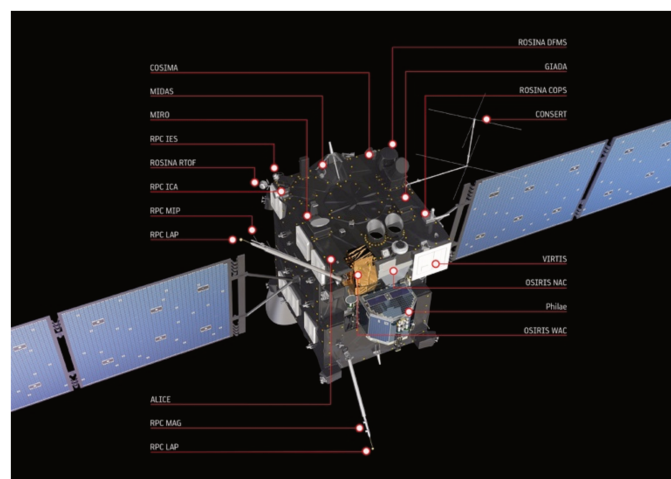


Figure 1: Rosetta's Instruments (Black Background). Credit :ESA/ATG medialab



One of the most surprising observations obtained was the first time detection of molecular oxygen by the Double Focusing Mass Spectrometer (DFMS) of ROSINA, with local abundances in the 1-10% range relative to water (Bieler et al. 2015). This led to the reinvestigation of the 1P/Halley data from the Giotto Neutral Mass Spectrometer (NMS), showing that there is also O<sub>2</sub> in the coma of 1P/Halley with an abundance of  $(3.7 \pm 1.7)\%$  with respect to water, suggesting that the O<sub>2</sub> molecule may be a common parent species in comets (Rubin et al. 2015). However, although oxygen is the third most abundant element in the universe, its molecular form has been detected rarely. Apart from these two comets, 67P and Halley, it has been observed in two interstellar clouds, the Orion Nebula (Goldsmith et al. 2011) and  $\rho$  Oph A dense core (Larsson et al. 2007). In the solar system, aside from Earth, it has only been detected in the moons of Jupiter (Hall et al. 1995), Saturn (Johnson et al. 2006) and on Mars (Barker et al. 1972).

Among other volatiles, the ROSINA mass spectrometer has also detected S<sub>2</sub> in the coma of comet 67P/C-G at a distance of  $\sim 3$  au from the Sun on October 2014 with  $4\text{--}13 \times 10^{-6}$  abundances with respect to water (Le Roy et al. 2015; Calmonte et al. 2016), which is much lower compared to O<sub>2</sub> abundance, though significant, and which, contrary to O<sub>2</sub>, shows no correlation with water. This leads to re-study the origin of S<sub>2</sub> in comets, which is still unclear, although its presence in such objects has been detected in multiple observations including the comet IRAS-Araki-Alcock (C/1983 H1) (Ahearn et al. 1983), 1P/Halley (Krishna Swamy & Wallis 1987), Hyakutake (C/1996 B2) (Laffont et al. 1998), Lee (C/1999 H1) (Kim et al. 2003), Ikeaya- Zhang (C/2002 C1) (Boice & Reyl   2005).

In this chapter, the origin of these two volatiles in comets will be studied in two consecutive sections, focusing first on O<sub>2</sub>, the most intriguing of the two. Sulfur having a rather similar chemistry to oxygen, although it may exist in the form of many allotropes (from S to the refractory ring molecules S<sub>8</sub>), the problem of its origin will then be treated in a similar manner to the O<sub>2</sub>'s.

For each section we will successively present 1) the tentative hypotheses actually available in the literature and the scenario we want to propose, 2) the computational procedure we have used, 3) the numerical results.

## I Tracking molecular oxygen in comets

### I.1 Origin of molecular oxygen in Comet 67P/Churyumov-Gerasimenko

According to the observations, the  $O_2/H_2O$  ratio is isotropic in the coma and does not change significantly with the heliocentric distances. This point, which clearly shows an ubiquitous presence of  $O_2$  in the water ice of the comet, might be considered as a marker of a primordial origin for  $O_2$ , which should have been incorporated into the nucleus, rather early during the comet's formation. Furthermore, for both observation periods (17 to 23 October 2014 and 1 September 2014 to 31 March 2015)  $O_2$  shows the strongest correlation with  $H_2O$  whereas for other compounds with a similar volatility, as CO and  $N_2$ , the correlation is low (see Figure 2). Again this indicates strongly that  $O_2$  and  $H_2O$  should have the same origin, contrary to  $N_2$  and CO.

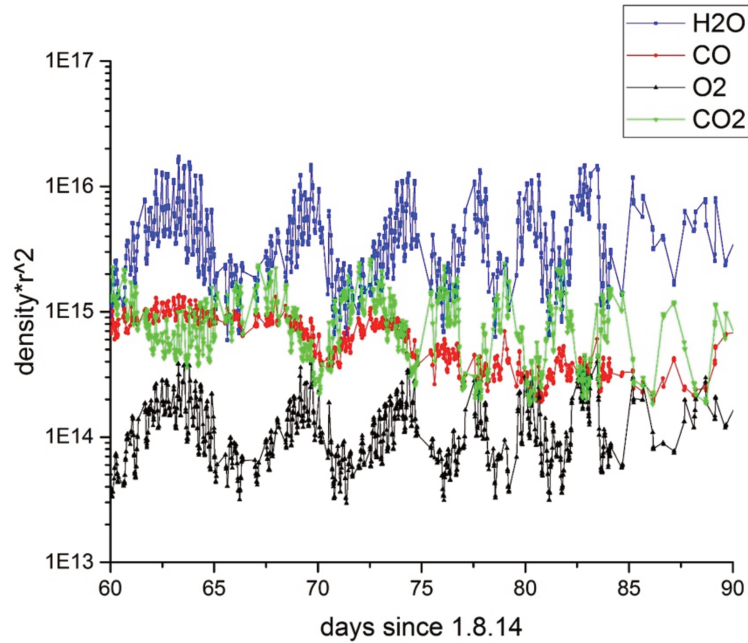


Figure 2: Correlations between volatile observed by ROSINA in comet 67P/C-G. Courtesy of K. Altwegg and the ROSINA team

However, in spite of such strong arguments in favor of a primordial origin, other hypotheses have been considered in several scenarios of formation, and we will present them as well.

### **I.1.1 Reviewing the astrophysical scenarios for the origin of O<sub>2</sub>**

The detection of O<sub>2</sub> in the coma of 67P/C-G has led to different theories for its origin, based on two opposite hypotheses; one calls on an extended ancient presence of O<sub>2</sub> in the comet icy bulk which allows the direct continuous sublimation from /with the cometary ice and points out a primordial origin whereas the other calls on a present chemical activity with various reactions occurring at the surface and in the coma.

According to Taquet and coworkers (Taquet et al. 2016), O<sub>2</sub> comes directly from the cometary ice and has a primordial origin, They discarded the possibility of the production of O<sub>2</sub> from the cometary surface by solar wind particles and UV radiation, since the penetration depth is not sufficient enough to process material in the bulk. Also, they argued that a decrease in O<sub>2</sub> to H<sub>2</sub>O ratio should have been detected, which is not the case, as the upper layer containing O<sub>2</sub>, would be removed during the six-month observation time. Therefore, they concluded that O<sub>2</sub> must have been present in the icy grains before the formation of the comet. They used astrochemical models with different physical conditions to compare possible O<sub>2</sub> production mechanisms and they proposed that it has been formed at the surface of interstellar ices through oxygen atom recombination in moderate temperature (~20 K), higher densities than usually expected in dark clouds and moderate ionization rates, suggesting a formation of the Solar System in dense clusters of stars. Thus, the formation of O<sub>2</sub> would rely on physical conditions that are warmer and denser than those usually expected in dark clouds.

The second type of approach involves the O<sub>2</sub> production during the sublimation of water ice. According to Dulieu and coworkers (Dulieu et al. 2017), O, O<sub>2</sub> and O<sub>3</sub>, being very volatile, cannot stay on the surface of the icy grains and they react to re-form H<sub>2</sub>O, eventually giving H<sub>2</sub>O<sub>2</sub>. Then, this H<sub>2</sub>O<sub>2</sub>/H<sub>2</sub>O ice mixture sublimates by heating and at the same time H<sub>2</sub>O<sub>2</sub> forms O<sub>2</sub> by dismutation/disproportionation reaction. The team performed two experiments aiming at the observed ratio of O<sub>2</sub>/H<sub>2</sub>O abundance; they could only reach a lower abundance ratio than expected, which might result from the fact that their experiments are not performed in space conditions, which cannot be proved in any way. Another weak point of this study is that the amount of O<sub>2</sub> produced is directly related to the quantity of H<sub>2</sub>O<sub>2</sub> present in the coma, which is still in question.

Another in situ  $O_2$  formation has been proposed by Yao and Giapis (Yao & Giapis 2017). According to them,  $O_2$  is directly formed by the collisions of energetic water ions with oxidized cometary surface analogues. In this kind of reactions, called Eley-Rideal (ER), energetic projectiles collide with surfaces and react with adsorbates to produce projectile-adsorbate molecules without equilibration with the surface (Yao & Giapi 2016). Their laboratory experiments showed that energetic water ions could abstract an oxygen atom on the surface, forming an excited precursor state which will eventually dissociates to produce the  $O_2^-$  negative ion. Further photo-detachment leads to molecular  $O_2$ , whose presence in the coma can be linked directly to water molecules and their interaction with the solar wind. However, in this study they cannot estimate the  $O_2$  yield for now and the reported accelerated water flux is too low to explain the observed  $O_2$  abundance. They proposed that the other ions present in the coma can participate in ER reactions ( $H_3O^+$ ,  $OH^+$  and  $O^+$ ) increasing the  $O_2$  yield, but their flux and energy distributions are not known yet.

### **I.1.2 Our scenario for trapping of $O_2$ in the cometary ice**

Agreeing on the primordial origin of  $O_2$ , we propose a scenario belonging to the first type, in which  $O_2$  is formed in the icy grain precursors of comets by irradiation (photolysis and/or radiolysis) of the  $H_2O$  ices. The process described below occurs on small icy grains, which later on agglomerate, but at that point are small enough to allow a full penetration of the radiations. The cosmic ray flux (CRF) breaks the  $H_2O$  molecules into small radicals as H, OH, O, which, being very reactive form rapidly molecules, and simultaneously creates voids in the matrix within which the produced molecules can accumulate. The main molecules formed are  $H_2$ , the smallest one, that most probably escapes easily from the matrix,  $H_2O$  that can agglomerate to the remaining ices to close the tracks produced by the CR, trapping the larger and heavier molecules produced like  $O_2$ .

Several cases of CR can be proposed for the irradiation of the icy grains. The first case considers the irradiation of icy grains located at 30 au from the sun in proto-solar nebula (PSN) whereas the second case considers the irradiation of icy grains in a low-density environment ( $\sim 10^{-3} \text{ g cm}^{-2}$ ). A third case might be added, which considers the upper layers of the PSN.

According to model calculations performed by Mousis et al. (2016) with the CRF value at 30 au (case 1), the  $O_2/H_2O$  ratio of 1-10% is reached in  $\sim 0.25$ -2.5 Gyr. This

extremely long time period conflicts with the lifetime of icy grains in the PSN, a few 100 years (Weidenschilling and Cuzzi 1993). The possibility of significant enhancement of the CRF by explosion of a close supernova (Fields & Ellis 1999) is also considered. Although such enhancements decrease the time needed to form sufficient amounts of  $O_2$  by a factor up to 100, this mechanism still requires a too long time for its production.

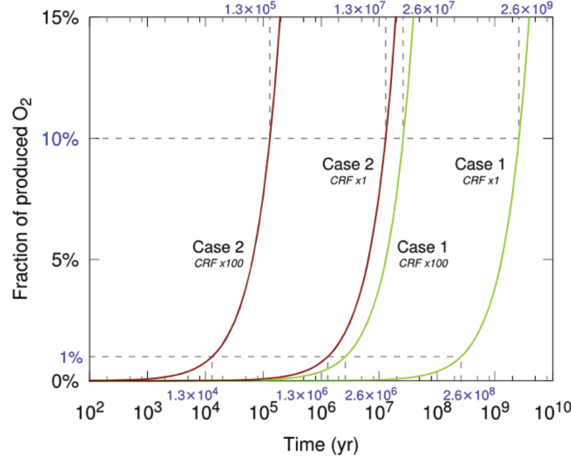


Figure 3: Time evolution of the fraction of  $O_2$  molecules produced by cosmic rays in an icy grain (Mousis et al. 2016)

We also considered the maximum CRF energy that an icy grain may receive (case 2). Such a high value of CRF energy can be achieved in low-density environments, which can only be found in molecular clouds. In such environments, 1-10% of  $O_2$  is formed in the icy grains on very short timescales (Figure 3). Therefore, to obtain significant amounts of  $O_2$  via radiolysis of icy grains, these grains must have formed in low-density environments such as the ISM. Consequently, 67P/C-G would have agglomerated from icy grains coming from ISM and their compositions remained pristine amorphous when entering the nebula. However, another possible scenario is that these icy grains would have experienced amorphous-to-crystalline phase transition when entering the disk. In spite of this transition,  $O_2$  would remain stable in the icy matrix because of the strong interactions between  $O_2$  and the surrounding  $H_2O$  molecules.

Another environment to favor  $O_2$  production is the irradiation of icy grains by CRF in the upper layers of PSN, which are also low-density environments. Here, turbulence plays an important role in the motion of small dust grains, so the grains initially settled in the midplane can be transported to high altitudes and low-density regions above the disk midplane. In such low-density environments, the CRF irradiation that grains received, should considerably be

enhanced compared to those in the mid-plane and be able to produce the amounts of  $O_2$  needed, before those grains be re-injected to the midplane zone.

Then two scenarios are possible. In the first one, comets would have agglomerated from interstellar icy grains that remained pristine when entering the nebula. In the second, comets would have formed from icy grains condensed in the proto-solar nebula and that would have been efficiently irradiated during their turbulent transport toward the upper layer of the disk.

To assert such scenarios that suggest a primordial origin for  $O_2$  in the comet, apart from the step of production of  $O_2$ , step that we will discuss about later on, the fundamental point to investigate is the stability of  $O_2$  in the more or less irregular icy matrix. Indeed, the very long time (a few  $10^4$  years) during which the molecular oxygen is supposed to stay embedded in the icy matrix, waiting for co-liberation with the surrounding water molecules, implies a strong trapping to be realistic hypothesis. This key point “how stable is the molecule  $O_2$  in the icy bulk?” is the topic of the following study.

## I.2 Modeling and computational details

### I.2.1 Modeling the ice structure

Water ice has about eighteen different crystalline phases, in which the oxygen atoms are in fixed relative positions while the hydrogen atoms may or may not be disordered, and three amorphous non-crystalline phases (Bartels-Rausch et al. 2012; Fuentes-Landete et al. 2015). This variety in crystalline phases comes from the open tetrahedrally arranged water molecule structure for hexagonal ice under normal atmospheric pressure. In all crystalline ices, the water molecules are bonded to neighboring water molecules by hydrogen bonds but keep their own symmetry. So doing, they obey the 'ice rules', also called Bernal-Fowler rules (Bernal & Fowler 1933), according to which, each water molecule has four hydrogen-bonded neighbors, two hydrogen atoms near each oxygen and one hydrogen atom on each  $O\cdots O$  bond; thus  $H-O-H\cdots OH_2$  and  $H_2O\cdots H-O-H$  are allowed but  $H-O-H\cdots H-O-H$  and  $H_2O\cdots OH_2$  are not (Figure 5).

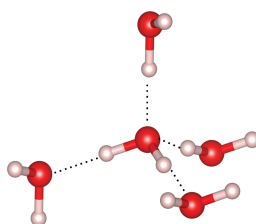


Figure 5: Water molecules in the ice structure

The existence of several crystalline and non-crystalline ice structures makes the modeling of the ice structure to be studied, a non-trivial task.

In this study, an apolar hexagonal ice model with surface hydrogen ordered as proposed by Fletcher (1992) is used; the same model was employed in previous studies about the origin of neutral sodium in cometary tails (Ellinger et al. 2015) and the trapping of noble gases in interstellar ices (Doronin 2015). It has been shown that this ice model is the most stable surface configuration of the hexagonal ice basal (0001) plane (Pan et al. 2010; Buch et al. 2008). More important, relying on the results, theoretical and experimental, by Doronin and coworkers (to be published), it seems that the choice of the type and the surface of ice has little effect on the adsorption energies.

Furthermore, in our case, it can be stated that our modeling of ices stands mainly for crystalline structure but somehow also for compact amorphous ices as we will introduce holes of different kinds into the bulk of crystalline ices. In the same frame of mind, it should be reminded of the Monte Carlo calculations by Buch and coworkers (2004) building ice aggregates constituted of hundreds of water molecules, whose core was found to be crystalline domains of apolar hexagonal ice Ih.

### **I.2.2 VASP parameters**

To model solid water ice structures and evaluate their interactions with “defaults” or “absorbates”, a method based on first principle periodic density functional theory is employed. All the simulations are carried out by means of the Vienna ab initio simulation package (VASP) (Kresse & Hafner 1993; 1994). This code has proved to be especially well adapted to model bulk and surface ice structures interacting with volatile species in several previous studies (Lattalais et al. 2011, 2015; Ellinger et al. 2015; Mousis et al. 2016).

More precisely, we used for this particular work a GGA type functional called (PBE), developed by Perdew et al. (1996), as it is considered to give good results for geometries and to reproduce correctly the hydrogen bonds (Calatayud et al. 2003) whose representation is determinant in such problems.

The systems studied in this thesis either shows H-bonding (the bonding between water molecules in the ice structure) or interactions by Van der Waals forces (the interaction between the small volatile and the H<sub>2</sub>O molecules surrounding it). In such a case, DFT alone is not sufficient to take into account the weak dispersion forces, so Van der Waals correction to the DFT has to be added. Different approaches including specially crafted functionals (Lee et al. 2010; Vydrov & Voorhis 2010; Dion et al. 2004) and semi-empirical (Grimme 2006) corrections exist. In this study, a semi empirical approach called DFT-D2 proposed by Grimme (2006) has been employed.

Since VASP is a periodical code, the ice cell is replicated periodically in 3 dimensions; x, y and z. A vacuum has to be introduced in the z direction perpendicular to the surface to obtain a two dimensional slab, modeling a surface. The role of the vacuum is to prevent undesired interactions between the surface layer and the bottom layer of the next periodical image. The important point in determining the vacuum z-dimension is to keep it minimum but sufficient to avoid these interactions efficiently, keeping in mind that the calculation time increases rapidly with the vacuum dimension. In a previous study by our team about an analogous case (cf Doronin 2015), an optimum distance of 15 Å was determined for the vacuum. An explicit representation of the model slab is given in Figure 4.

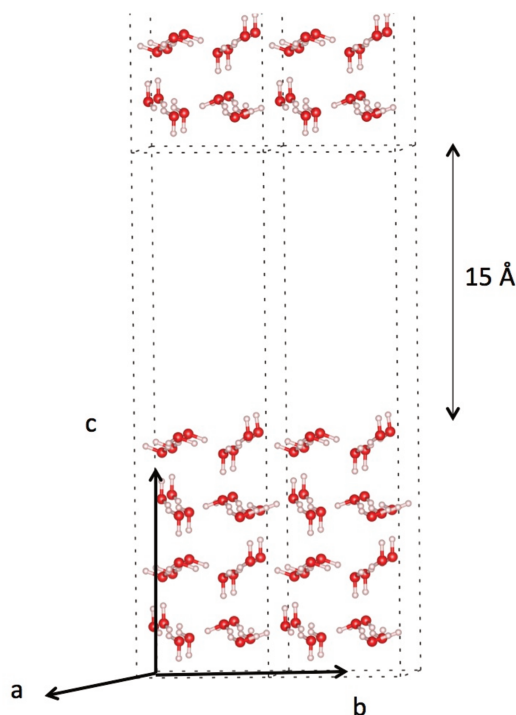


Figure 4: Representation of the ice slab



The number of K-points to be used depends on the cell. As explained, the ice slab is periodic in two dimensions (x & y) and the cell parameters in the direction of x and y are found to have a 1:1 ratio. Therefore, a 3x3x1 K points grid automatic Monkhorst & Pack sampling has been applied with the same number of K points in (ox) and (oy) directions. Note that one K point is enough in the direction perpendicular to the surface because the slab we model is not periodic in that direction. The standard energy cut-off of 400 eV was chosen (cf Doronin 2015).

To prepare the slab model, the bulk structure was fully optimized to obtain the ground state geometry of ice. Then a unit cell is defined with a 15 Å vacuum in the z direction (perpendicular to the surface) as stated before. Concerning the slab dimensions in the x and y directions, the starting unit cell referred hereafter as the “primitive cell” has a length of 8 Å in both directions and is composed of 4 ice bi-layers, the minimum required to study the insertion of small volatiles (like Na, Ar or O<sub>2</sub>) (cf Doronin 2015).

When modeling solid structures with periodic codes, we have to keep in mind, on the one hand that the computing time is directly linked to the dimension of the cell, increasing rapidly with each dimension, on the other hand that the main problem is to define a cell with parameters large enough to avoid the interaction between the periodic images. In our case, those periodic images imply those of the adsorbate as well as those of the cavities created inside the icy bulk, which may all lead to spurious interactions. An analogous problem arises with the parameter thickness of the slab when other interaction than simple adsorption is looked for, especially if large cavities are to be considered. Consequently, the stabilization energies have been calculated as functions of the sensitive parameters (number of ice bi-layers in the slab and different x-y dimensions of the unit cell) to obtain an optimum protocol in regards of both, efficiency and reliability of the calculations as detailed further on.

### **I.2.3 Stabilization energy**

The stabilization energy of O<sub>2</sub> is defined as the difference between the energy of the total system, O<sub>2</sub> interacting with the ice, and the sum of the energies of the pure ice and isolated O<sub>2</sub> (equation 1). One has to note that, by “pure ice”, we mean the system constituted only with water molecules featuring a regular or irregular icy bulk with or without cavities depending of the case, not the perfect crystallographic system; in any case it is the same system as the one in interaction with the molecule O<sub>2</sub>.

$$E_{stabilization} = (E_{ice} + E_{O_2}) - E_{(O_2+ice)} \quad (eqn1)$$

A negative sign for the stabilization energies signifies an endothermic process whereas positive stabilization energy values shows that the trapping in that particular environment is exothermic.

### I.3 Tests and Results

#### I.3.1 Preliminary results (primitive cell)

As a preliminary test, all cases have been calculated with the primitive cell.

In the simple case of adsorption on the surface, the molecules positions of the two bi-layers starting from the bottom have been kept fixed to mimic the bulk of ice while the molecules of the two upper bi-layers were allowed to relax and their geometries optimized. In all other cases, insertion into the perfect crystalline ice or into the cavities dug inside the bulk, the upper and the bottom bi-layers have been kept frozen whereas the two in between bi-layers geometries have been optimized, in order to allow O<sub>2</sub> to fit in.

The ices being irradiated by the CR present different cavities that are modeled as presented in Figure 6.

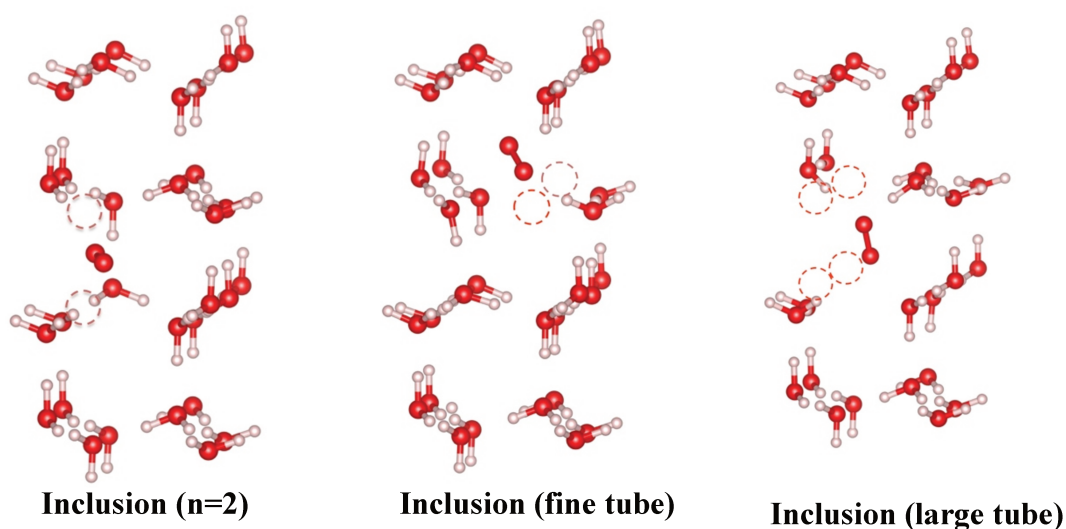


Figure 6: Optimized geometries for O<sub>2</sub> trapped in different types of cavities (missing water molecules visualized by the dotted circles)

All the results obtained with the primitive cell are reported in Table 1.

Environment	Stabilization Energy
Adsorption (singlet)	-0.83
Adsorption (triplet)	0.12
Inclusion (n=0)	-0.35
Inclusion (n=1)	-0.06
Inclusion (n=2)	0.20
Inclusion (fine tube) (n=2)	0.24
Inclusion (large tube) (n=4)	0.27

Table 1: Stability (eV) of O<sub>2</sub> in voids within the ice (n: number of molecules removed to create the void) calculated in the primitive cell model

From these results we can deduce the following comments:

i) As a first test, the simple adsorption of the O<sub>2</sub> molecule onto the ice surface has been investigated to get the stability of O<sub>2</sub> once it has reached the surface and compare insertion with adsorption. O<sub>2</sub> in its ground state is triplet but, by interacting with the ice surface, the orbital levels degeneracy may disappear. This phenomenon is called spin quenching and it is seen in some adsorption cases. For this reason, the adsorptions for both triplet and singlet state were calculated. The triplet state was found to be the most stable with adsorption energy of 0.12 eV, which is much lower than the adsorption energy of 1 H<sub>2</sub>O molecule onto the ice surface (~0.6 eV).

ii) Inclusion of O<sub>2</sub> into the perfect crystalline ice is not thermodynamically allowed; it is an endothermic process. Similarly, the position with the molecule trapped into the void obtained by the removal of one H<sub>2</sub>O molecule is not stable.

iii) Nevertheless, O<sub>2</sub> seems to be stabilized efficiently inside the cavities obtained by the removal of more than one H<sub>2</sub>O molecule. Different cases have been considered as presented in Figure 6. Because of the limitation of the dimension of the unit cell, the void obtained by the removal of 2 H<sub>2</sub>O molecules forms a real limited cavity inside the ice bulk whereas the cavities obtained by the removal of more than two water molecules result into a hollow tube in the ice structure, due to the periodicity of the VASP. Inclusion called “fine tube” is obtained by the removal of 2 successive H<sub>2</sub>O molecules in the same plane in the direction of one of the cell vector (x or y). With the periodicity of the ice cell, this creates a hollow tube in the direction of the other cell vector. The removal of 4 H<sub>2</sub>O molecules can also

lead to the formation of a hollow tube, called “large tube” whose dimensions are much larger. These hollow tubes are interesting in themselves because they could figure the irradiation tubes induced by the CR.

The stabilization energy is found to be 0.20 eV for the cavity obtained by the removal of the 2 H<sub>2</sub>O. For the tubes, the stabilization energy is steady, remaining around 0.2 – 0.3 eV and showing that O<sub>2</sub> can be effectively trapped inside the cavities obtained by the removal of at least 2 H<sub>2</sub>O molecules. Although, these stabilization energies are lower than the ice cohesion energy (~0.55 eV), they are in the order of that of a water dimer (~0.25 eV), meaning that the presence of O<sub>2</sub> should not disturb the ice structure until the sublimation. Interestingly, this is a little larger than the adsorption energy on the surface.

However, this model with the primitive cell has to be checked and improved if needed.

### **I.3.2 Improving the model**

The same cases of inclusion as in the preceding calculations have been investigated increasing the number of bi-layers and the cell dimensions in both x and y directions.

#### **a) Extended primitive cell with a 6 bi-layers slab**

The first parameter to be checked is the thickness of the slab. Since only two bi-layers molecular positions were optimized in the previous case study, due to the 4 bi-layers limitation of the model, the larger cavities may not have been described properly. Here, while the cell dimensions in the x-y directions are kept identical to those of the primitive cell, the thickness of the slab is increased to 6 bi-layers. To study the different cases of insertion, again the positions of the upper and the bottom layers are kept fixed but now the geometry of 4 bi-layers are to be optimized. The adsorption has not been investigated again since the 4 bi-layers system appears sufficient to describe this kind of process, since even within 4 bi-layers cell, the upper layer in interaction with the adsorbate and the bi-layer next to it are allowed to relax.

Environment	Stabilization Energy
Inclusion (n=1)	-0.01
Inclusion (n=2)	0.23
Inclusion (fine tube) (n=2)	0.24

Inclusion (large tube) (n=4, type 2)	0.20
Inclusion (large tube) (n=4, type 3)	0.25
Inclusion (large tube) (n=4, type 1)	0.24

Table 2: Stability (eV) of O<sub>2</sub> in voids within the ice (n: number of molecules removed to create the void) calculated in the extended slab primitive cell model. Report to Figure 7 for the signification of types 1, 2, 3.

The results obtained with this extended slab are displayed in Table 2.

Compared to the results obtained with the 4 bi-layers slab, all cases reported in Table 2 give similar results. Again, inclusion of O<sub>2</sub> into the smallest cavity with the removal of one H<sub>2</sub>O molecule is endothermic. Similarly, starting from the cavity (n=2), O<sub>2</sub> can be trapped with stabilization energies of 0.2-0.3 eV in different environments. The cavities are mostly formed in a manner similar to the 4 bi-layers case. However, for the formation of the large tubes, since more bi-layers are available in this model, different sites have been tested. In particular, three sites (Figure 7) were chosen to test the effect of the cavity position in the model, while keeping the cavity size constant. First, two cavities are formed within the two middle bi-layers; one of them is on the edge of the cell (1 in Figure 7) whereas the other is in the inner position (2 in Figure 7). The stabilization energies in all cases remain very close, in the range of 0.20 – 0.25 eV. Then, a third cavity is considered, closer to the bottom layer than the preceding ones (3 in Figure 7). Again the energy value obtained stays in the same range of 0.25 eV, showing that the cavity position in the inner layers does not affect at all the energetic stability.

Globally, these results show that O<sub>2</sub> can be trapped inside the ice, in accordance with the former results of Table 1, and that it is stabilized with analogous energies (variations within 10%). Indeed, we can conclude that the 4 bi-layer representation of the ice bulk was reliable and that the energies seem converged with respect to the thickness of the slab.

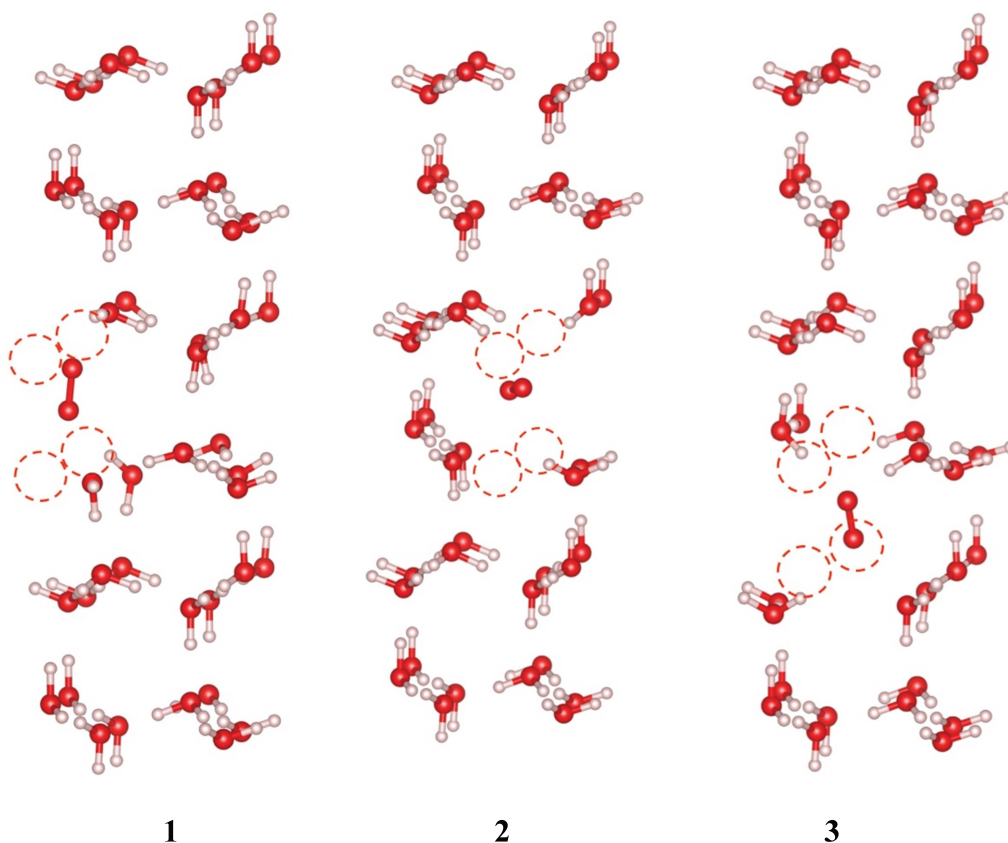


Figure 7: The optimized structures for  $O_2$  trapped in different types of cavities (large tube type)

### b) Double and quadruple cells with a 4 bi-layers slab

Designing limited cavities of different sizes instead of unlimited empty tubes in the ice bulk might be considered a more realistic situation susceptible to occur following the process of ice reconstruction. This implies to use larger cells in x and y directions.

Up to now, we have found that the trapping of  $O_2$  stabilizes around 0.2-0.3 eV starting from the smallest cavity ( $n=2$ ) to the largest (large tube), although the stabilization energy values have not been tested with respect to the cell parameters in x and y directions. Within the 4 bi-layers or 6 bi-layers primitive cell, even the smallest cavities have a limited water environment. This could make them closer to the tube cases, eventually resulting in over-estimated stabilization energies. For this reason, two cases of cavities are selected as tests, to calculate  $O_2$ 's stabilization energy with a double-sized cell and a quadruple-sized cell. They are respectively obtained by the removal of 2 and 4  $H_2O$  molecules in different bi-layers, forming a larger cavity, though not a proper tube (see Figure 8).

Note that a quadruple cell is four times larger than the primitive cell in volume, whereas the double cell is two times.

Environment	primitive cell	double cell	quadruple cell
Adsorption	0.12	0.13	-
Inclusion (n=2)	0.20	0.20	0.20
Inclusion (n=4)	0.27	0.24	0.20

Table 3: Stability (eV) of  $O_2$  in voids within the ice (n: number of molecules removed to create the void) calculated in the successive extended cell models. Note that more Figures are given for precise comparison as the calculations are supposed to have increased precision with the extension of the cell.

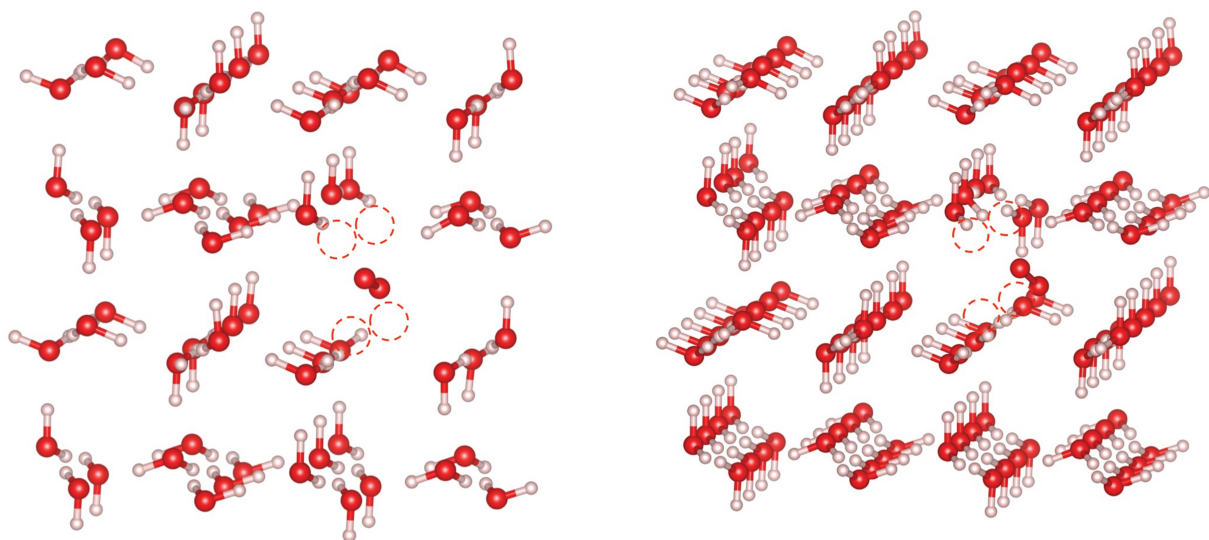


Figure 8: The optimized crystalline structures for  $O_2$  trapped inside the cavity (n=4) with a double (left) and a quadruple cell (right).

The results reported in Table 3 induce the conclusion that, whatever the conditions of the calculation, double or quadruple cell, small or large cavity, the stabilization energy of  $O_2$  inside the ice bulk remains in the range of 0.2-0.3 eV, confirming the preceding results. Consequently, the values of the stabilization energies within cavities obtained in the primitive cell model could be considered as reliable. However, looking closely to the numbers obtained with the different cells, some sort of convergence is to be observed with a narrowing of the value range, pointing to a final value of 0.20 eV to be retained for the stability of  $O_2$  embedded into water ices.

### I.3.3 Case of O<sub>2</sub> double trapping

Once we have asserted our hypothesis that O<sub>2</sub> is trapped and well stabilized into the icy bulk, so that it can only desorb together with the H<sub>2</sub>O molecules, we may try to address the delicate point of explaining the ratio O<sub>2</sub> to H<sub>2</sub>O ratio detected by ROSINA. The preceding calculations have shown that the smallest reliable representative cell to trap O<sub>2</sub> is the simple cell with 4 bi-layers, in which there are 30 (for inclusion n=2) and 28 (for inclusion n=4, large tube) H<sub>2</sub>O molecules embedding 1 molecule of O<sub>2</sub>, which leads to a O<sub>2</sub> to H<sub>2</sub>O ratio around 3 %. This implies that, when the comet water sublimates, the water molecules drag with them the trapped O<sub>2</sub> molecules in the same proportion. This is in accordance with the mean value observed in the coma of 67P, though we have to keep in mind that it is not an average value but an upper limit for our model. In the present state, it cannot account for more.

Now, taking into account that several molecules of O<sub>2</sub> could be formed in the same environment, we have to consider the possibility that these O<sub>2</sub> molecules could agglomerate into the voids as a dimer.

The triplet ground state of the O<sub>2</sub> molecule give rise to three different potential energy surfaces (PES) of singlet and triplet, (plus a quintet multiplicity). According to multi reference ab initio calculations, O<sub>2</sub> dimer is in singlet state in its ground state with a rectangular D<sub>2h</sub> geometry in isolation (Bartolomei et al. 2008).

To trap the O<sub>2</sub> dimer, a rather large cavity should be needed. Consequently, we considered only cavities obtained by the removal of 4 H<sub>2</sub>O molecules taking note that, when calculating with the primitive cell, a large tube is formed.

Keeping in mind the different multiplicities of the ground states of O<sub>2</sub> and its dimer, we note that there are two ways of calculating the stabilization energy coming from the interaction of the dimer with the surrounding H<sub>2</sub>O molecules. One is the difference between the energy of the total system and the sum of the energy of the ice with cavity and twice the energy of the isolated O<sub>2</sub>, named (E1) in Table 5 and corresponding to (eqn. 2), whereas the second way is the energy difference between the energy of the total system and the sum of the energy of the ice with cavity and the energy of the isolated O<sub>2</sub> dimer (named (E2) in Table 5 and related to (eqn 3)).



$$E_{stabilization} = (E_{ice} + 2 \times E_{O_2}) - E_{(O_2dimer+ice)} \quad (eqn2)$$

$$E_{stabilization} = (E_{ice} + E_{O_2dimer}) - E_{(O_2dimer+ice)} \quad (eqn3)$$

The stabilization energy given in Table 5 shows only small variation with the two different types of ice cells considered, with a value around 0.40 eV for (E1) and 0.32 eV for (E2). The order of magnitude indicates that the O<sub>2</sub> dimer can also easily be trapped in the voids within the ice either in the form of two O<sub>2</sub> molecules in triplet state or as a proper O<sub>2</sub> dimer in its ground singlet state. Moreover the dimer seems to be stabilized even more than a lonely O<sub>2</sub> molecule.

Environment	primitive cell	double cell
Inclusion (n=4) (E1)	0.43	0.40
Inclusion (n=4) (E2)	0.35	0.32

Table 5: Stability (eV) of [O<sub>2</sub> – O<sub>2</sub>] in voids within the ice (n: number removed to create the void)

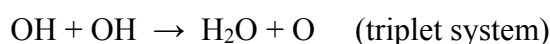
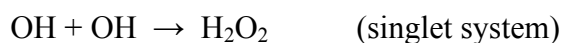
Altogether, taking the optimum smallest cell and realizing the same evaluation as for the simple O<sub>2</sub>, the O<sub>2</sub> to H<sub>2</sub>O ratio rises up to around 7%, close to the maximum value of 10% observed in particular spots of the comet. Finally combination of O<sub>2</sub> monomers and dimers trappings seems able to reproduce more than fairly the oxygen-water ratios observed in the coma.

#### **I.4 Chemical aspect: Perspective**

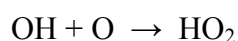
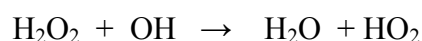
Going back to the global scenario, we should now deal with the step of formation of O<sub>2</sub> within the tubes produced by the irradiation of the cosmic rays. Except for the various atomic or molecular inclusions eventually present in the ices but in very small quantities, and apart the H<sub>2</sub>O molecules themselves, the main species present after irradiation are those resulting from the breaking of the water molecules along the tube, that can be only the radicals H, O and OH. These small radicals are all very reactive and rapidly recombine according the following reactions:



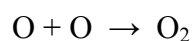
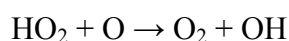
$\text{H}_2$  being a small and light molecule most probably escapes quickly from the icy matrix



$\text{H}_2\text{O}_2$  being particularly fragile to radiation eventually breaks back to OH radicals, which participate essentially to the reconstruction of the icy matrix by producing  $\text{H}_2\text{O}$



The formation of  $\text{HO}_2$  may eventually be followed by



Hence, two ways of formation for  $\text{O}_2$  are to be investigated, one as a direct recombination of the oxygen atoms, the other via the formation and destruction of the molecule  $\text{HO}_2$ .

These reactions have been studied in gas phase and some in presence of a few water molecules. However no proper study on a solid surface, a fortiori within a solid matrix has been performed.

## **II Tracking molecular sulfur in comets**

### **II.1 Origin of molecular sulfur in Comet 67P/ Churyumov-Gerasimenko**

According to the first measurements by the Double Focusing Mass Spectrometer (DFMS), part of the Rosetta Orbiter Sensor for Ion and Neutral Analysis (ROSINA) on 20 October 2014 between 07:54 and 08:37 (UTC) and on 19 October 2014 between 00:39 and 01:22 (UTC) at a distance of 3.15 au from the Sun (Le Roy et al. 2015),  $\text{S}_2$  has been detected

with an abundance of 0.0004 – 0.0013 % relative to water. However, these measurements were done outside of the water snow line, where water is stable as a solid and does not remain in the gas phase so that the abundances relative to water are not expected to be representative of the bulk composition.

The second set of measurements is more demonstrative as it was obtained between equinox in May 2015 and perihelion in August 2015 in an interval, which covers heliocentric distances from 3.5 to 1.24 au. There, the abundance obtained for S<sub>2</sub> with respect to water is in the order of 0.001% (Calmonte et al. 2016), showing that the value of this ratio is maintained even in lower heliocentric distances. However, contrary to O<sub>2</sub> strongly correlated to H<sub>2</sub>O, S<sub>2</sub> shows no correlation to H<sub>2</sub>O nor to H<sub>2</sub>S the most abundant S-bearing species. (Calmonte et al 2016)

### **II.1.1 Reviewing the astrophysical scenarios for the origin of S<sub>2</sub>**

Only two types of scenarios have been proposed to identify the origin of molecular sulfur. The first one considers that S<sub>2</sub> is a parent molecule of the comets, desorbing directly from the cometary ices. A'Hearn & Feldman (1985) proposed that S<sub>2</sub> originating from the icy matrix of comets should be formed by UV or high-energy proton irradiation of other S-containing species already trapped in the icy grains in the ISM. In particular, they pointed out that the S<sub>2</sub> abundance in the interstellar medium (ISM) could not explain the S<sub>2</sub> abundance observed in the comets and that consequently S<sub>2</sub> could not come directly from the ISM in the form of S<sub>2</sub>. This proposition was followed by experimental studies including the one by Grim & Greenberg (1986). These authors argued for the formation of S<sub>2</sub> from H<sub>2</sub>S molecules embedded in dirty ices composed of molecules such as H<sub>2</sub>O, CO and CH<sub>4</sub>, and submitted to UV radiation. They also pretended that S<sub>2</sub> molecules could remain trapped in the amorphous material until the water molecules sublime. Jimenez-Escobar & Caro (2011) irradiated H<sub>2</sub>S and H<sub>2</sub>S:H<sub>2</sub>O ices with UV and observed that, passing through intermediate products as HS, HS<sub>2</sub> and H<sub>2</sub>S<sub>2</sub>, they finally got the formation of S<sub>2</sub> together with S-polymers up to S<sub>8</sub>. Later on, they (Jimenez-Escobar et al. 2012) showed that the formation of S<sub>2</sub> was also possible with X-ray irradiation. After A'Hearn & Feldman (1985), Calmonte et al. in 2016 proposed the formation of S<sub>2</sub> from the radiolysis of S-bearing compounds in cometary ices. However, if experimental data exist for UV and X-ray irradiation of ices, the experimental conditions are not those in space and there is a lack of computational study about the stability of S<sub>2</sub> in H<sub>2</sub>O or H<sub>2</sub>S ice.

The second type of scenario considers that  $S_2$  is a product of reactions occurring in the coma. Saxena & Misra (1995) explained the  $S_2$  abundance observed in Comet IRAS-Araki-Alcock (1983d) by a formation process of  $S_2$  from sulfur atoms with ethylene acting as a catalyst in the inner coma. It has to be noted that the sulfur atoms are formed by photolytic reactions from the parent molecules,  $CS_2$ ,  $H_2S$ ,  $OCS$ ,  $HS$ ; hence the efficiency of such a mechanism relies on the hypothetical abundance of these molecules together with the production and abundance of ethylene.

The same mechanism has been used to explain the  $S_2$  abundance in comet C/1996 B2 (Saxena et al. 2003). However, according to A'Hearn et al (2000), taking into account the abundance of  $C_2H_4$  and the relatively slow rate of the reaction, this mechanism cannot produce the required amount of  $S_2$ ; they proposed another mechanism, implying extremely fast reactions: metastable atomic sulfur (in 1D state) formed from the dissociation of  $CS_2$  would react with the  $OCS$  present in the inner coma to produce  $S_2$ . But,  $S_2$  was already seen at distances larger than 3 au (Bieler et al. 2015) in cometary coma and there, densities are very low, so that collisions among volatiles are very rare.

This induces to rule out the second type of scenarios where  $S_2$  originates from reactions occurring in the coma and give more credit to a primordial origin for  $S_2$  as for  $O_2$ .

### **II.1.2 Our scenario for trapping $S_2$ in the cometary ice**

The case of  $S_2$  is less straightforward than the case of  $O_2$ . As stated above, the fact that  $S_2$  is already seen at distances larger than 3 au, suggests a primordial origin for this molecule as for molecular oxygen. It is then tempting to set a parallel between the two species, origin, formation and history combined. However, we have to keep in mind that, unlike  $O_2$ , the emission observed for  $S_2$  shows no correlation with  $H_2O$  which composes its majority environment, nor with  $H_2S$  the sulfur analogous of  $H_2O$  and the most abundant of S-bearing compounds.

Here we propose a first type of scenario, in which  $S_2$ , like  $O_2$ , is formed in the icy grain precursors of comets by irradiation (photolysis and/or radiolysis) of the  $H_2O$  ices and the S-bearing molecules embedded in the  $H_2O$  ice.

The detection of  $H_2S$  in comets, up to 1.5% relative to  $H_2O$  as inferred from millimeter and submillimeter observations (Bockelée-Morvan et al. 2000, 2010; Boissier et al. 2007),

also suggests that this molecule should be present in interstellar icy grain mantles. Other S-species ( $\text{CS}_2$ ,  $\text{SO}_2$ ,  $\text{OCS}$ , and  $\text{H}_2\text{CS}$ ) were detected in comet Hale–Bopp with abundances between 0.02% and 0.4% (Bockelée-Morvan et al. 2000), though much lower than  $\text{H}_2\text{S}$ . Indeed, sulfur atoms in interstellar icy grains are expected to form  $\text{H}_2\text{S}$  preferentially because of the high hydrogen abundances and the mobility of hydrogen in the ice. Eventually, kind of  $\text{SH}_2$  clumps should be found in places, embedded into the water ices.

The cosmic ray flux breaks the  $\text{SH}_2$  molecules to produce  $\text{S}_2$  in a similar pattern as for  $\text{O}_2$  from  $\text{H}_2\text{O}$  molecules while simultaneously creating voids in the matrix within which the produced molecules can accumulate. The conditions are very similar to those of the formation of  $\text{O}_2$ . Again, at that point, the possibility of a long-lasting sequestration of the molecule into the icy bulk has to be seriously checked. Compared to the  $\text{O}_2$  case, the  $\text{S}_2$  case is somewhat more complex as  $\text{S}_2$  might be trapped into two kinds of reservoirs:  $\text{H}_2\text{O}$  ices and  $\text{H}_2\text{S}$  clumps themselves embedded in  $\text{H}_2\text{O}$  ices.

Therefore, these two types of icy environments have been investigated in the following part.

## **II.2 Tests and results**

### **II.2.1 The case of $\text{S}_2$ embedded in $\text{H}_2\text{O}$ ice**

Most of the cavities formed by irradiation should be surrounded by  $\text{H}_2\text{O}$  molecules, since  $\text{H}_2\text{O}$  is the dominant volatile in comets (Bockelée-Morvan et al. 2004). Therefore, the stability of  $\text{S}_2$  molecules has been investigated first in  $\text{H}_2\text{O}$  ices. In a similar approach to the study of the  $\text{O}_2$  trapping inside the water ice, the sequestration of  $\text{S}_2$  has been investigated in different environments, i.e. inside cavities of different sizes. The convergence of the results with respect to the cell size (double & quadruple cell) and the thickness of the slab (4 bi-layer & 6 bi-layer cell) have also been tested for the sulfur species, though already checked for  $\text{O}_2$ ; indeed, it has to be taken into account that the sizes of the trapped molecules were different enough to lead to eventual behavior changes inside the cavities from  $\text{O}_2$  to  $\text{S}_2$ .

#### **II.2.1.1 Preliminary results (primitive cell)**

The protocol is strictly identical to the one used in the  $\text{O}_2$  study. Apolar Ih crystalline ice structure has been employed. The cell called “primitive” is constituted by a 4 ice bi-layers

slab with cell parameters of 8 Å in the x and y directions. The cavities (n=1 to 4) introduced in the regular icy bulk are identical to those in the O<sub>2</sub> study. To model the adsorption, two bi-layers from the bottom are kept fixed while molecules in the two upper bi-layer are allowed to relax. In all other cases (inclusion (n=0,1,2,4)), the outer layers are kept frozen whereas the two bi-layers in between are optimized.

The results are displayed in Table 6 and lead to the following comments:

Environment	E stability
Adsorption	0.26
Inclusion (n=0)	-1.20
Inclusion (n=1)	-0.12
Inclusion (n=2)	0.25
Inclusion (fine tube) (n=2)	0.51
Inclusion (large tube) (n=4)	0.56

Table 6: Stability (eV) of S<sub>2</sub> in voids within the ice (n: number of molecules removed to create the void)

i) The adsorption of S<sub>2</sub> molecule onto the ice surface has first been calculated. The adsorption energy found is 0.26 eV. This value is nearly twice larger than the adsorption of O<sub>2</sub>, implying that S<sub>2</sub> can be absorbed much better than O<sub>2</sub>, once it is on the surface. Weak forces between molecules, especially dispersion forces are proportional to the number of electrons. Therefore, the possible reason behind this difference might be the fact that S<sub>2</sub> has more electrons and is more polarizable than O<sub>2</sub>.

ii) Inclusion of S<sub>2</sub> forced into a perfect crystalline ice disturbs the system enough to produce an endothermic process; this is also the case for the inclusion of S<sub>2</sub> into the cavity obtained with the removal of only one H<sub>2</sub>O molecule in the ice structure. This cavity does not provide enough space for one S<sub>2</sub> molecule, resulting in an unstable structure. It has to be noted that both cases (n=0 and 1) lead to repulsive effects even larger than for O<sub>2</sub>.

iii) The situation differs when trapping S<sub>2</sub> inside the cavities obtained with the removal of more than one H<sub>2</sub>O molecule. The same cavity structures obtained for the O<sub>2</sub> case were used (Figure 9). Inside a small cavity (n=2), S<sub>2</sub> can be trapped with stabilization energy of 0.25 eV. For larger cases, inclusion in the fine and large tube, S<sub>2</sub> is trapped with a much higher stabilization energy, around 0.5 eV. The stabilization energies for wider cavities are

larger than the adsorption of  $S_2$  onto the surface (more than double). This shows that a particular chemistry is likely to occur within cavities compared with standard surfaces. Compared to  $O_2$ , the stabilization energies for  $S_2$  does not converge as quickly with the size of the cavity, starting from 0.25 eV for inclusion in a small cavity to  $\sim 0.5$  eV for higher cavities. One can put forward that  $S_2$  molecules, being much larger than  $O_2$  molecules, require a higher cavity size to be at ease without constraints.

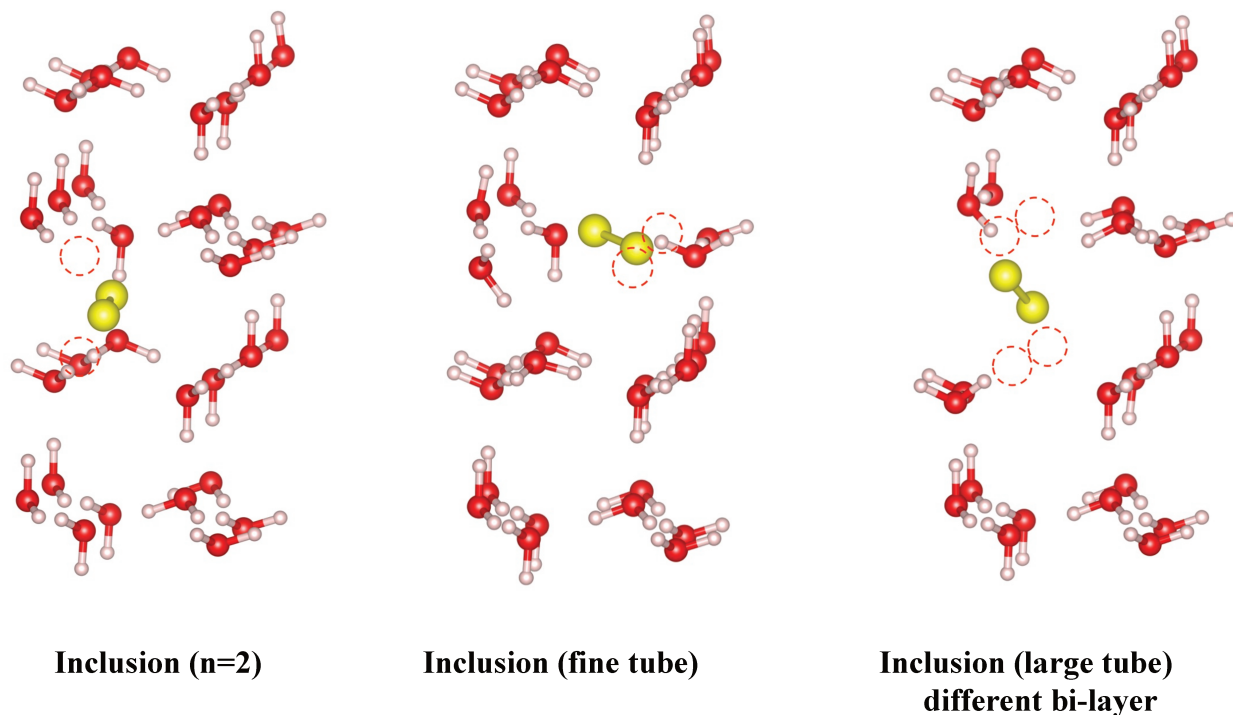


Figure 9: The optimized geometries for  $S_2$  trapped in different type of cavities with the 4 bi-layers slab.

### II.2.1.2 Improving the model

In such a case, we have even more reasons than in the oxygen case, to have the primitive cell model to be tested in terms of both the slab thickness and the cell size. The same extensions as for the  $O_2$  study will be investigated.

#### a) Extending the primitive cell with a 6 bi-layers slab

Two cases, inclusion in the fine tube and inclusion in the large tube (Figure 10) are considered in order to study the effect of the number of bi-layers used to model the ice slab and see whether convergence is reached with respect to the thickness of the slab. The

inclusion in the large tube, having two hollow tubes in two bi-layers, is the most difficult case to model with a 4 bi-layer cell, since only the layers with the tubes are optimized. For this reason, this case has been chosen to test the slab thickness convergence together with the other less problematic extreme case, the inclusion in the fine tube. As in the  $O_2$  case, the two outer bi-layers are kept frozen while the 4 bi-layers situated in between are allowed to relax. The results are given in table 7.

Environment	Stabilization Energy
Inclusion (fine tube)	0.50
Inclusion (large tube)	0.53

Table 7: Stability (eV) of  $S_2$  in voids within the ice

It can be seen that increasing the slab thickness of the unit cell does not change significantly the stabilization energy, which slightly diminishes by a few percents but roughly stays around 0.5 eV. This implies that 4 bi-layers of ice can be considered as sufficient enough to represent the environment and at the same time, it shows that the stabilization energy of  $S_2$  is indeed in the order of 0.5 eV for larger cavities compared to 0.2 eV within a small cavity.

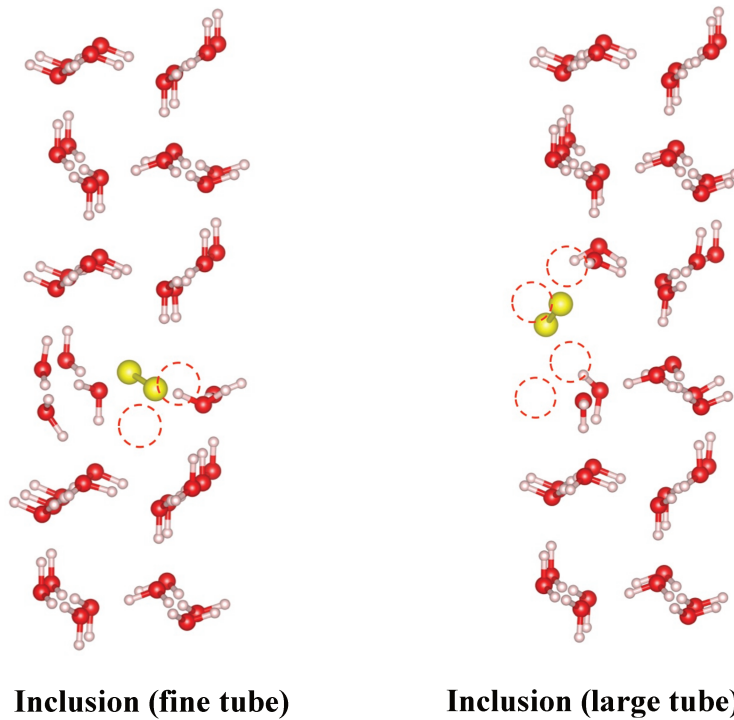


Figure 10: The optimized crystalline structures for  $S_2$  trapped in different type of cavities for inclusion with the 6 bi-layer slab.



## b) Double Cell

The cavities obtained with the removal of more than 1 H<sub>2</sub>O molecules in the primitive cell model form hollow tubes in the ice structure, either fine (n=2) or large (n=4). These tube models are the extreme cases, which may be formed along the way of the irradiation and they represent a limit for the stabilization energy of S<sub>2</sub>, forming the largest space possible. However, the stability of S<sub>2</sub> in different cavity sizes, not only in the hollow tubes should be tested, and we have to note that, within the primitive cell model, it is not possible to obtain mere cavities by the removal of more than 2 H<sub>2</sub>O molecules. So, we have retained two representative cases of inclusion to investigate with a double cell model: S<sub>2</sub> within the cavity obtained by the removal of 2 H<sub>2</sub>O and S<sub>2</sub> into a larger cavity formed when removing from the lattice 4 H<sub>2</sub>O molecules (Figure 11). The two outer bi-layers are kept constant; whereas two core bi-layers are optimized.

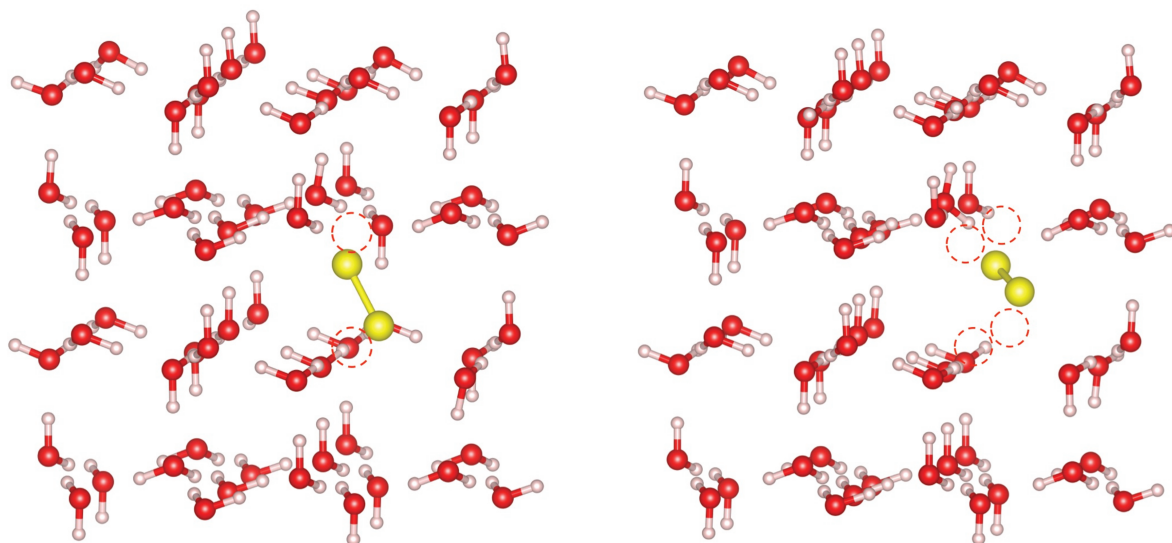


Figure 11: The optimized crystalline structures for S<sub>2</sub> trapped in the cavity (n=2) (left) and n=4 (right) within double cell (right) with the 4 bi-layer slab.

The calculated energy values for these two cases are reported in Table 8. The stabilization energy for the trapping of S<sub>2</sub> in a small cavity (n=2) is found to be 0.28 eV, which is the same order of magnitude as obtained with the primitive cell (0.25 eV). In the

case of a larger cavity ( $n=4$ ), the stabilization energy is found to be 0.50 eV, which is very close to the values obtained for the inclusion in fine & large tubes (0.51 & 0.56 eV). These results show that, when the space available is sufficient, the energy stabilizes around 0.5 eV.

Environment	Stabilization Energy
Inclusion ( $n=2$ )	0.28
Inclusion ( $n=4$ )	0.50

Table 8: Stability (eV) of  $S_2$  in voids within the ice ( $n$ : number of molecules removed to create the void)

From the preceding results we may conclude that  $S_2$  can be trapped in  $H_2O$  ice efficiently enough to remain stable until the sublimation of the water ice. The stabilization energy stands around 0.5 eV within the cavities large enough to host  $S_2$ . We note that this value is even larger than the trapping of  $O_2$  (0.2 – 0.4 eV), meaning that  $S_2$  is even more stable than  $O_2$  molecule inside the cavities. Trapping of volatiles inside cavities is governed by the weak dispersion forces, which are proportional to the number of electrons involved and the polarizability.  $S_2$  with a higher number of electrons may form more stable structures than  $O_2$ . These results are consistent with the laboratory experiments of Grim & Greenberg (1987), who showed that  $S_2$  remains trapped in icy grains until heated up to  $\sim 160$  K, at which, water ice sublimates at PSN conditions.

### II.2.2 The case of $S_2$ embedded in $H_2S$ ice

Before agglomerating to form comets, the icy grains are submitted to a strong cosmic radiation flux; under such irradiation the S-bearing compounds within the water ice are expected to turn mostly into  $H_2S$ , forming small domains of  $H_2S$  inside the water ice. Under more irradiation, these  $H_2S$  domains may form radicals and produce  $S_2$  in a process similar to the production of  $O_2$  from  $H_2O$ . The formation of  $S_2$  from the  $H_2S:H_2O$  ice has been already investigated experimentally and it was shown that  $H_2S$  can be photolyzed easily to  $S_2$  and even to S polymers until  $S_8$  (Escobar & Caro 2011). Consequently we have to consider the possibility that these molecules can accumulate in the voids created simultaneously in the icy matrix. Since the temperature of the medium of interest is low,  $H_2S$  ice is taken as pure condensates and it is the most stable phase at the lowest temperature that is used in our model.

### II.2.2.1 Stability of H<sub>2</sub>S in H<sub>2</sub>O ice

The first hypothesis to be tested is that small H<sub>2</sub>S domains can form and stay incorporated inside the water ice. The stabilization of such H<sub>2</sub>S domains is addressed by replacing H<sub>2</sub>O molecules progressively by H<sub>2</sub>S in the water ice lattice. Different domains have been investigated, starting with the substitution of 1 H<sub>2</sub>O molecule by 1 H<sub>2</sub>S (No. 1 in Figure 12). For the substitution of 2 H<sub>2</sub>O molecules, two different cases are considered, one is called “far away”, the 2 H<sub>2</sub>O molecules substituted not being directly bounded by H-bonding (No 1 and 2 in Figure 12); the other one is called “close”, the 2 H<sub>2</sub>O molecules substituted being bounded by H-bonding (Position No 2 and 3 in Figure 12). Then a bigger H<sub>2</sub>S domain is formed by the substitution of 3 H<sub>2</sub>O molecules, all of them bounded by H-bond to each other. Finally the biggest domain considered is obtained by the substitution of 4 H<sub>2</sub>O molecules yielding a tube of H<sub>2</sub>S molecules. For each case, the outer bi-layers are kept fixed, whereas 4 core bi-layers are optimized.

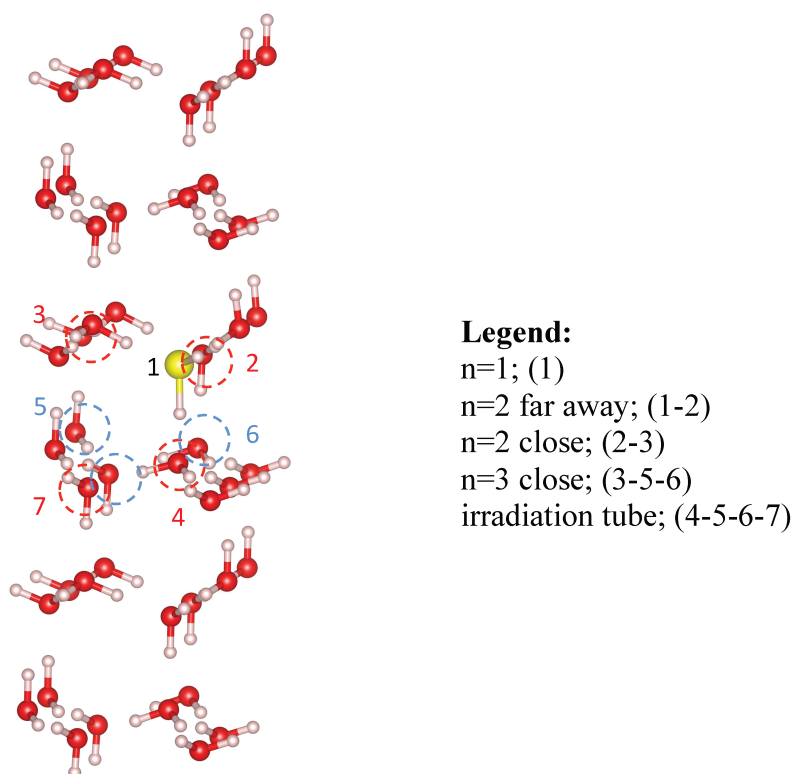


Figure 12: The position of H<sub>2</sub>O molecules substituted by H<sub>2</sub>S in H<sub>2</sub>O ice crystalline structure

The stabilization energies for the substitution of H<sub>2</sub>S is calculated as the difference between the total system with H<sub>2</sub>S and the sum of H<sub>2</sub>S in isolation and the energy of the water ice structure obtained by removing substituted H<sub>2</sub>O molecules, then this difference is divided by the number of H<sub>2</sub>O substituted by H<sub>2</sub>S (Eqn 4).

$$E_{stabilization} = \frac{\left( (E_{ice} + n \times E_{H_2S}) - E_{(H_2S+ice)} \right)}{n} \quad (4)$$

The results are reported in Table 9. H<sub>2</sub>S in the hexagonal water ice structure stabilizes between 0.5-0.8 eV. The stabilization energies decrease when the H<sub>2</sub>S molecules are closer in the structure. In this approach, H<sub>2</sub>S molecules are forced to be stay in hexagonal water ice crystalline structure, which causes a constraint in the final structure composed of H<sub>2</sub>O and H<sub>2</sub>S. Combined with the fact that H<sub>2</sub>S molecules are much larger and have longer bond distances, cell parameters optimized for H<sub>2</sub>O ice might not be effective to model the combined ice. For this reason, although H<sub>2</sub>S molecules may form small domains inside the water ice bulk, in the cases in which the substituted H<sub>2</sub>O positions are closer, the stabilization energy decreases. A full theoretical study of mixed ices of H<sub>2</sub>O/ SH<sub>2</sub> would be necessary to have a clear cut view of such an environment but is still to be done.

The important result for our study, pointed by these calculations, is that small H<sub>2</sub>S clumps are stabilized in H<sub>2</sub>O ice. In the next section, the stability of S<sub>2</sub> inside H<sub>2</sub>S ice will be investigated.

Environment	Stabilization Energy
Adsorption	0.61
Substitution (n=1)	0.77
Substitution (n=2) far away	0.73
Substitution (n=2) close	0.56
Substitution (n=3) close	0.50
Substitution (irradiation tube)	0.51

Table 9: Stability (eV) of H<sub>2</sub>S interacting with H<sub>2</sub>O ice (n: number of H<sub>2</sub>O molecules replaced by H<sub>2</sub>S).

### II.2.2.2 The stability of S<sub>2</sub> in H<sub>2</sub>S ice

Compared to H<sub>2</sub>O primitive cell, the corresponding H<sub>2</sub>S one has much longer cell parameters (the procedure to obtain the H<sub>2</sub>S cell is explained in appendix A.) as the distance between the periodic images of the S<sub>2</sub> that 13 Å instead of 8 Å in the case of O<sub>2</sub>. So, we could cut down our tests for parameters and only keep those based on the effect of the thickness of the H<sub>2</sub>S layers.

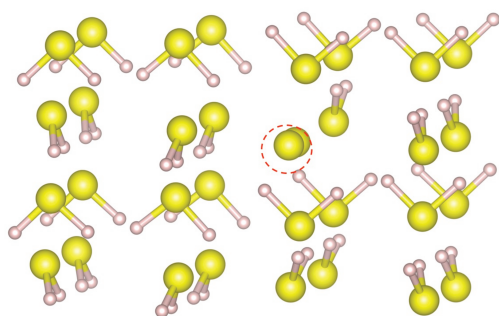
#### a) Primitive cell (4 layer cell)

Similarly to the previous calculations, inclusion of the volatile (S<sub>2</sub> in this case) into the perfect crystalline H<sub>2</sub>S ice was first considered. Again, the trapping of the volatile in the perfect ice is found not thermodynamically stable. Then different cavities supposed to be formed by irradiation have been designed to search for the stability of S<sub>2</sub> within the irregular H<sub>2</sub>S ice. Four cases were studied: small cavities formed by the removal of 1 and 2 H<sub>2</sub>S molecules followed by a larger cavity formed by the removal of 4 H<sub>2</sub>S molecules in different layers; and finally the cavity called large tube in this study, obtained by the removal of 4 H<sub>2</sub>S molecules in a way to form a hollow tube. For a better understanding, the positions of the H<sub>2</sub>S molecules removed are visualized in Figure 12 with red circles.

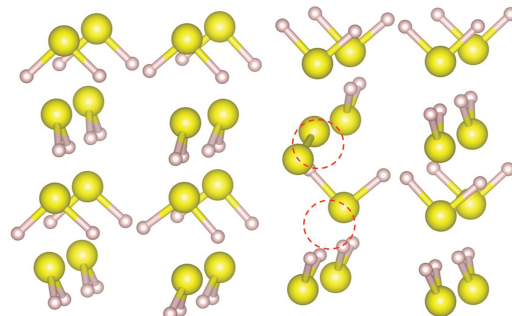
The results are reported in Table 10, according to which, S<sub>2</sub> unlike O<sub>2</sub>, can even be trapped in the smallest cavity obtained by the removal of only one H<sub>2</sub>S molecule. Again, this can be explained with the higher number of electrons of S compared with O: weak interactions are stronger in the case of H<sub>2</sub>S and S<sub>2</sub>. For the larger cavities, the stabilization energy stands around 0.3 eV, implying that S<sub>2</sub> can effectively be trapped within H<sub>2</sub>S ices as well as H<sub>2</sub>O ices. However, as for the other preceding models, the convergence of these results has to be verified with respect to the slab thickness.

Environment	Stabilization Energy
Inclusion	-0.94
Inclusion (n=1)	0.21
Inclusion (n=2)	0.32
Inclusion (n=4)	0.29
Inclusion (large tube)	0.31

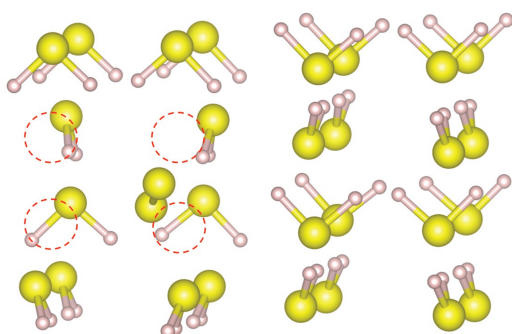
Table 10: Stability (eV) of S<sub>2</sub> in voids within the H<sub>2</sub>S ice (n: number of molecules removed to create the void)



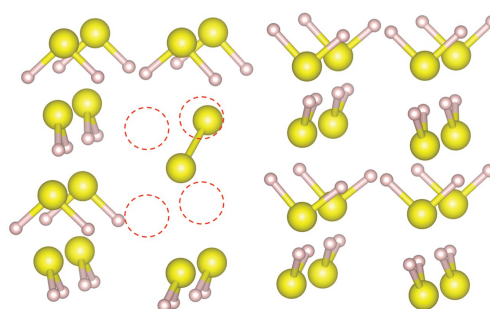
**Inclusion (n=1)**



**Inclusion (n=2)**



**Inclusion (n=4)**



**Inclusion (large tube)**

Figure 13: The optimized crystalline structures of  $S_2$  trapped in  $H_2S$  ice within different types of cavities

### **b) Extended cell (6 layer cell)**

The 6 layers cell is obtained by addition of two layers to the initial  $H_2S$  ice slab. The two outer layers positions are kept constant whereas the other four layers in between optimized with  $S_2$  in it.

Without surprise, as in all models considered, the simple inclusion of  $S_2$  into the perfect crystalline ice is not stable thermodynamically. As can be seen in Table 11, similarly to the results obtained above with the primitive cell,  $S_2$  can be trapped within all the cavities formed in the  $H_2S$  ice bulk. Five different cavities are considered, starting from the removal of 1  $H_2S$  molecules to the removal of 4. Smaller cavities are obtained with the removal of 1 and 2  $H_2S$  molecules, whereas a larger cavity obtained with the removal of 4  $H_2S$  molecules



in different layers. Among them, two cases might be qualified extreme, the “fine tube”, obtained by the removal of 2  $\text{H}_2\text{S}$  molecules from a layer parallel to the side of the slab and the “large” tube, obtained by the removal of 4  $\text{H}_2\text{S}$  molecules, both forming hollow tubes of  $\text{H}_2\text{S}$ .

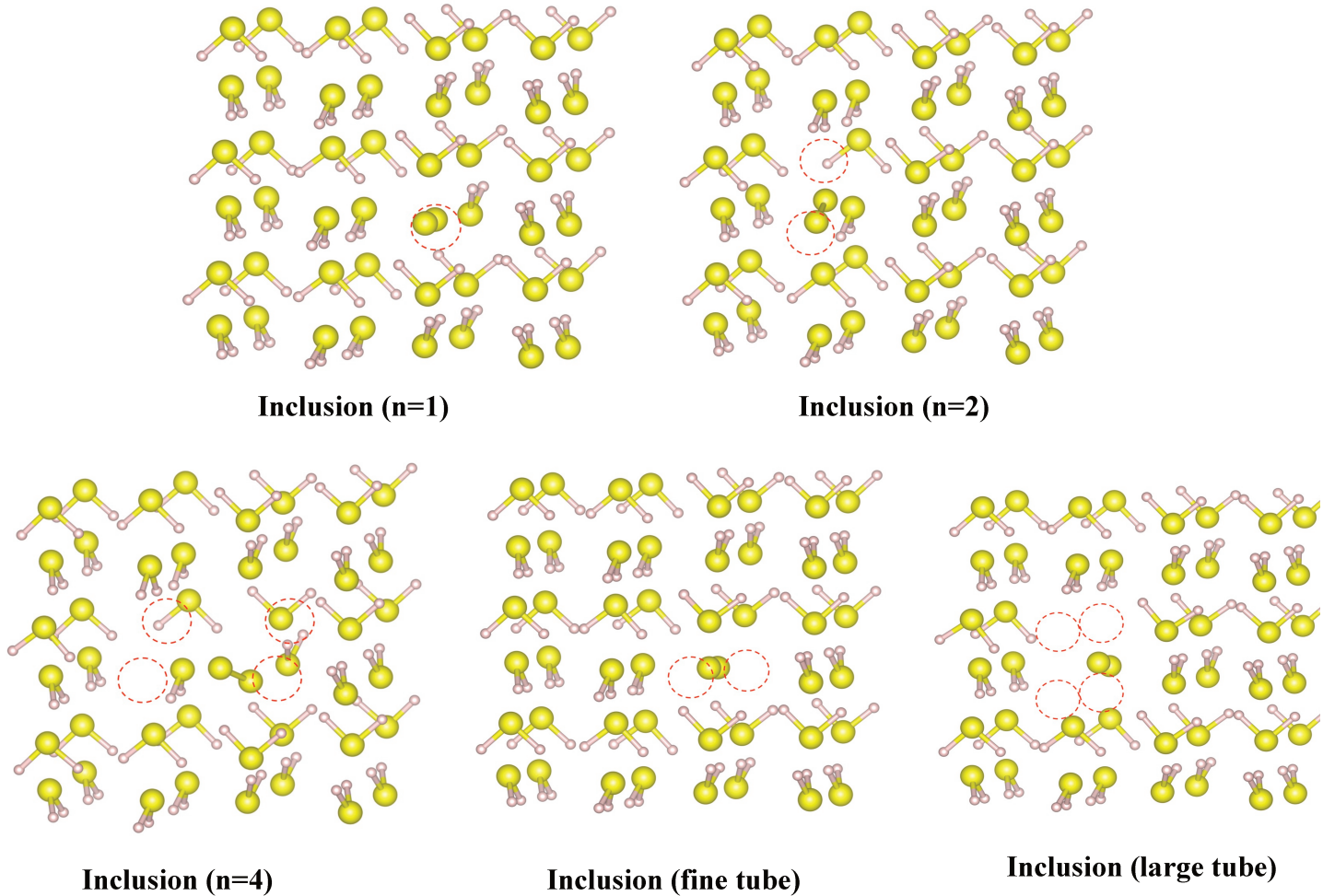


Figure 13: The optimized crystalline structures of  $\text{S}_2$  trapped in  $\text{H}_2\text{S}$  ice within different type of cavities

As in the 4 layer cell model,  $\text{S}_2$  can be trapped even inside a small cavity ( $n=1$ ) with a stabilization energy of 0.29 eV, (a value close to the 0.21 eV in the small model) and this value increases with the size of the cavity, tending to an asymptotic value. But the values obtained in this larger model, 0.45 eV with a cavity produced by the removal of 2  $\text{H}_2\text{S}$  and 0.4 – 0.5 eV for the even larger cavities, including tubes, shows a stronger stabilization.

In the case of the trapping of  $\text{S}_2$  in  $\text{H}_2\text{O}$  ice, the stabilization energy remains same passing from 4 bi-layers model to 6 bi-layers. However, the trapping of  $\text{S}_2$  in  $\text{H}_2\text{S}$  is different,



the stabilization energy values increase systematically about 0.1 eV in average passing from the 4 bi-layer model to the 6 bi-layer model. This is significant and could indicate that the 4 bi-layer model might be considered as too limited to represent the inclusion cases in H<sub>2</sub>S ice; so we rely on the 6 bi-layer model results to answer about the stability of S<sub>2</sub> in H<sub>2</sub>S ice.

Environment	Stabilization Energy
Inclusion	-0.69
Inclusion (n=1)	0.29
Inclusion (n=2)	0.45
Inclusion (n=4)	0.41
Inclusion (fine tube)	0.41
Inclusion (large tube)	0.49

Table 11: Stability (eV) of S<sub>2</sub> in voids within the H<sub>2</sub>S ice (n: number of molecules removed to create the void)

Globally, S<sub>2</sub> can be trapped into the H<sub>2</sub>S ice bulk efficiently enough to remain stable until the sublimation of the ice. The stabilization energy sets up around 0.4 - 0.5 eV within the cavities large enough to host S<sub>2</sub>, a value in the same order of magnitude as with the trapping of S<sub>2</sub> in H<sub>2</sub>O ice. Thus, being stable in H<sub>2</sub>S ice as much as in H<sub>2</sub>O ice, S<sub>2</sub> can sublime in the same way and at the same time with both, H<sub>2</sub>S and H<sub>2</sub>O surrounding molecules.

## Appendix A

Assuming that  $\text{H}_2\text{S}$  ice domains in the water ice, are pure condensates, we chose the most stable crystalline structure of  $\text{H}_2\text{S}$  in low temperature and pressure to study the trapping of  $\text{S}_2$ . Solid  $\text{H}_2\text{S}$  has three crystalline phases (I, II and III), which were observed below the melting point at ambient pressure (Sandor & Ogunade 1969; Anderson et al. 1977). Phase I is stable between 187.6 and 126.2 K and II between 126.2 and 103.5 K and both of them have cubic lattices with four molecules in the unit cells with phase I having  $\text{Fm}\bar{3}\text{m}$  space group, phase II, having  $\text{Pa}\bar{3}$ . The phase III observed below 103.5 K, has an orthorhombic ( $\text{Pbcm}$ ) lattice (Cockcroft et al. 1990); being present at the lowest temperature, it is the most adapted to our study, taking into account the environment conditions.

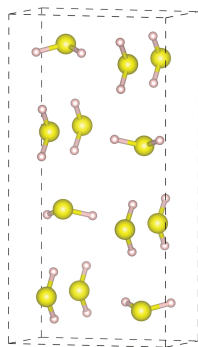


Figure 10: The unit cell of phase III  $\text{H}_2\text{S}$  ice

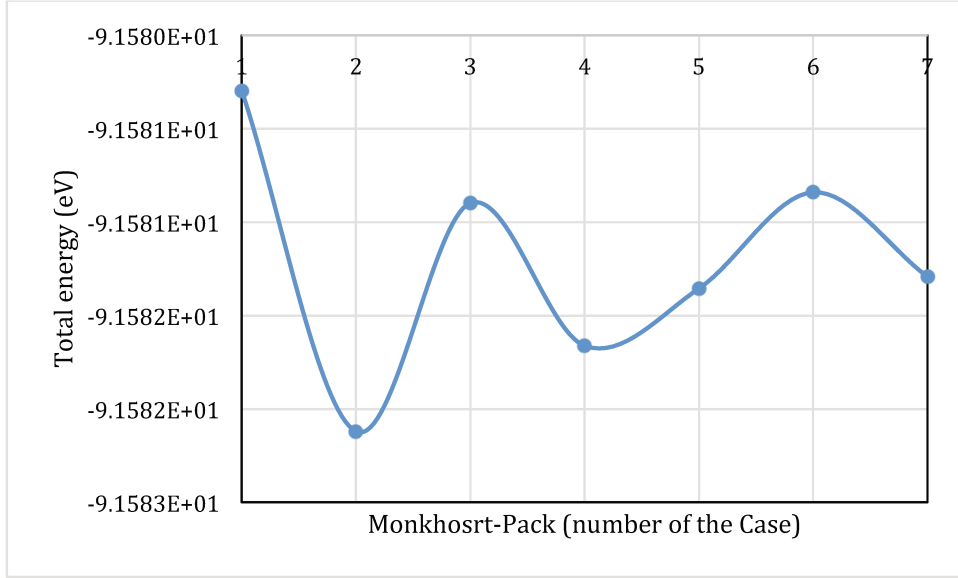
### Technical Procedure to Model Ice Slab

This structure (phase III) was determined by powder neutron diffraction studies of  $\text{D}_2\text{S}$  solid. It is orthorhombic with space group  $\text{Pbcm}$  and its cell constants are  $a=4.0760 \text{ \AA}$ ,  $b=13.3801 \text{ \AA}$  and  $c=6.7215 \text{ \AA}$ , which is taken as a starting point for the unit cell in our calculations. Before optimizing the cell parameters, the number of k-points has been tested to properly define the grid points in k-space. The length of the cell parameters being in a 3:1:2 ratio, the k-points have been chosen according to this ratio.

The total energies obtained with increasing number of k-points have been reported in table 10 and in graphic 1. We choose the 12 4 8 Monkhorst-Pack which gives the converged energy of -91.581 eV.

Case	Monkhorst-Pack	Total Energy (eV)
1	6 2 4	-91.58029718
2	9 3 6	-91.58212037
3	12 4 8	-91.58089840
4	18 6 12	-91.58166210
5	24 8 16	-91.58135569
6	27 9 18	-91.58084044
7	36 12 24	-91.58129311

Table 10: The Monkhorst-Pack vs. total energy of the ice (eV)



Graphic 1: The Monkhorst-Pack grid (for the number of the case, please refer to table10) vs. total energy of the ice (eV)

Once the number of k-points is chosen, the dimensions of the cell parameters have been optimized with `isif=7` option in VASP. Within this option, the position of the ions and the cell shape remain fixed whereas volume of the cell changes. However, in case volume changes, an error called the Pulay stress arises from the fact that the plane wave basis set is not complete with respect to changes of the volume. It affects the stress tensor calculated by the VASP; the diagonal components of the stress tensor are incorrect. Also all volume relaxation algorithms in VASP work with a constant basis set, so all energy changes are strictly consistent with the calculated stress tensor, as a result of which, the equilibrium

volume is calculated underestimated. To prevent it, a large energy cut off must be used (ENMAX=1.3 x default value) and with high precision option (PREC=High). In this study also, the large energy cut off have been applied to optimize cell parameters. The optimized cell parameters are:  $a=4.1410 \text{ \AA}$ ,  $b=13.5932 \text{ \AA}$  and  $c=6.8285 \text{ \AA}$ .

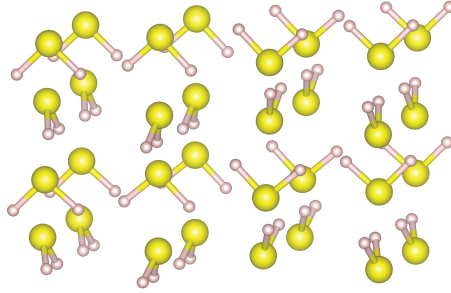


Figure 11: The crystalline structure of  $\text{H}_2\text{S}$  slab

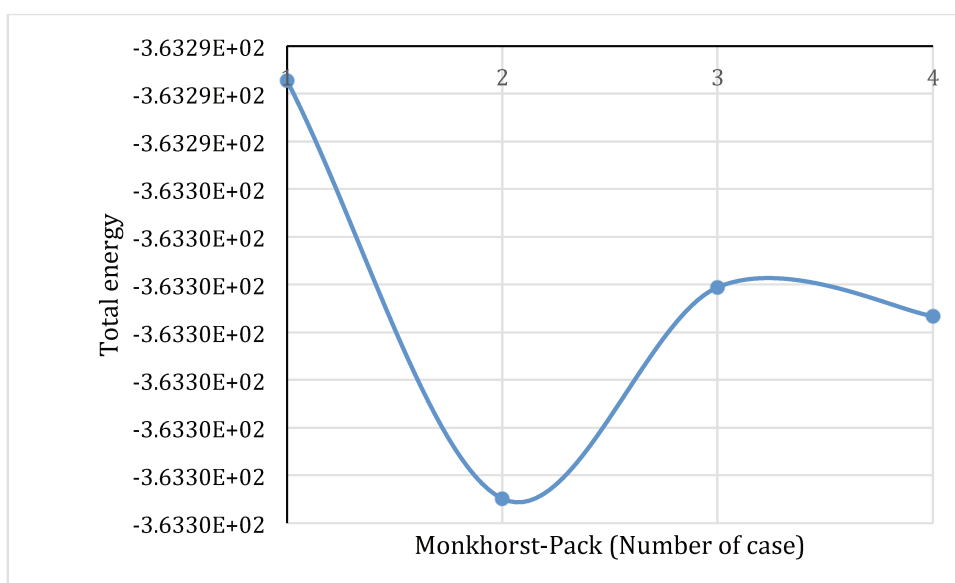
To obtain the slab to model ice structures for the adsorption and inclusion cases, the unit cell with optimized cell parameters are multiplied in two directions (b and c) and then this multiple cell has been cut from 0001 plane. Within this new structure, a new set of k-points has been tested. The total energies with respect to the number of k-points has been given in table 11 and graphic 2. According to the results, we chose the 4 4 1 Monkhorst-Pack for which the total energy is converged.

Monkhorst-Pack	Total Energy (eV)
2 2 1	-363.2927302
3 3 1	-363.3014857
4 4 1	-363.2970542
6 6 1	-363.2976579

Table 11 : The Monkhorst-Pack vs. total energy of the ice (eV)

To describe properly the two-dimension surface, since VASP code is periodic code in three dimensions, we recall that there should be sufficient width of vacuum in the direction perpendicular to the surface direction to avoid interaction of the adsorbate with the image of the ice cell. However, increase in vacuum also demands higher calculation resources. For this

reason, the total energy of the system is calculated with increasing vacuum width until the total energy reaches the convergence and this value is kept for all calculations.



Graphic 2 The Monkhorst-Pack grid (for the number of the case, please refer to table 11) vs. total energy of the ice (eV)

### III Published articles

THE ASTROPHYSICAL JOURNAL LETTERS, 823:L41 (5pp), 2016 June 1  
© 2016. The American Astronomical Society. All rights reserved.

doi:10.3847/2041-8205/823/2/L41



#### ORIGIN OF MOLECULAR OXYGEN IN COMET 67P/CHURYUMOV–GERASIMENKO

O. MOUSIS<sup>1</sup>, T. RONNET<sup>1</sup>, B. BRUGGER<sup>1</sup>, O. OZGUREL<sup>2</sup>, F. PAUZAT<sup>2</sup>, Y. ELLINGER<sup>2</sup>, R. MAGGIOLIO<sup>3</sup>, P. WURZ<sup>4</sup>, P. VERNAZZA<sup>1</sup>,  
J. I. LUNINE<sup>5</sup>, A. LUSPAY-KUTI<sup>6</sup>, K. E. MANDT<sup>6</sup>, K. ALTWEGG<sup>4</sup>, A. BIELER<sup>4</sup>, A. MARKOVITS<sup>2</sup>, AND M. RUBIN<sup>4</sup>

<sup>1</sup> Aix Marseille Université, CNRS, LAM (Laboratoire d'Astrophysique de Marseille) UMR 7326, F-13388, Marseille, France; [olivier.mousis@lam.fr](mailto:olivier.mousis@lam.fr)

<sup>2</sup> Laboratoire de Chimie Théorique, Sorbonne Universités, UPMC Univ. Paris 06, CNRS UMR 7616, F-75252 Paris CEDEX 05, France

<sup>3</sup> Royal Institute for Space Aeronomy, 3 Avenue Circulaire, Brussels, Belgium

<sup>4</sup> Physikalisches Institut, University of Bern, Sidlerstrasse 5, CH-3012 Bern, Switzerland

<sup>5</sup> Department of Astronomy and Carl Sagan Institute, Space Sciences Building Cornell University, Ithaca, NY 14853, USA

<sup>6</sup> Department of Space Research, Southwest Research Institute, 6220 Culebra Rd., San Antonio, TX 78228, USA

Received 2016 March 28; revised 2016 April 25; accepted 2016 April 26; published 2016 June 1

#### ABSTRACT

Molecular oxygen has been detected in the coma of comet 67P/Churyumov–Gerasimenko with abundances in the 1%–10% range by the *Rosetta* Orbiter Spectrometer for Ion and Neutral Analysis-Double Focusing Mass Spectrometer instrument on board the *Rosetta* spacecraft. Here we find that the radiolysis of icy grains in low-density environments such as the presolar cloud may induce the production of large amounts of molecular oxygen. We also show that molecular oxygen can be efficiently trapped in clathrates formed in the protosolar nebula (PSN), and that its incorporation as crystalline ice is highly implausible, because this would imply much larger abundances of Ar and N<sub>2</sub> than those observed in the coma. Assuming that radiolysis has been the only O<sub>2</sub> production mechanism at work, we conclude that the formation of comet 67P/Churyumov–Gerasimenko is possible in a dense and early PSN in the framework of two extreme scenarios: (1) agglomeration from pristine amorphous icy grains/particles formed in ISM and (2) agglomeration from clathrates that formed during the disk's cooling. The former scenario is found consistent with the strong correlation between O<sub>2</sub> and H<sub>2</sub>O observed in comet 67P/Churyumov–Gerasimenko's coma while the latter scenario requires that clathrates formed from ISM icy grains that crystallized when entering the PSN.

**Key words:** astrobiology – comets: general – comets: individual (67P/Churyumov–Gerasimenko) – methods: numerical – solid state: volatile

#### 1. INTRODUCTION

The *Rosetta* Orbiter Spectrometer for Ion and Neutral Analysis (ROSINA) Double Focusing Mass Spectrometer (DFMS) on board the *Rosetta* spacecraft (Balsiger et al. 2007) enabled the detection of O<sub>2</sub> in the coma of comet 67P/Churyumov–Gerasimenko (67P/C–G) with local abundances in the 1%–10% range and a mean value of  $3.80 \pm 0.85\%$  (Bieler et al. 2015). A subsequent reinvestigation of the 1P/Halley data from the Giotto Neutral Mass Spectrometer also indicates that the coma of comet 1P/Halley should contain O<sub>2</sub> with an abundance of  $3.7 \pm 1.7\%$  with respect to water, suggesting that this molecule may be a rather common parent species in comets (Rubin et al. 2015b).

To investigate the origin of O<sub>2</sub> in 67P/C–G, Bieler et al. (2015) considered the possibility of O<sub>2</sub> production via the radiolysis of water ice incorporated within the nucleus. Based on 67P/C–G's known orbital history, they estimated that any O<sub>2</sub> produced during the residence time of 67P/C–G in the Kuiper Belt was quickly lost during the first pass or two around the Sun. The authors further found that radiolysis on closer orbit to the Sun would most likely only affect the top few micrometers of the nucleus' active surface. In this case, the O<sub>2</sub>/H<sub>2</sub>O ratio produced in these conditions would decrease with depth. Because they did not observe any variation of the O<sub>2</sub>/H<sub>2</sub>O ratio during the sampling period, Bieler et al. (2015) ruled out the hypothesis of O<sub>2</sub> production via the radiolysis and determined that O<sub>2</sub> must have been incorporated into 67P/C–G at the time of its formation in the protosolar nebula (PSN).

In order to explain how O<sub>2</sub> could have been incorporated into the ices of 67P/C–G, we investigate here the radiolysis

hypothesis at epochs prior to the formation of comets, when icy grains were the dominant solid phase of the outer PSN. Furthermore, we examine the different trapping scenarios of O<sub>2</sub> that could explain its presence. Because some recent works suggest that this comet may have been accreted from a mixture of clathrates and pure crystalline ices formed in the PSN (Luspay-Kuti et al. 2016; Mousis et al. 2016), we study the propensity for O<sub>2</sub> trapping in clathrates, and also evaluate if its condensation as pure crystalline ice is consistent with the comet's inferred composition. Among all these investigated mechanisms, we find that clathration of O<sub>2</sub> is efficient in the PSN and that radiolysis can explain the formation of O<sub>2</sub> and its stabilization in icy grains. However, to produce enough O<sub>2</sub> molecules, the radiolysis of icy grains must have happened in a low-density environment such as the presolar cloud.

#### 2. O<sub>2</sub> FORMATION VIA RADIOLYSIS

We first investigate the possibility of radiolytic production of O<sub>2</sub> in icy grains present in the outer PSN prior to their agglomeration by 67P/C–G. The energy available for radiolysis is provided by the galactic cosmic ray flux (CRF) impacting icy grains. In the following, since galactic CRF can penetrate into water ice down to depths of a few tens of meters (Cooper et al. 1998), we only consider icy grains with sizes below this limit, implying that no H<sub>2</sub>O ice can be out of reach of radiolysis. In our calculations, we use the energy range and CRF distribution from Yeghikyan (2011) and Cooper et al. (2003), respectively. The CRF energy dose absorbed by icy grains located at 30 au from the Sun is within the  $\sim(5\text{--}60) \times 10^{16} \text{ eV kg}^{-1} \text{ yr}^{-1}$  range, depending on the disk's



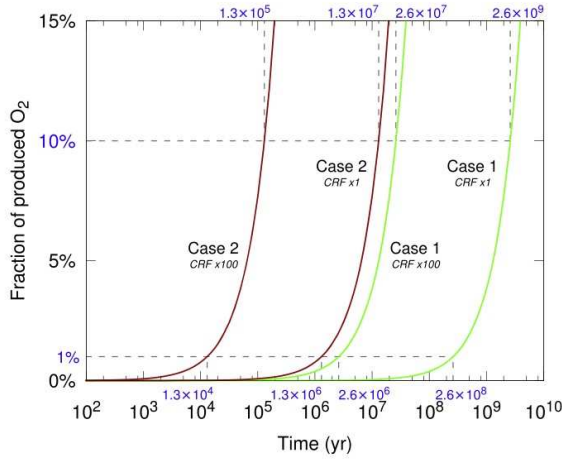


**Figure 1.** Time evolution of the fraction of  $O_2$  molecules produced by cosmic rays in an icy grain. Case 1 (green curves) considers the irradiation of an icy grain placed at 30 au in the PSN. Case 2 (red curves) considers the irradiation of an icy grain located in a low-density environment ( $\sim 10^{-3} \text{ g cm}^{-2}$ ). Two CRF values are explored in each case, namely 1 and 100 times the nominal CRF value (see the text).

surface density (between 10 and  $10^3 \text{ g cm}^{-2}$ ; see Hersant et al. 2001).

$O_2$  is produced by radiolysis of water ice through the chemical reaction  $2 \text{ H}_2\text{O} \rightarrow 2 \text{ H}_2 + \text{O}_2$ , with an amount of energy needed to alter one  $\text{H}_2\text{O}$  molecule  $W_r = 235 \text{ eV}$  (Johnson 1991).  $\text{H}_2$  is then rapidly lost from the water ice due to its fast diffusion. Further reactions with  $\text{O}_2$  are precluded because the diffusion of these molecules is slowed down by the disk's low temperatures (Johnson 1990). We have thus assumed that all the energy absorbed by water ice is used to form  $\text{O}_2$ . To reach the molecular ratio  $\text{O}_2/\text{H}_2\text{O}$  (1%–10%) measured by Bieler et al. (2015) in 67P/C-G, cosmic rays must alter twice as many  $\text{H}_2\text{O}$  molecules in icy grains. The time  $\tau$  needed to reach this ratio is then given by

$$\tau = \frac{W_r \cdot N_A}{E_{\text{CR}} \cdot M_{\text{H}_2\text{O}}} \times f_{\text{H}_2\text{O}} \quad (1)$$

where  $N_A$  ( $\text{mol}^{-1}$ ) is the Avogadro constant,  $M_{\text{H}_2\text{O}}$  ( $\text{kg mol}^{-1}$ ) is the molar mass of water,  $E_{\text{CR}}$  ( $\text{eV kg}^{-1} \text{ yr}^{-1}$ ) is the CRF energy dose received by water ice and  $f_{\text{H}_2\text{O}}$  is the fraction of altered  $\text{H}_2\text{O}$  molecules, which corresponds to two times the fraction of  $\text{O}_2$  produced.

Figure 1 shows the results of our calculations. An  $\text{O}_2$  fraction in the 1%–10% range is reached in  $\sim 0.25$ – $2.5 \text{ Gyr}$  at the aforementioned nominal CRF value (Case 1). These extremely long time periods are incompatible with the lifetime of icy grains in the PSN (a few  $10^4$  year; Weidenschilling & Cuzzi 1993). If icy grains have grown to sizes larger than tens of meters in the PSN, then the deepest layers should remain unaltered. In this case, even longer timescales would be needed for  $\text{O}_2$  formation. However, the CRF may have undergone significant enhancements throughout the history of the solar system, by a factor of  $\sim 3$  during its passages through the Milky Way's spiral arms (a few tens of Myr every 400–500 Myr; Effenberger et al. 2012; Werner et al. 2015; Alexeev 2016), or even by a factor of  $\sim 100$  during a few kyr because of a close supernova explosion ( $< 30 \text{ pc}$ ; Fields &

Ellis 1999). Such enhancements can decrease the time needed to form  $\text{O}_2$  by up to a factor of 100, which is still too long for our consideration.

We also consider the possibility of an icy grain receiving the maximum CRF energy dose estimated by Yeghikyan (2011), namely  $\sim 1.20 \times 10^{20} \text{ eV kg}^{-1} \text{ yr}^{-1}$ . This value leads to a time  $\tau$  in the  $\sim 1$ – $10 \text{ Myr}$  range (see case 2 of Figure 1), or  $\sim 10$ – $100 \text{ kyr}$  with a CRF enhanced by a factor of 100. However, such a high value of  $E_{\text{CR}}$  corresponds to a surface density of  $10^{-3} \text{ g cm}^{-2}$ , which can only be reached in molecular clouds. In such environments, the column densities would be low enough to form 1%–10% of  $\text{O}_2$  in the icy grains even on very short timescales. Therefore, to incorporate significant amounts of  $\text{O}_2$  produced via radiolysis of icy grains, cometary grains must have formed in the presolar cloud prior to disk formation.

### 3. $O_2$ STABILITY IN WATER ICE

An important question is whether  $\text{O}_2$  molecules produced via radiolysis of ice grains can remain stabilized within the water icy matrix of 67P/C-G. The stabilization energy is defined as the difference between the energy of the system of  $\text{O}_2$  interacting with the ice and the sum of the energies of the pure ice and  $\text{O}_2$  at infinite separation. To investigate this problem, a sampling of the representative structures of  $\text{O}_2$  in solid water ice has been obtained using a strategy based on first principle periodic density functional theory quantum calculations, that has been proven to be appropriate for modeling bulk and surface ice structures (Lattalais et al. 2011, 2015; Ellinger et al. 2015). Among the different forms, we considered the apolar variety of hexagonal ice *Ih* because these structures have a balanced distribution of alternating hydrogen and oxygen avoiding computational artifacts for surface optimizations and at the same time reproduce the bulk properties (Casassa et al. 2005). How  $\text{O}_2$  behaves as a function of the number of  $\text{H}_2\text{O}$  molecules removed is illustrative of the storage capability of the ice as a function of porosity. The results of our calculations, performed using the Vienna ab initio simulation package (Kresse & Hafner 1993, 1994), are presented below.

1. Starting with no  $\text{H}_2\text{O}$  removed, i.e., the pure crystalline ice, we found no stabilization for the inclusion of  $\text{O}_2$  in the hexagonal lattice. It is in fact an endothermic process.
2. With one  $\text{H}_2\text{O}$  removed, and replaced by one  $\text{O}_2$ , we have a substitution structure whose stabilization, in the order of  $10^{-3} \text{ eV}$ , is meaningless.
3. With 2, 3, and 4 adjacent  $\text{H}_2\text{O}$  molecules removed from the hexagonal lattice we obtained well defined cavities that, after reconstruction, show different shapes according to the positions of the entities removed. The stabilization energies were found to be on the order of 0.2–0.3 eV, going to 0.4–0.5 eV for an embedded  $\text{O}_2$  dimer. A typical structure of embedding is illustrated in Figure 2 where  $\text{O}_2$  is stabilized with an energy of  $\sim 0.23 \text{ eV}$ . This energy is on the order of that of a water dimer, which means that the presence of  $\text{O}_2$  should not perturb the ice structure until it is ejected into the coma via sublimation with the surrounding  $\text{H}_2\text{O}$  molecules.

It should be stressed that the formation of one  $\text{O}_2$  requires at least the destruction of two  $\text{H}_2\text{O}$ . The present simulation is fully consistent with the aforementioned radiolysis hypothesis, where the irradiation process is at the origin of both the formation of  $\text{O}_2$  and the development of the cavity in which it



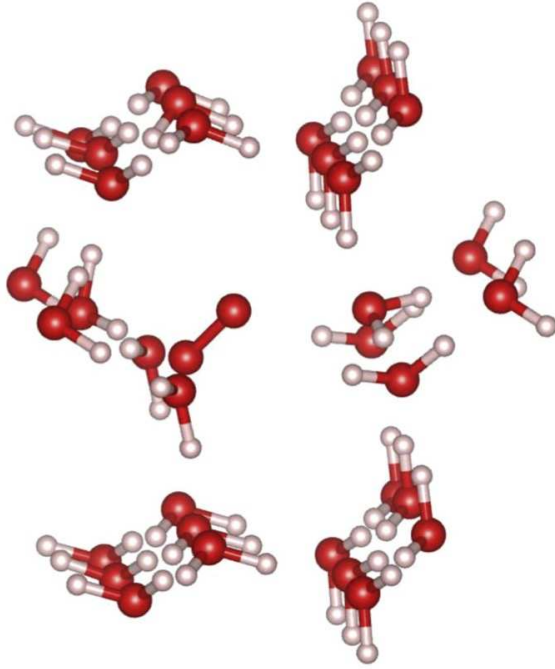


**Figure 2.** Side view of  $O_2$  embedded in a cavity inside compact amorphous ice. The cavity corresponds to a void of 3  $H_2O$  molecules from an hexagonal apolar lattice.

remains sequestered. Similar results are obtained in the case of  $O_2$  stabilization in amorphous ice.

#### 4. $O_2$ CLATHRATION IN THE PSN

One possible source of  $O_2$  in the nucleus of 67P/C-G is the trapping of  $O_2$  in clathrates that formed in the PSN prior to having been agglomerated by the comet as it formed. This is supported by recent works showing that the  $Ar/CO$  and  $N_2/CO$  ratios and the time variation of other volatile species measured in 67P/C-G's coma are found to be consistent with the presence of clathrates in its nucleus (Luspay-Kuti et al. 2016; Mousis et al. 2016). To investigate the amount of  $O_2$  that could have been trapped in clathrates and now be present in 67P/C-G, we use the same statistical thermodynamic model as the one described in Mousis et al. (2010, 2016), which is used to estimate the composition of these crystalline structures formed in the PSN. To evaluate the trapping efficiency of  $O_2$ , we consider a gas constituted of  $O_2$  and  $CO$ . After  $H_2O$ ,  $CO$  is one of the dominant gases found in 67P/C-G (Le Roy et al. 2015) and in most of comets (Bockelée-Morvan et al. 2004, p. 391). The Kihara parameters for the molecule-water interactions employed in our calculations are derived from Mohammadi et al. (2003) for  $O_2$  and from Mohammadi et al. (2005) for  $CO$ . These represent the most recent sets of data found in the literature for the two species. We refer the reader to the model description provided in Mousis et al. (2010) for further details.

When clathrates destabilize in the nucleus, the trapped volatiles are released prior to water sublimation, implying that the water vapor measured at the time of the  $O_2$  sampling by ROSINA should be derived from the vaporization of crystalline

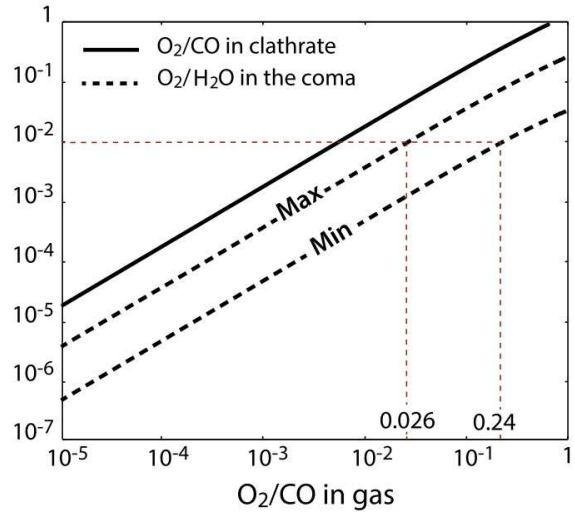


**Figure 3.**  $O_2/CO$  ratio in clathrates formed at 45 K and the corresponding  $O_2/H_2O$  ratio in the coma, as a function of the coexisting  $O_2/CO$  ratio in the PSN gas phase. The “Min” and “Max” labels correspond to calculations of the  $O_2/H_2O$  ratio in 67P/C-G's coma, assuming that the  $CO/H_2O$  abundance is between 2.7% and 21% (see the text). The vertical red dashed lines represent the  $O_2/CO$  ratio in the PSN gas phase needed to form clathrates giving 1%  $O_2$  relative to  $H_2O$  in the coma.

ice layers located closer to the surface. Hence, the  $O_2$  depletion is better quantified by comparing the  $O_2/CO$  ratio in clathrates and the coma value since these two species are expected to be released simultaneously from destabilized clathrates. Figure 3 represents the value of the  $O_2/CO$  ratio in structure I clathrates<sup>7</sup> as a function of the  $O_2/CO$  ratio in the coexisting gas phase at a chosen disk's temperature of  $\sim 45$  K. This value is within the temperature range needed for clathrates to form in the PSN from a gaseous mixture of protosolar composition that reproduces the  $Ar/CO$  and  $N_2/CO$  ratios measured in 67P/C-G's coma (Mousis et al. 2016). We find that, whatever the  $O_2/CO$  ratio considered for the initial PSN gas phase, it is enriched by a factor of  $\sim 1.4$ – $1.8$  in the formed clathrate. Figure 3 also shows that the  $O_2/CO$  ratio must be in the 0.026–0.24 range in the PSN gas phase for the clathrate trapping mechanism to agree with the measured range of  $O_2/H_2O$  in the coma ( $\sim 1\%$ ), assuming that all cavities are filled by guest molecules and that the  $CO/H_2O$  abundance ratio in the coma corresponds to the sampled value ( $\sim 2.7\%$ – $21\%$ ; Le Roy et al. 2015). This range of  $O_2/CO$  ratios is consistent with values obtained at distances beyond  $\sim 5$  au in a T Tauri disk (Walsh et al. 2015). Therefore, our calculations show that the clathration of  $O_2$  in the PSN is a realistic mechanism to account for the  $O_2/H_2O$  ratio observed by ROSINA in 67P/C-G's coma.

#### 5. $O_2$ CONDENSATION IN THE PSN

An alternative possibility for the observed presence of  $O_2$  in the coma of 67P/C-G is that the  $O_2$  could have been agglomerated as pure crystalline ice by the nucleus forming at cooler PSN temperatures than those required for clathration.

<sup>7</sup> Both  $O_2$  and  $CO$  molecules are expected to form this structure (Mohammadi et al. 2003, 2005).

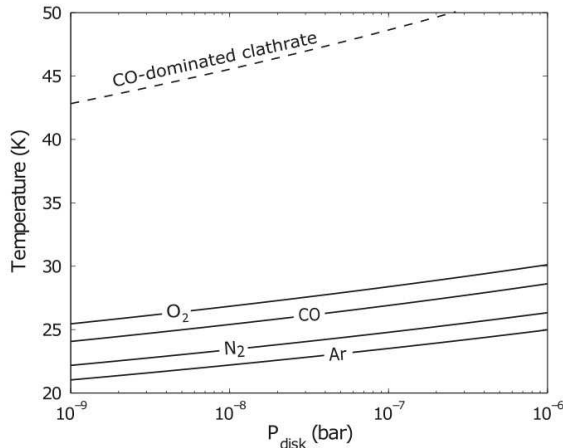


**Figure 4.** Solid lines: equilibrium curves of  $O_2$ ,  $CO$ ,  $N_2$ , and  $Ar$  pure crystalline ices as a function of total disk pressure. Dashed line: equilibrium curve of the CO-dominated clathrate as a function of total disk pressure (see the text).

To investigate this scenario, we calculated the temperature dependence of the equilibrium curves of  $O_2$ ,  $CO$ ,  $N_2$ , and  $Ar$  pure crystalline ices via the use of the polynomial relations reported by Fray & Schmitt (2009). To derive the partial pressures for each gas, we assumed that  $O$ ,  $C$ ,  $N$ , and  $Ar$  exist in protosolar abundances in the PSN (Lodders et al. 2009), with all  $C$  and all  $N$  in the forms of  $CO$  and  $N_2$ , respectively. The partial pressure of  $O_2$  is derived from the  $O_2/CO$  gas phase ratio ( $\sim 33\%$ ) predicted beyond the snowline of a T Tauri disk via an extensive chemical model (Walsh et al. 2015). The equilibrium curves of  $O_2$ ,  $CO$ ,  $N_2$ , and  $Ar$  pure crystalline ices are represented along with the equilibrium curve of the  $CO$ - $N_2$ - $Ar$  multiple guest clathrate proposed by Mousis et al. (2016) to explain 67P/C-G's composition, as a function of the total PSN pressure in Figure 4. Because the  $CO$ - $N_2$ - $Ar$  multiple guest clathrate is by far dominated by  $CO$  (see Figure 1 of Mousis et al. 2016), we assume that its partial pressure is the same as for  $CO$  crystalline ice. The equilibrium curve of the clathrate is taken from Lectez et al. (2015).

From the examination of the condensation sequence presented in Figure 4, we find that the hypothesis of  $O_2$  agglomeration as pure crystalline ice is inconsistent with 67P/C-G's current composition. The fact that  $Ar/CO$  and  $N_2/CO$  ratios are found to be significantly depleted by factors of  $\sim 90$  and  $10$  in 67P/C-G's coma, respectively, compared to the protosolar values (Balsiger et al. 2015; Rubin et al. 2015a; Mousis et al. 2016), implies that  $Ar$  and  $N_2$  cannot form substantial amounts of pure crystalline ices at the formation location of the comet in the PSN (Mousis et al. 2016). Instead, it has been proposed that these volatiles were mostly trapped in  $CO$ -dominated clathrates (Mousis et al. 2016). Under these circumstances, because the equilibrium curve of  $O_2$  ice is in the vicinity of those of  $Ar$  and  $N_2$  ices, the incorporation of  $O_2$  in this form would require the trapping of larger amounts of  $Ar$  and  $N_2$ , incidentally leading to quasi protosolar  $Ar/CO$  and  $N_2/CO$  ratios. This does not agree with the depleted ratios observed in 67P/C-G.

## 6. CONCLUSIONS

In this study, we have investigated several scenarios that may explain the presence of molecular oxygen in the nucleus of 67P/C-G. Our results are the following:

1. Even with a strong CRF enhancement due to the presence of a nearby supernova, we find that the radiolysis of icy grains is not fast enough in the PSN to create amounts of  $O_2$  comparable with those observed in 67P/C-G. Instead, icy grains must be placed in low-density environments such as molecular clouds to allow radiolysis to work efficiently. The irradiation process also favors the stabilization of  $O_2$  molecules in the icy matrix via the development of cavities and is compatible with both amorphous and crystalline ice structures.
2.  $O_2$  can be efficiently trapped in clathrates formed in the PSN. The  $O_2/CO$  ratio in the clathrate phase is up to  $\sim 2$  times the  $O_2/CO$  ratio in the coexisting PSN gas phase.
3. The incorporation of  $O_2$  as pure crystalline ice is unlikely in 67P/C-G because the condensation of this species in the PSN would imply much larger abundances of  $Ar$  and  $N_2$  than those observed in the coma.

Based on these results, and assuming that radiolysis has been the only mechanism for producing  $O_2$ , we find that the formation of 67P/C-G is possible in a dense and early PSN in the framework of two extreme scenarios: (1) agglomeration from pristine amorphous icy grains/particles formed in the ISM and (2) agglomeration from multiple guest clathrates including  $O_2$  that formed during the cooling of the disk subsequent to the vaporization of the amorphous icy grains entering the PSN. However, scenario 1 was found inconsistent with ROSINA pre-perihelion observations of volatile abundances in the coma. In contrast, Mousis et al. (2016) and Luspay-Kuti et al. (2016) have shown that scenario 2 could match these data if 67P/C-G agglomerated from a mixture of clathrates and crystalline ices that condensed in the PSN. Also, scenario 2 is compatible with a possible chemical production of  $O_2$  in the PSN gas phase (Walsh et al. 2015). In this picture, whatever the considered source, i.e., radiolysis of ISM grains or/and PSN gas phase chemistry,  $O_2$  is efficiently entrapped in clathrates prior to their agglomeration by 67P/C-G.

On the other hand, with the incorporation of  $O_2$  in the cavities created by CRF in the icy matrix, scenario 1 naturally provides an explanation for the strong correlation found between the  $O_2$  and  $H_2O$  production rates observed in 67P/C-G's coma (Bieler et al. 2015). If this scenario is correct, this would make implausible the accretion of 67P/C-G from clathrates and crystalline ices originating from the PSN. Meanwhile, a way to reconcile scenario 2 with the strong  $O_2$ - $H_2O$  correlation would be to assume that the icy grains initially formed as in scenario 1. These icy grains/particles would have then subsequently experienced an amorphous-to-crystalline phase transition in the  $130$ – $150$  K temperature range when entering the disk (Kouchi et al. 1994; Maldoni et al. 2003; Ciesla 2014). In this alternative scenario, all volatiles initially adsorbed by ISM amorphous ice would be released in the PSN gas phase during phase transition. With the cooling of the disk, these volatiles would have been later trapped in the clathrates formed with the crystallized icy grains. The case of  $O_2$  is unique because, due to its formation process, this molecule is inserted into the icy matrix. In spite of the phase transition,  $O_2$  would remain stable within the icy matrix because the strength of the



interaction between O<sub>2</sub> and the surrounding H<sub>2</sub>O molecules is expected not to decrease (eventually increase) upon crystallization. In this scenario, CO, Ar, and N<sub>2</sub> would be trapped in clathrates with O<sub>2</sub> remaining embedded in water, in a way consistent with the observed correlation.

To conclude, further post-perihelion *ROSINA* data, in particular the precise measurements of the relative abundances of the different volatiles as a function of geography and time, are needed to disentangle between the existing formation scenarios. It is also possible that only the in situ sampling of a nucleus by a future lander will provide a definitive answer to the question of the formation conditions of 67P/C-G and other Jupiter Family Comets in the PSN.

O.M. acknowledges support from CNES. This work has been partly carried out thanks to the support of the A\*MIDEX project (n° ANR-11-IDEX-0001-02) funded by the “Investissements d’Avenir” French Government program, managed by the French National Research Agency (ANR). This work also benefited from the support of CNRS-INSU national program for planetology (PNP). R.M. was supported by the Belgian Science Policy Office through the Solar-Terrestrial Centre of Excellence and by PRODEX/ROSETTA/ROSINA PEA 4000107705. J.I.L. acknowledges support from JWST. K.E. M. acknowledges support from JPL Subcontract 1345493.

#### REFERENCES

- Alexeev, V. A. 2016, *SoSyR*, **50**, 24
- Balsiger, H., Altwegg, K., Bar-Nun, A., et al. 2015, *SciA*, **1**, e1500377
- Balsiger, H., Altwegg, K., Bochsler, P., et al. 2007, *SSRv*, **128**, 745
- Bieler, A., Altwegg, K., Balsiger, H., et al. 2015, *Natur*, **526**, 678
- Bockelée-Morvan, D., Crovisier, J., Mumma, M. J., & Weaver, H. A. 2004, in *Comets II*, ed. M. C. Festou, H. U. Keller, & H. A. Weaver (Tucson, AZ: Univ. Arizona Press), 391
- Casassa, S., Calatayud, M., Doll, K., Minot, C., & Pisani, C. 2005, *CPL*, **409**, 110
- Ciesla, F. J. 2014, *ApJL*, **784**, L1
- Cooper, J. F., Christian, E. R., & Johnson, R. E. 1998, *AdSpR*, **21**, 1611
- Cooper, J. F., Christian, E. R., Richardson, J. D., & Wang, C. 2003, *EM&P*, **92**, 261
- Effenberger, F., Fichtner, H., Scherer, K., & Büsching, I. 2012, *A&A*, **547**, A120
- Ellinger, Y., Pautz, F., Mousis, O., et al. 2015, *ApJL*, **801**, L30
- Fields, B. D., & Ellis, J. 1999, *NewA*, **4**, 419
- Fray, N., & Schmitt, B. 2009, *P&SS*, **57**, 2053
- Hersant, F., Gautier, D., & Hure, J.-M. 2001, *ApJ*, **554**, 391
- Johnson, R. E. 1990, *PCS*, 19
- Johnson, R. E. 1991, *JGR*, **96**, 17
- Kouchi, A., Yamamoto, T., Kozasa, T., Kuroda, T., & Greenberg, J. M. 1994, *A&A*, **290**, 1009
- Kresse, G., & Hafner, J. 1993, *PhRvB*, **48**, 13115
- Kresse, G., & Hafner, J. 1994, *PhRvB*, **49**, 14251
- Lattalais, M., Bertin, M., Mokrane, H., et al. 2011, *A&A*, **532**, A12
- Lattalais, M., Pautz, F., Ellinger, Y., & Ceccarelli, C. 2015, *A&A*, **578**, A62
- Lectez, S., Simon, J.-M., Mousis, O., et al. 2015, *ApJL*, **805**, L1
- Le Roy, L., Altwegg, K., Balsiger, H., et al. 2015, *A&A*, **583**, A1
- Lodders, K., Palme, H., & Gail, H.-P. 2009, *Landolt Börnstein*, ed. J. E. Trümper Springer Materials
- Luspay-Kuti, A., Mousis, O., Fuselier, S. A., et al. 2016, *SciA*, **2**, e1501781
- Maldoni, M. M., Egan, M. P., Smith, R. G., Robinson, G., & Wright, C. M. 2003, *MNRAS*, **345**, 912
- Mohammadi, A. H., Anderson, R., & Tohidi, B. 2005, *Am. In. Chem. Eng.*, **51**, 2825
- Mohammadi, A. H., Tohidi, B., & Burgass, R. W. 2003, *J. Chem. Eng. Data*, **48**, 612
- Mousis, O., Lunine, J. I., Luspay-Kuti, A., et al. 2016, *ApJL*, **819**, L33
- Mousis, O., Lunine, J. I., Picaud, S., & Cordier, D. 2010, *FaDi*, **147**, 509
- Mumma, M. J., & Charnley, S. B. 2011, *ARA&A*, **49**, 471
- Parrish, W. R., & Prausnitz, J. M. 1972, *Ind. Eng. Chem. Process Design Dev.*, **11**, 26 (Erratum: Parrish, W. R., Prausnitz, J. M. 1972, *Ind. Eng. Chem. Process Design Dev.*, **11**, 462)
- Rubin, M., Altwegg, K., Balsiger, H., et al. 2015a, *Sci*, **348**, 232
- Rubin, M., Altwegg, K., van Dishoeck, E. F., & Schwehm, G. 2015b, *ApJL*, **815**, L11
- Walsh, C., Nomura, H., & van Dishoeck, E. 2015, *A&A*, **582**, A88
- Weidenschilling, S. J., & Cuzzi, J. N. 1993, in *Protostars and Planets III* (Tucson, AZ: Univ. Arizona Press), 1031
- Werner, M., Kissmann, R., Strong, A. W., & Reimer, O. 2015, *APh*, **64**, 18
- Yeghikyan, A. G. 2011, *Ap*, **54**, 87



## Stability of Sulphur Dimers ( $S_2$ ) in Cometary Ices

O. Mousis<sup>1</sup>, O. Ozgurel<sup>2</sup>, J. I. Lunine<sup>3</sup>, A. Luspai-Kuti<sup>4</sup>, T. Ronnet<sup>1</sup>, F. Pauzat<sup>2</sup>, A. Markovits<sup>2</sup>, and Y. Ellinger<sup>2</sup>  
<sup>1</sup> Aix Marseille Université, CNRS, LAM (Laboratoire d'Astrophysique de Marseille) UMR 7326, F-13388, Marseille, France; [olivier.mousis@lam.fr](mailto:olivier.mousis@lam.fr)  
<sup>2</sup> Laboratoire de Chimie Théorique, Sorbonne Universités, UPMC Univ. Paris 06, CNRS UMR 7616, F-75252 Paris CEDEX 05, France  
<sup>3</sup> Department of Astronomy and Carl Sagan Institute, Space Sciences Building Cornell University, Ithaca, NY 14853, USA  
<sup>4</sup> Department of Space Research, Southwest Research Institute, 6220 Culebra Road, San Antonio, TX 78228, USA  
 Received 2016 July 27; revised 2016 October 21; accepted 2016 December 5; published 2017 January 23

### Abstract

$S_2$  has been observed for decades in comets, including comet 67P/Churyumov–Gerasimenko. Despite the fact that this molecule appears ubiquitous in these bodies, the nature of its source remains unknown. In this study, we assume that  $S_2$  is formed by irradiation (photolysis and/or radiolysis) of S-bearing molecules embedded in the icy grain precursors of comets and that the cosmic ray flux simultaneously creates voids in ices within which the produced molecules can accumulate. We investigate the stability of  $S_2$  molecules in such cavities, assuming that the surrounding ice is made of  $H_2S$  or  $H_2O$ . We show that the stabilization energy of  $S_2$  molecules in such voids is close to that of the  $H_2O$  ice binding energy, implying that they can only leave the icy matrix when this latter sublimates. Because  $S_2$  has a short lifetime in the vapor phase, we derive that its formation in grains via irradiation must occur only in low-density environments such as the ISM or the upper layers of the protosolar nebula, where the local temperature is extremely low. In the first case, comets would have agglomerated from icy grains that remained pristine when entering the nebula. In the second case, comets would have agglomerated from icy grains condensed in the protosolar nebula and that would have been efficiently irradiated during their turbulent transport toward the upper layers of the disk. Both scenarios are found consistent with the presence of molecular oxygen in comets.

**Key words:** astrobiology – comets: general – comets: individual (67P/Churyumov–Gerasimenko) – methods: numerical – solid state: volatile

### 1. Introduction

The nature of the source of sulphur dimers ( $S_2$ ) observed in comets is still unknown. The first detection of  $S_2$  in a celestial body was in the UV spectra of Comet IRAS-Araki-Alcock (C/1983 H1) acquired with the *International Ultraviolet Explorer* (IUE) space observatory (Ahearn et al. 1983). Emission bands of  $S_2$  were subsequently identified in many comets observed with IUE in the eighties, including 1P/Halley (Krishna Swamy & Wallis 1987).  $S_2$  was also identified in comets Hyakutake (C/1996 B2), Lee (C/1999 H1), and Ikeya-Zhang (C/2002 C1; Laffont et al. 1998; Kim et al. 2003; Boice & Reylé 2005). More recently,  $S_2$  has been detected in comet 67P/Churyumov–Gerasimenko (hereafter 67P/C-G) by the ROSINA mass spectrometer on board the *Rosetta* spacecraft at a distance of  $\sim 3$  au from the Sun in 2014 October ( $\sim 4\text{--}13 \times 10^{-6}$  with respect to water; Le Roy et al. 2015; Calmonte et al. 2016). All of these observations suggest that  $S_2$  is ubiquitous in comets.

Because the lifetime of  $S_2$  is very short in comae (approximately a few hundred seconds at most; Reylé & Boice 2003), two main scenarios have been invoked in the literature to account for its presence in comets. In the first scenario,  $S_2$  is the product of reactions occurring in the coma. Ethylene was thus proposed to act as a catalyst allowing the formation of  $S_2$  molecules in the inner coma (Saxena & Misra 1995; Saxena et al. 2003). Also, the presence of atomic S (as the photodissociation product of  $CS_2$ ) reacting with OCS was suggested to form  $S_2$  in comae (A'Hearn et al. 2000). However, models depicting the chemistry occurring in cometary comae show that these two mechanisms do not account for the observed levels of  $S_2$  (Rodgers & Charnley 2006).

In the second scenario,  $S_2$  molecules are believed to be of parent nature and reside in cometary ices (Ahearn et al. 1983;

Ahearn & Feldman 1985; Feldman 1987; Grim & Greenberg 1987; A'Hearn 1992). Ahearn & Feldman (1985) proposed that the UV photolysis of S-bearing species embedded in ISM ices could form sufficient amounts of  $S_2$  that remains trapped in the icy matrix. Since then, a number of mechanisms based on UV or X-ray irradiation have been proposed, starting mainly from  $H_2S$  (the most abundant S-bearing volatile observed in comets; Irvine et al. 2000; Bockelée-Morvan et al. 2004) and  $H_2S_2$ , and involving radicals like HS and  $HS_2$  (Grim & Greenberg 1987; Jiménez-Escobar & Muñoz-Caro 2011; Jiménez-Escobar et al. 2012). It has also been proposed that  $S_2$  could be formed from the radiolysis of S-bearing compounds in cometary ices (Ahearn & Feldman 1985; Calmonte et al. 2016) despite the fact that so far, there is no experimental proof showing that this mechanism is effective.

In the present study, we postulate that  $S_2$  is formed from  $H_2S$  molecules embedded in icy grains by irradiation of UV, X-ray, and cosmic ray fluxes (CRF), whether icy grain precursors of comets formed in the protosolar nebula or the ISM. Because radiolysis generated by the impact of cosmic rays simultaneously creates voids in ices within which the produced molecules can accumulate (Carlson et al. 2009; Mousis et al. 2016b), we investigate the stability of  $S_2$  molecules in such cavities, assuming that the surrounding ice is made of  $H_2S$  or  $H_2O$ . We show that the stabilization energy of  $S_2$  molecules in such voids is close to that of the  $H_2O$  ice binding energy, implying that they can only leave the icy matrix when this latter sublimates. We finally discuss the implications of our results for the origin of cometary grains, with a particular emphasis on those agglomerated by comet 67P/C-G.



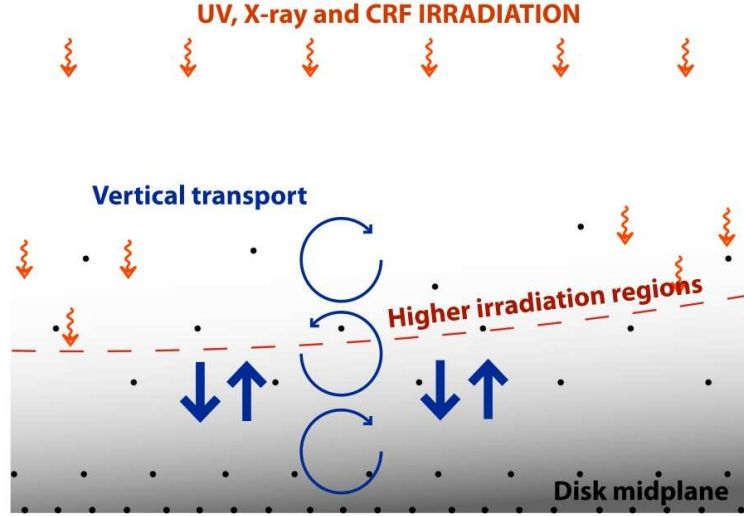


**Figure 1.** Illustration of the vertical transport of small icy grains toward disk regions where they are efficiently irradiated. Dust is concentrated in the midplane of the disk due to gravitational settling and gas drag. However, turbulent eddies lift the icy grains toward the upper regions and also drag them down because the direction of the velocity is random and coherent during a timescale comparable to the local keplerian period. Small dust grains finally spend a non-negligible fraction of their lifetime in the disk's upper regions, where the irradiation attenuation is low.

## 2. Irradiation of Icy Grains

Three irradiation mechanisms leading to the formation of  $S_2$  are considered in this study. The first two mechanisms, namely UV and X-ray irradiation, have been proven to produce  $S_2$  from  $H_2S$  and  $H_2S_2$  (Grim & Greenberg 1987; Jiménez-Escobar & Muñoz-Caro 2011; Jiménez-Escobar et al. 2012). Experiments have shown that  $S_2$  can be produced and stabilized in icy grains over thicknesses of a few tenths of microns. Despite the lack of experimental data, radiolysis has also been considered as a potential candidate for  $S_2$  formation from S-bearing compounds in cometary icy grains (Ahearn & Feldman 1985). This mechanism has recently been proposed to explain the detection of  $S_2$  in 67P/C-G (Calmonte et al. 2016) and is often invoked to account for its presence in Europa's exosphere (Carlson et al. 1999; Cassidy et al. 2010). Cosmic rays reach deeper layers than photon irradiation and simultaneously creates voids in which some irradiation products such as  $O_2$  or here  $S_2$  can be sequestered (Mousis et al. 2016b). Whatever the irradiation process considered, we assume that, once  $S_2$  has been created and trapped in the microscopic icy grains, the latter agglomerated and formed the building blocks of comets.

## 3. Stability of $S_2$ Molecules in an Icy Matrix

The  $S_2$  stabilization energy arises from the electronic interaction between the host support ( $H_2O$  ice or  $H_2S$  ice) and the  $S_2$  foreign body. The stabilization energy is evaluated as

$$E_{\text{stab}} = (E_{\text{ice}} + E_{S_2}) - E, \quad (1)$$

where  $E_{S_2}$  is the energy of the isolated molecule,  $E_{\text{ice}}$  the energy of the pristine solid host and  $E$  is the total energy of the [host +  $S_2$ ] complex, with all entities optimized in isolation.

All simulations are carried out by means of the Vienna ab-initio simulation package (Kresse & Hafner 1993, 1994; Kresse & Furthmüller 1996; Kresse & Joubert 1999). The long range interactions in the solid and the hydrogen bonding being the

critical parameters in the ices, we use the PBE generalized gradient approximation functional (Perdew et al. 1996), in the (PBE+D2) version corrected by Grimme et al. (2010), that has been specifically designed to deal with the present type of problem. This theoretical tool has proved to be well adapted to model bulk and surface ice structures interacting with volatile species (Lattalais et al. 2011, 2015; Ellinger et al. 2015; Mousis et al. 2016b). More details on the computational background can be found in the aforementioned publications.

Since  $S_2$  is created well inside the icy grain mantles, the initial description of the irradiated ice is taken as that of the internal structures of ice clusters obtained from Monte-Carlo simulations of ice aggregates constituted of hundreds of water molecules. The important point in the simulations by Buch et al. (2004) is that the core of the aggregates consists in crystalline domains of apolar hexagonal ice  $I_h$ . However, in the present context, the irradiation creates significant defects inside the ice, namely, voids and irradiation tracks that, at least locally, modify the crystalline arrangement.

### 3.1. $S_2$ Embedded in $H_2O$ Ice

Because  $H_2O$  is the dominant volatile in comets (Bockelée-Morvan et al. 2004), most of the cavities created by CRF irradiation are expected to be surrounded by  $H_2O$  molecules. Table 1 shows the stabilization energy of  $S_2$  as a function of the size of these cavities. How the  $S_2$  stabilization evolves as a function of their size is summarized below.

1. Starting with no  $H_2O$  removed, we find no stabilization for the inclusion of  $S_2$  in the ice lattice. It is in fact an endothermic process, as it is for  $O_2$  inclusion (Mousis et al. 2016b).
2. With one  $H_2O$  removed, we have an inclusion structure for which stabilization is negative, meaning that  $S_2$  cannot stay in such a small cavity.
3. With somewhat larger cavities obtained by removing two to four adjacent  $H_2O$  molecules from the ice lattice, we

**Table 1**Computed Stabilization Energies (eV) of S<sub>2</sub> Interacting with H<sub>2</sub>O Ice or H<sub>2</sub>S Ice

Environment	H <sub>2</sub> O Ice	H <sub>2</sub> S Ice
Adsorption	0.28	...
Inclusion ( $n = 1$ ) <sup>a</sup>	-0.12	0.30
Inclusion ( $n = 2$ )	0.28	0.45
Inclusion ( $n = 4$ )	0.50	0.40
Inclusion (fine track)	0.51	0.41
Inclusion (large track)	0.53	0.50

**Note.**<sup>a</sup>  $n$  = number of H<sub>2</sub>O or H<sub>2</sub>S molecules destroyed to create the void in which S<sub>2</sub> is trapped.

obtain increasing stabilization energies from 0.3 to 0.5 eV.

4. With larger cavities that form along the irradiation track, the stabilization energies are found to be at least of the order of 0.5 eV.

In short, as soon as the space available is sufficient, the energy stabilizes around 0.5 eV. This stabilization energy is (1) higher (more stabilizing) than what is found in the case of O<sub>2</sub> (0.2–0.4 eV; Mousis et al. 2016b) and (2) larger than that of a water dimer (~0.25 eV). Hence, the presence of S<sub>2</sub> should not perturb the ice structure until it is ejected into the coma via sublimation with the surrounding H<sub>2</sub>O molecules. The results of our computations are consistent with the laboratory experiments of Grim & Greenberg (1987) who showed that S<sub>2</sub> remains trapped in icy grains until they are heated up to ~160 K, a temperature at which water ice sublimates at PSN conditions.

### 3.2. S<sub>2</sub> Embedded in H<sub>2</sub>S Ice

H<sub>2</sub>S behaves similarly to H<sub>2</sub>O because of its ability to establish hydrogen bonds. This implies that small domains of H<sub>2</sub>S could have formed in the bulk of the ice and served as local sources for the formation of S<sub>2</sub>. The stabilization of these aggregates is addressed by numerical simulations in which H<sub>2</sub>S entities are progressively introduced by replacing an equal number of H<sub>2</sub>O molecules in the water-ice lattice. Table 2 shows the stabilization energies with values around 0.5 and 0.75 eV for neighboring and far away H<sub>2</sub>S, respectively. Consequently, substituting several neighboring H<sub>2</sub>O by H<sub>2</sub>S is a possibility to be considered if the H<sub>2</sub>S is abundant enough, thus creating small islands of H<sub>2</sub>S within the water ice.

If small clumps of H<sub>2</sub>S ices in the bulk of water ice are a plausible hypothesis, as suggested by the aforementioned numbers, then the proper conditions are realized for the in situ formation of S<sub>2</sub> by deep irradiation. The case in which H<sub>2</sub>S molecules replace H<sub>2</sub>O along the irradiation track is a less favorable situation but it could be at the origin of the S<sub>n</sub> oligomers observed in some laboratory experiments (Meyer et al. 1972; Jiménez-Escobar et al. 2012). We evaluate the stabilization of S<sub>2</sub> in H<sub>2</sub>S clumps, assuming that they behave as pure condensates. The results, presented in Table 1 and summarized below, are quite close to those derived for water ice.

1. With one H<sub>2</sub>S removed, we have a substitution structure whose stabilization is on the order of 0.30 eV.

**Table 2**Computed Stabilization Energies (eV) of H<sub>2</sub>S Interacting with H<sub>2</sub>O Ice

Environment	H <sub>2</sub> S
Adsorption	0.61
Substitution ( $n = 1$ ) <sup>a</sup>	0.77
Substitution ( $n = 2$ far away)	0.73
Substitution ( $n = 2$ close)	0.56
Substitution ( $n = 3$ close)	0.50
Substitution (irradiation track)	0.51

**Note.**<sup>a</sup>  $n$  = number of H<sub>2</sub>O molecules replaced by H<sub>2</sub>S.

2. With larger cavities obtained by removing two to four adjacent H<sub>2</sub>S molecules, we obtain increasing stabilization energies between 0.40 and 0.45 eV.
3. With even larger cavities, extended in the direction of the irradiation, the stabilization energies are found to be similar to the preceding ones, between 0.40 and 0.50 eV.

Again we find that the presence of S<sub>2</sub> should not perturb the ice structure, even when trapped in H<sub>2</sub>S clumps, until the latter sublimate, due to increasing local temperature.

### 4. Implications for Cometary Ices

It has recently been shown that the radiolysis of icy grains in low-density environments, such as the presolar cloud, may induce the production of amounts of molecular oxygen high enough to be consistent with the quantities observed in 67P/C-G (Mousis et al. 2016b). Higher density environments such as the PSN midplane were excluded because the timescales needed to produce enough O<sub>2</sub> in cometary grains exceeded by far their lifetimes in the disk. Also, the efficiency of ionization by cosmic rays in the PSN midplane is now questioned because of the deflection of galactic CRF by the stellar winds produced by young stars (Cleeves et al. 2013, 2014).

On the other hand, because the lifetime of S<sub>2</sub> is very short in the gas phase (approximately a few hundred seconds at most; Reylé & Boice 2003), its formation conditions are even more restrictive than those required for O<sub>2</sub>. Assuming that S<sub>2</sub> indeed formed from H<sub>2</sub>S or any other S-bearing molecule via UV, X-ray, or CRF irradiation, this implies that this molecule never left the icy matrix in the time interval between its formation and trapping. In other words, S<sub>2</sub> never condensed from the PSN before being trapped in cometary grains. This stringent constraint requires S<sub>2</sub> to form within icy grains irradiated by CRF in low-density environments such as ISM, where the local temperature is extremely cold. In this picture, comets, including 67P/C-G, would have agglomerated in the PSN from icy grains originating from ISM, whose compositions and structures remained pristine when entering the nebula.

Alternatively, because the CRF irradiation should be poorly attenuated in the upper layers of the PSN, these regions also constitute an adequate low-density environment, allowing the formation of S<sub>2</sub> in cometary grains. Turbulence plays an important role in the motion of small dust grains that are well coupled to the gas (see Figure 1). Micron-sized grains initially settled in the midplane are entrained by turbulent eddies and diffuse radially and vertically with an effective viscosity roughly equal to that of the gas for such small particles (see Ciesla 2010, 2011 for details). Consequently, solid particles



follow a Gaussian distribution in the vertical direction. The scale height of dust (corresponding to the standard deviation of the distribution) is a fraction of the gas scale height, this fraction being larger and possibly equal to the gas scale height in the cases of small grains and higher degrees of turbulence (Dubrulle et al. 1995; Youdin & Lithwick 2007).

The vertical transport of solids exposes them to very different disk environments. Dust grains are stochastically transported to high altitude and low-density regions above the disk midplane. Ciesla (2010) developed a numerical simulation to integrate the motion of individual particles and showed that micron-sized grains spent  $\sim 32\%$  of their lifetime at altitudes above the scale height of the disk, including  $\sim 5\%$  at heights above four times its scale height, regardless of the distance from the Sun. In such low-density environments, photochemistry plays a primordial role, as demonstrated by Ciesla & Sandford (2012), because UV photons are weakly attenuated at those heights. This also holds for the CRF irradiation of grains that should be substantially enhanced compared to the dose received by particles residing in the midplane. Under those circumstances, the production of  $S_2$  should be favored in icy grains over several cycles of vertical transport toward the surface of the disk. This scenario should also favor the formation of  $O_2$  from irradiation of  $H_2O$  ice (see Mousis et al. 2016b for details).

## 5. Discussion and Conclusions

It is reasonable to assume that the multiple forms of irradiation hitting the microscopic icy grains in low-density environments such as ISM or the upper layers of protoplanetary disks can lead both to the formation of  $S_2$  molecules and the development of cavities in these grains, in which the molecule remains sequestered. The same scenario has been proposed for  $O_2$  formation and stabilization in cometary icy grains (Mousis et al. 2016b). In the case of  $S_2$  formation, the possibility of forming the dimer via the radiolysis of S-bearing ices remains an open question. Future experimental work is needed to check the viability of this mechanism.

The possible formation of  $S_2$  in icy grains via their irradiation in ISM, together with the short lifetime of this molecule in the gas phase, leads to the plausible possibility that comets agglomerated from pristine amorphous grains that never vaporized when entering the PSN, as already envisaged for the origin of 67P/C-G's material (Rubin et al. 2015a; Mousis et al. 2016b). On the other hand, the formation of  $S_2$  in icy grains that migrated toward the upper layers of the disk is compatible with their condensation in the PSN midplane. This mechanism leaves open the possibility that these grains are made of crystalline ices and clathrates, as proposed by Mousis et al. (2016a) and Luspay-Kuti et al. (2016) to account for several pre-perihelion compositional measurements made by the *Rosetta* spacecraft in 67P/C-G. The same process could explain the presence of  $O_2$  measured in situ in comets 67P/C-G and 1P/Halley (Bieler et al. 2015; Rubin et al. 2015b). Interestingly, whatever the ice structure considered for the icy grains, the voids allowing the stabilization of  $S_2$  can be considered as analogs of clathrates in terms of cage sizes and intermolecular interactions.

The fact that one  $H_2S$  replacing one  $H_2O$  has little influence on the stability of the solid lattice is a favorable situation for the formation of a mixed ice. It is plausible that some segregation occurs with the formation of  $H_2S$  islands in the bulk of

crystalline or amorphous water ice. Then, the proper conditions would be realized for the in situ formation of  $S_2$ , especially if we remember that the formation of one  $S_2$  requires at least the destruction of two imprisoned sulphur species. The plausible formation of  $H_2S$  clumps is a strong argument in favor of a non-uniform distribution of  $S_2$  within cometary ices. Note that in the case of irradiation of crystalline grains condensed in the PSN and transported toward the upper layers of the disk, the formed  $S_2$  may be entrapped in clathrates (Grim & Greenberg 1987), also forming a solid phase distinct from water ice in cometary grains.

The immediate consequence of the presence of distinct  $S_2$ -bearing solid phases is the difficulty to predict the  $S_2$  correlation with  $H_2O$  or  $H_2S$  in 67P/C-G from *Rosetta* measurements. The  $S_2/H_2O$  abundance ratio is directly linked to the region of the comet whose desorption is observed. Contrary to  $O_2$  whose apparent good correlation with  $H_2O$  is explained by its trapping in water ice (Bieler et al. 2015; Mousis et al. 2016b), no global trend should be drawn between the variation of  $S_2$  and  $H_2O$  abundances if  $S_2$  is distributed within both the S-bearing and  $H_2O$  ices. Indeed,  $S_2$  may be released simultaneously from the  $H_2O$  layer present close to the surface and from  $H_2S$  clusters localized deeper in the subsurface. Our results are supported by the ROSINA data collected between 2015 May (equinox) and 2015 August (perihelion), showing that there is no clear correlation of  $S_2$  with  $H_2O$  or  $H_2S$  in 67P/C-G (Calmonte et al. 2016). These observations allow us to exclude the trapping of  $S_2$  in a dominant ice reservoir. If  $S_2$  was mainly trapped in  $H_2S$ -bearing ice, then the outgassing rates of  $S_2$  and  $H_2S$  should have been well correlated during the period sampled by the ROSINA instrument. The same statement applies if  $S_2$  had been essentially trapped in water ice.

O.M. acknowledges support from CNES. This work has been partly carried out thanks to the support of the A\*MIDEX project (n° ANR-11-IDEX-0001-02) funded by the "Investissements d'Avenir" French Government program, managed by the French National Research Agency (A.N.R.). This work also benefited from the support of CNRS-INSU national program for planetology (P.N.P.). J.L.L. appreciates support from NASA through the *JWST* project. A.L.-K. acknowledges support from NASA JPL (subcontract no. 1496541).

## References

- A'Hearn, M. F. 1992, in IAU Symp. 150, *Astrochemistry of Cosmic Phenomena*, ed. P. D. Singh (Dordrecht: Kluwer), 415
- A'Hearn, M. F., Arpigny, C., Feldman, P. D., et al. 2000, *BAAS*, 32, 44.01
- A'Hearn, M. F., & Feldman, P. D. 1985, *ASIC*, 156, 463
- A'Hearn, M. F., Schleicher, D. G., & Feldman, P. D. 1983, *ApJL*, 274, L99
- Bieler, A., Altwegg, K., Balsiger, H., et al. 2015, *Natur*, 526, 678
- Bockelée-Morvan, D., Crovisier, J., Mumma, M. J., & Weaver, H. A. 2004, in *Comets II*, ed. M. C. Festou, H. U. Keller, & H. A. Weaver (Tucson, AZ: Univ. Arizona Press), 391
- Boice, D. C., & Reylé, C. 2005, *HiA*, 13, 501
- Buch, V., Sigurd, B., Devlin, J. P., Buck, U., & Kaziminski, J. K. 2004, *IRPC*, 23, 375
- Calmonte, U., Altwegg, K., Balsiger, H., et al. 2016, *MNRAS*, 462, S253
- Carlson, R. W., Calvin, W. M., Dalton, J. B., et al. 2009, in *Europa*, ed. R. T. Pappalardo et al. (Tucson, AZ: Univ. Arizona Press), 283
- Carlson, R. W., Johnson, R. E., & Anderson, M. S. 1999, *Sci*, 286, 97
- Cassidy, T., Coll, P., Raulin, F., et al. 2010, *SSRv*, 153, 299
- Ciesla, F. J. 2010, *ApJ*, 723, 514
- Ciesla, F. J. 2011, *ApJ*, 740, 9
- Ciesla, F. J., & Sandford, S. A. 2012, *Sci*, 336, 452



- Cleeves, L. I., Adams, F. C., & Bergin, E. A. 2013, *ApJ*, 772, 5
- Cleeves, L. I., Bergin, E. A., Alexander, C. M. O., et al. 2014, *Sci*, 345, 1590
- Dubrulle, B., Morfill, G., & Sterzik, M. 1995, *Icar*, 114, 237
- Ellinger, Y., Pauzat, F., Mousis, O., et al. 2015, *ApJL*, 801, L30
- Feldman, P. D. 1987, in IAU Symp. 120, *Astrochemistry* (Dordrecht: D. Reidel), 417
- Grim, R. J. A., & Greenberg, J. M. 1987, *ApJ*, 321, L91
- Grimme, S., Antony, J., Ehrlich, S., & Krieg, H. 2010, *JChPh*, 132, 154104
- Irvine, W. M., Schloerb, F. P., Crovisier, J., Fegley, B., Jr., & Mumma, M. J. 2000, in *Protostars and Planets IV*, ed. V. Mannings, A. P. Boss, & S. Russell (Tucson, AZ: Univ. Arizona Press), 1159
- Jiménez-Escobar, A., & Muñoz-Caro, G. M. 2011, *A&A*, 536, A91
- Jiménez-Escobar, A., Muñoz Caro, G. M., Ciaravella, A., et al. 2012, *ApJL*, 751, L40
- Kim, S. J., A'Hearn, M. F., Wellnitz, D. D., Meier, R., & Lee, Y. S. 2003, *Icar*, 166, 157
- Kresse, G., & Furthmüller, J. 1996, *PhRvB*, 54, 11169
- Kresse, G., & Hafner, J. 1993, *PhRvB*, 48, 13115
- Kresse, G., & Hafner, J. 1994, *PhRvB*, 49, 14251
- Kresse, G., & Joubert, D. 1999, *PhRvB*, 59, 1758
- Krishna Swamy, K. S., & Wallis, M. K. 1987, *MNRAS*, 228, 305
- Laffont, C., Boice, D. C., Moreels, G., et al. 1998, *GeoRL*, 25, 2749
- Lattalais, M., Bertin, M., Mokrane, H., et al. 2011, *A&A*, 532, A12
- Lattalais, M., Pauzat, F., Ellinger, Y., & Ceccarelli, C. 2015, *A&A*, 578, A62
- Le Roy, L., Altwegg, K., Balsiger, H., et al. 2015, *A&A*, 583, A1
- Luspay-Kuti, A., Mousis, O., Hässig, M., et al. 2016, *SciA*, 2, e1501781
- Meyer, B., Stroyer-Hansen, T., & Oommen, T. V. 1972, *JMoSp*, 42, 335
- Mousis, O., Lunine, J. I., Luspay-Kuti, A., et al. 2016a, *ApJL*, 819, L33
- Mousis, O., Ronnet, T., Brügger, B., et al. 2016b, *ApJL*, 823, L41
- Perdew, J. P., Burke, K., & Ernzerhof, M. 1996, *PhRvL*, 77, 3865
- Reylé, C., & Boice, D. C. 2003, *ApJ*, 587, 464
- Rodgers, S. D., & Charnley, S. B. 2006, *AdSpR*, 38, 1928
- Rubin, M., Altwegg, K., Balsiger, H., et al. 2015a, *Sci*, 348, 232
- Rubin, M., Altwegg, K., van Dishoeck, E. F., & Schwegm, G. 2015b, *ApJL*, 815, L11
- Saxena, P. P., & Misra, A. 1995, *MNRAS*, 272, 89
- Saxena, P. P., Singh, M., & Bhatnagar, S. 2003, *BASI*, 31, 75
- Youdin, A. N., & Lithwick, Y. 2007, *Icar*, 192, 588

#### IV References

- Ahearn, M. F., Schleicher, D. G., & Feldman, P. D. (1983). The discovery of S<sub>2</sub> in comet IRAS-Araki-Alcock 1983d. *The Astrophysical Journal*, 274, L99-L103.
- Barker, E. S. (1972). Detection of Molecular Oxygen in the Martian Atmosphere. *Nature*, 238, 447-448.
- Bartels-Rausch, T., Bergeron, V., Cartwright, J. H., Escibano, R., Finney, J. L., Grothe, H., ... & Price, S. D. (2012). Ice structures, patterns, and processes: A view across the icefields. *Reviews of Modern Physics*, 84(2), 885.
- Bartolomei, M., Hernández, M. I., Campos-Martínez, J., Carmona-Novillo, E., & Hernández-Lamonedá, R. (2008). The intermolecular potentials of the O<sub>2</sub>–O<sub>2</sub> dimer: a detailed ab initio study of the energy splittings for the three lowest multiplet states. *Physical Chemistry Chemical Physics*, 10(35), 5374-5380.
- Bernal, J. D., & Fowler, R. H. (1933). A theory of water and ionic solution, with particular reference to hydrogen and hydroxyl ions. *The Journal of Chemical Physics*, 1(8), 515-548.
- Bieler, A., Altwegg, K., Balsiger, H., Bar-Nun, A., Berthelier, J. J., Bochsler, P., ... & van Dishoeck, E. F. (2015). Abundant molecular oxygen in the coma of comet 67P/Churyumov-Gerasimenko. *Nature*, 526(7575), 678-681.
- Boice, D. C., & Reylé, C. (2005). The nature of diatomic sulfur in comets. *Highlights of Astronomy*, 13, 501.
- Buch, V., Sigurd, B., Paul Devlin, J., Buck, U., & Kazimirski, J. K. (2004). Solid water clusters in the size range of tens–thousands of H<sub>2</sub>O: a combined computational/spectroscopic outlook. *International Reviews in Physical Chemistry*, 23(3), 375-433.
- Buch, V., Groenzin, H., Li, I., Shultz, M. J., & Tosatti, E. (2008). Proton order in the ice crystal surface. *Proceedings of the National Academy of Sciences*, 105(16), 5969-5974.

- Calmonte, U., Altwegg, K., Balsiger, H., Berthelier, J. J., Bieler, A., Cessateur, G., ... & Gasc, S. (2016). Sulphur-bearing species in the coma of comet 67P/Churyumov–Gerasimenko. *Monthly Notices of the Royal Astronomical Society*, 462, S253-S273.
- Calatayud, M., Courmier, D., & Minot, C. (2003). Ionization of HCl and HF in ice: a periodic DFT study. *Chemical Physics Letters*, 369(3), 287-292.
- Dion, M., Rydberg, H., Schröder, E., Langreth, D. C., & Lundqvist, B. I. (2004). Van der Waals density functional for general geometries. *Physical Review Letters*, 92(24), 246401.
- Doronin, M. V. (2015). *Adsorption on Interstellar Analog Surfaces: from Atoms to Organic Molecules* (Doctoral dissertation). UPMC, Paris, France.
- Dulieu, F., Minissale, M., & Bockelée-Morvan, D. (2017). Production of O<sub>2</sub> through dismutation of H<sub>2</sub>O<sub>2</sub> during water ice desorption: a key to understanding comet O<sub>2</sub> abundances. *Astronomy & Astrophysics*, 597, A56.
- Ellinger, Y., Pauzat, F., Mousis, O., Guilbert-Lepoutre, A., Leblanc, F., Ali-Dib, M., ... & Doressoundiram, A. (2015). Neutral Na in cometary tails as a remnant of early aqueous alteration. *The Astrophysical Journal Letters*, 801(2), L30.
- Fields, B. D., & Ellis, J. (1999). On deep-ocean <sup>60</sup>Fe as a fossil of a near-earth supernova. *New Astronomy*, 4(6), 419-430.
- Fletcher, N. H. (1992). Reconstruction of ice crystal surfaces at low temperatures. *Philosophical Magazine B*, 66(1), 109-115.
- Fuentes-Landete, V., Mitterdorfer, C., Handle, P. H., Ruiz, G. N., Bernard, J., Bogdan, A., ... & Loerting, T. (2015, May). Crystalline and amorphous ices. In *Proceedings of the International School of Physics “Enrico Fermi”* (Vol. 187, pp. 173-208). Amsterdam: IOS Press.
- Grimme, S. (2006). Semiempirical GGA-type density functional constructed with a long-range dispersion correction. *Journal of Computational Chemistry*, 27(15), 1787-1799.

Goldsmith, P. F., Liseau, R., Bell, T. A., Black, J. H., Chen, J. H., Hollenbach, D., ... & Neufeld, D. (2011). Herschel measurements of molecular oxygen in Orion. *Astrophysical Journal*, 737, 96.

Hall, D. T., Strobel, D. F., Feldman, P. D., McGrath, M. A., & Weaver, H. A. (1995). Detection of an oxygen atmosphere on Jupiter's moon Europa. *Nature*, 373(6516), 677-679.

Johnson, R. E., Luhmann, J. G., Tokar, R. L., Bouhram, M., Berthelier, J. J., Sittler, E. C., ... & Liu, M. (2006). Production, ionization and redistribution of O<sub>2</sub> in Saturn's ring atmosphere. *Icarus*, 180(2), 393-402.

Kim, S. J., A'Hearn, M. F., Wellnitz, D. D., Meier, R., & Lee, Y. S. (2003). The rotational structure of the B–X system of sulfur dimers in the spectra of Comet Hyakutake (C/1996 B2). *Icarus*, 166(1), 157-166.

Kresse, G., & Hafner, J. (1993). Ab initio molecular dynamics for liquid metals. *Physical Review B*, 47(1), 558.

Kresse, G., & Hafner, J. (1994). Ab initio molecular-dynamics simulation of the liquid-metal–amorphous-semiconductor transition in germanium. *Physical Review B*, 49(20), 14251.

Laffont, C., Boice, D. C., Moreels, G., Clairemidi, J., Rousselot, P., & Aernach, H. (1998). Tentative identification of S<sub>2</sub> in the IUE spectra of comet Hyakutake (C/1996 B2). *Geophysical research letters*, 25(14), 2749-2752.

Larsson, B., Liseau, R., Pagani, L., Bergman, P., Black, J. H., Booth, R., ... & Olberg, M. (2007). Molecular oxygen in the p Ophiuchi cloud. *Astronomy & Astrophysics*, 466, 999.

Lattalais, M., Bertin, M., Mokrane, H., Romanzin, C., Michaut, X., Jeseck, P., ... & Baouche, S. (2011). Differential adsorption of complex organic molecules isomers at interstellar ice surfaces. *Astronomy & Astrophysics*, 532, A12.

Lattalais, M., Pauzat, F., Ellinger, Y., & Ceccarelli, C. (2015). Differential adsorption of CHON isomers at interstellar grain surfaces. *Astronomy & Astrophysics*, 578, A62.

- Le Roy, L., Altwegg, K., Balsiger, H., Berthelier, J. J., Bieler, A., Briois, C., ... & Fiethe, B. (2015). Inventory of the volatiles on comet 67P/Churyumov-Gerasimenko from Rosetta/ROSINA. *Astronomy & Astrophysics*, 583, A1.
- Mousis, O., Ronnet, T., Brugger, B., Ozgurel, O., Pauzat, F., Ellinger, Y., ... & Luspay-Kuti, A. (2016). Origin of molecular oxygen in comet 67P/Churyumov-Gerasimenko. *The Astrophysical Journal Letters*, 823(2), L41.
- Pan, D., Liu, L. M., Tribello, G. A., Slater, B., Michaelides, A., & Wang, E. (2010). Surface energy and surface proton order of the ice Ih basal and prism surfaces. *Journal of Physics: Condensed Matter*, 22(7), 074209.
- Perdew, J. P., Burke, K., & Ernzerhof, M. (1996). Generalized gradient approximation made simple. *Physical Review Letters*, 77(18), 3865.
- Rubin, M., Altwegg, K., van Dishoeck, E. F., & Schwehm, G. (2015). Molecular oxygen in Oort cloud comet 1P/Halley. *The Astrophysical Journal Letters*, 815(1), L11.
- Taquet, V., Furuya, K., Walsh, C., & Van Dishoeck, E. F. (2016). A primordial origin for molecular oxygen in comets: a chemical kinetics study of the formation and survival of O<sub>2</sub> ice from clouds to discs. *Monthly Notices of the Royal Astronomical Society*, 462(Suppl 1), S99-S115.
- Vydrov, O. A., & Van Voorhis, T. (2010). Nonlocal van der Waals density functional: The simpler the better. *The Journal of chemical physics*, 133(24), 244103.
- Weidenschilling, S. J., & Cuzzi, J. N. (1993). Formation of planetesimals in the solar nebula. *In Protostars and planets III* (pp. 1031-1060). Tucson: Univ. Arizona.
- Yao, Y., & Giapis, K. P. (2016). Kinematics of Eley-Rideal reactions at hyperthermal energies. *Physical review letters*, 116(25), 253202.
- Yao, Y., & Giapis, K. P. (2017). Dynamic molecular oxygen production in cometary comae. *Nature Communications*, 8, 15298.



### **Chapter 3: On the origin of alkali (Na, K) and alkaline earth (Mg, Ca) metals in Europa exosphere**

Jupiter's moon Europa, with its geologically young surface (Pappalardo et al. 1999), its possible salty subsurface ocean (Kivelson et al. 2000) and its tenuous atmosphere (Hall et al., 1995) is one of the most intriguing objects in the Solar System. Its surface and atmosphere are bathed with the external radiation field (Carlson et al. 1999; Cooper et al. 2001, Paranicas et al. 2000). Therefore, studying the origin, evolution and composition of the extended atmosphere can help to understand the surface composition, which in turn provides information on the subsurface material (Johnson et al. 1998), since the surface is young with an average age of ~50 Myr (Pappalardo et al. 1999; Zahnle et al. 2003).

Europa's atmosphere was first detected with Hubble Space Telescope observations of the 1304 and 1356 Å emission lines of neutral atomic oxygen coming from dissociation of molecular dioxygen (Hall et al. 1996). According to initial modeling (Ip 1996) the oxygen atmosphere could be originated from the sputtering of water ice on the surface of Europa, as originally suggested by Johnson et al (1998) and that a very thin extended atmosphere should also form in the process. The first detection of this extended atmosphere, including sodium observations, was made by Brown & Hill (1996) at distances of up to 20 Europa radii (1 RE = 1569 km) from the surface. The detection of sodium (an atomic open-shell) showed that the composition of Europa's atmosphere is not only important to understand the interaction of the magnetosphere with the surface, but also to determine the non-water-ice composition. After the detection of Na component of the atmosphere, different hypothesis were proposed for its origin. One way, among others, to progress in the understanding of the origin of Na on the Europa's surface is to measure the abundances of additional trace elements in Europa's atmosphere.

Simultaneous observations of potassium and sodium in Europa's extended atmosphere were made on September 9th 1998 at the W. M. Keck telescope using HIRES, the facility echelle spectrograph (Vogt et al. 1994). Identical observations on Io's extended atmosphere were obtained on November 15th 1998.



In 2001, Brown reported the sodium-to-potassium ratio in Europa's extended atmosphere as  $25 \pm 3$  together with the first measurements of this ratio in Io's extended atmosphere as  $10 \pm 3$  and a value of  $6 \pm 1$  in Io's high-speed jet.

In this chapter, we propose a scenario for the origin and relative abundances of sodium and potassium in Europa's exosphere. An extension of this scenario is also presented for calcium and magnesium, which are the two next most easily detectable metallic trace elements candidates for future mission (ESA's JUICE and NASA's CLIPPER).

## **I Astrophysical context**

The first time detection of Na in Europa's exosphere in 1996 followed by the simultaneous detection of Na and K with a Na/K ratio of  $\sim 25$  led to different hypotheses about the origin of these trace elements. These can be divided into two different approaches. The first relies on exogenous theories, proposing that Na and K present in the exosphere come from an outer source, Io or meteorite; the second is supported by endogenous theories, suggesting that Na and K are intrinsic to Europa's surface.

According to Brown and Hill (1996), Na in the ice surface of Europa may be originated from the volcanic activity in Io nearby. They suggested that sodium is injected to the Io neutral clouds from the volcanos, then ionized by the Io plasma torus and finally collide to Europa's surface. They calculated the implantation rate of sodium into Europa's surface to be  $24 \text{ gs}^{-1}$ , which was the amount of Na required to supply the atmosphere in steady state. However, the first quantitative measurement of the sodium-to-potassium ratio in Io's atmosphere showed that it was nearly three times smaller than the Na/K ratio in Europa (Brown 2001).

Since this ratio should decrease even more in the process of transfer between Io's surface and its implantation in Europa's surface, it is clear that the origin of Na and K in Europa's exosphere cannot be from Io

The other possibility of exogenous origin of Na and K is the meteorite bombardment. According to this theory (Brown, 2001), meteorite bombardments of the surface of Europa should bring sodium and potassium. Analyses of the terrestrial meteorites show a Na/K ratio of 13 on average, which is approximately consistent with the measured value in Europa.

However, within similar reasoning, the other satellite of Jupiter, Ganymede should also have a sodium component in the atmosphere, which is non-detected so far.

The second type of hypothesis is based on the endogenous origins for Na and K. One of such arguments is that Na and K are intrinsic to the ices on the surface, as part of salts deposited as evaporates in liquid water resurfacing events (Brown 2001). Accordingly, aqueous alteration of Europa's kernel in the past may have removed certain salts selectively from the surfaces and enriched them in the liquid fraction. Assuming that dominant sodium and potassium containing compounds are sulfates, with  $\text{Na}_2\text{SO}_4$  being more soluble than  $\text{K}_2\text{SO}_4$  (Lide 1996), sodium would be depleted relative to potassium in the remaining solid material and would be enriched in the liquid. Therefore, one can expect a lower value of Na/K for intrinsic surface materials than for the resurfacing materials that originate from the sub-surface ocean. However, since the pre-alteration value of Na/K for Europa is not known, it is not possible to differentiate between solid and liquid sources.

## **II Trapping of alkali and earth-alkali metals in icy crust of Europa**

In this study, we propose a second type approach for the endogenous origin of the observed Na/K ratio. The global process starts during the condensation of refractory material in the proto-solar nebula. Thermochemical equilibrium calculations show that Na, for example, is mainly trapped in rocks in the proto-solar nebula, mostly in the form of silicates (Ellinger et al. 2015) and that these rocks incorporate into the building blocks of Europa. Then the metallic ions are transferred from the solid refractory compounds to the liquid phase of the surrounding ocean. During the cooling phase, the metallic ions are trapped into the icy crust then they migrate to the surface of the icy crust. Finally, they can be ejected from the surface as neutral atoms together with the surrounding water molecules by surface sputtering. The evolution of their electronic structure from positive ions to neutral atoms during their migration in the icy crusts is followed in the next developments.

Taking into account the proto-solar composition of the disk (Asplund et al. 2009), all Na-bearing compounds formed as refractory materials, irrespective of the proto-solar disk's temperature in an extended domain between 0°K and 800°K (Ellinger et al. 2015). Assuming the formation of the K-, Ca- and Mg-bearing compounds in the same conditions, their abundances can also be considered as solar (Asplund et al. 2009) within the kernel of Europa. Accordingly, their abundances relative to H are Na/H ( $2 \times 10^{-6}$ ), K/H ( $1.3 \times 10^{-7}$ ), Ca/H ( $2.2 \times$

$10^{-6}$ ), and Mg/H ( $3.8 \times 10^{-5}$ ). From these values, it can be seen that the abundances of Na and Ca are close to each other, that K is less abundant by one order of magnitude, whereas Mg is largely the most abundant of all, one order of magnitude above Na and Ca.

In the early times of Europa, it is assumed that an ocean of liquid water starts to form and surrounds the solid kernel of the satellite. In such a situation, the fact that the rocks being washed by water for a long periods, enables the transfer of metallic ions from refractory material to liquid water. This same procedure was considered as an effective process for  $\text{Na}^+$ ,  $\text{K}^+$ ,  $\text{Mg}^{++}$ , and  $\text{Ca}^{++}$  ions present in the primitive rocks on earth (De Ronde et al. 1997). However, the quantities of ions transferred into water are directly related to their respective solubility.

Considering Europa as differentiated (like the Earth), the relative molality in aqueous phase can be estimated from the studies of water-rock interaction in a terrestrial geothermal field in SW-Iceland (Zhang Zhanski, 2001), as well as from evaluation of the composition of the Archean ocean (De-Ronde et al. 1997). According to these studies, the molalities of the ions depend on the water/rock ratio and in a lesser extent on the temperature. According to Kuskov & Kronrod (2005), the ocean surrounding the rocky kernel has to be in a shell of dimensions comprised between 80 and 160 km, taking into account the constraints on the mass and moment of Europa. Therefore, no saturation phenomenon can occur and the molalities obtained for large water/rock ratio (water/rock =  $10^6$ ) can be employed (Table 1).

Ion	$\text{Na}^+$	$\text{K}^+$	$\text{Mg}^{++}$	$\text{Ca}^{++}$
T=120°C Water/rock = $10^6$	$750 \times 10^{-3}$	$25 \times 10^{-3}$	$10 \times 10^{-3}$	$100 \times 10^{-3}$
Archean ocean	$789 \times 10^{-3}$	$19 \times 10^{-3}$	$51 \times 10^{-3}$	$232 \times 10^{-3}$

Table 1: Ions molalities (mole/l) of alkali and Earth alkali of selected elements deduced from experimental work by Zhang Zhanshi (2001) and evaluations from De Ronde et al. (1997).

The values in Table 1 show that the molalities are spread over two orders of magnitude, decreasing from sodium to calcium, potassium and magnesium. In principle, the relative molalities in Europa's ocean should be proportional to both their initial abundances in the rock material and their respective solubility into the water. However, since the abundances of these ions in the rocks can be considered as unlimited, it is their capacity to dissolve into water, measured by their molality that should be the determining factor. Therefore, sodium will be in higher quantity than others, followed by calcium, potassium and magnesium.

Step 2 happens with the cooling down of Europa. As the temperature decreases, the ocean water starts to freeze from the top, forming an ice crust whose thickness increases with time. During this process, foreign bodies are embedded in the ice matrix, in particular metallic ions are also trapped inside the icy crust. Then, the metals are transferred from deep inside to the top ice layers via the already mentioned ice convection mechanism (Pappalardo et al. 1998). In this step, the determining factor is the stability of the metal inside the icy structure. Finally, the metallic atoms are ejected into the exosphere as neutral atoms by the sputtering of water ice surface.

In this chapter, the stability of metallic ions in different layers of the icy crust has been investigated using periodic quantum chemistry numerical simulations based on "first principle" periodic density functional theory. Throughout the calculations, the evolution of the charge density around metallic ions is also studied.

### **III Computational procedure**

#### **III.1 VASP Parameters**

Here again, we have used the type of GGA functional (PBE) as developed by Perdew et al. (1996). The systems of interest show both H-bonding (the bonding between the water molecules in the ice structure) and interactions by Van der Waals forces (the interaction between the metallic ions and the H<sub>2</sub>O molecules surrounding them). For this kind of non-covalent weak dispersion forces, Van der Waals corrections have to be added to the DFT. To this end, a semi-empirical approach, DFT-D2, proposed by Grimme (2006) has been employed.

Though the computational machinery is the same as previously, the aim of the study is completely different from the other solid-state calculations presented in the preceding chapter of this thesis. In chapter 3, the main goal was to determine the stability of atomic species in various situations inside the bulk of the ice, whereas here, we follow the migration of the metals from the bottom of the ice crust to the topmost layer. No attempt at quantifying a diffusion process was done. Instead, besides the stability aspect, we now focus on the evolution of the electronic structure of the atoms from their trapping as cations to their ejection towards the exosphere as neutral atoms.

In the solid state treatments, especially when using plane waves basis sets, the result of the calculation is a continuous electron charge density so that it is no clear how to partition electrons amongst fragments of the system such as atoms and molecules. To bypass this conceptual difficulty, different schemes for the electron partitioning have been proposed. In the present study we used Bader charge density analysis (Bader 1990) as implemented by Graeme Henkelman's group in the VASP code (Henkelman et al. 2006)

As in the comet's chapter, the apolar Ih crystalline ice structure has been employed with a primitive unit cell composed of 4 ice bi-layers whose cell parameters are 8 Å in x and y directions; a vacuum of 15 Å high between two successive slabs is maintained to avoid any spurious interaction. A K-point grid of 3x3x1 for x, y, and z directions respectively, has been applied allowing automatic Monkshort & Pack sampling to generate a satisfactory representation of the plane wave basis set. A standard kinetic energy cut-off of 400 eV was employed for all calculations.

### **III.1.1 Preliminary results (primitive cell)**

The main idea behind this study is to follow the evolution of metallic ions from their trapping in the ice bulk to their ejection from the icy surface to the exosphere. For this reason, several positions inside the bulk and on the way toward the surface of ice are considered, starting from bottom to top. These positions, characterized by the number  $n$  of H<sub>2</sub>O molecules missing in the unit cell network, can be visualized in Figure 1.

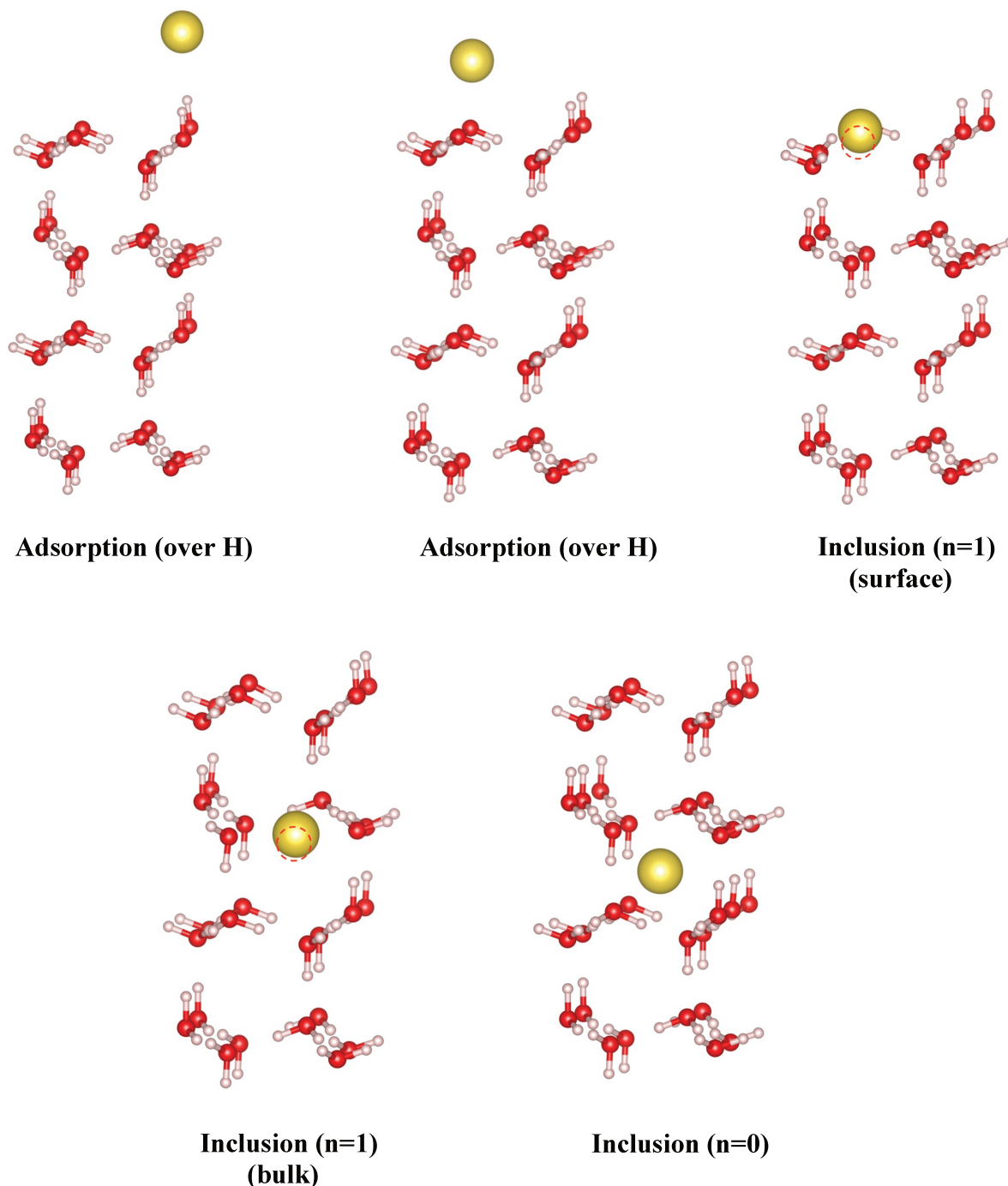


Figure 1 : The optimized structures for Na trapped in different type of cavities.

- Inclusion (n=0) represents the trapping of metals into the perfect crystalline ice, although at the end of this procedure, the perfect crystalline structure is lost.

Then, like in the previous chapter, cavities with different sizes are studied.

- Inclusion (n=1) is a cavity obtained when one  $\text{H}_2\text{O}$  molecule is missing in the cell. Two different positions are considered for this cavity, one is labelled “bulk”, when the



cavity is formed in the middle of bi-layers; the other “surface”, when the cavity is formed in the upper bi-layer. It is intended to represent the last trapping situation of the metals before their arrival to the surface.

- Inclusion (n=2) is a larger cavity with two missing H<sub>2</sub>O molecules that is appropriate to study the effect of the size cavity.

Finally, the adsorption of metals on two sites is studied (n=0).

- One is the adsorption through the oxygen atom of H<sub>2</sub>O molecules on the surface whereas the other site is through the hydrogen atom. It is the final interaction point of metals with the icy crust before ejection in the gas phase.

Atom	Adsorption (over H)	Adsorption (over O)	Inclusion (n=1) (surface)	Inclusion (n=1) (bulk)	Inclusion (n=0)
Na	0.11 / 0.18	0.66 / 0.55	0.85 / 0.56	1.03 / 0.77	0.07/0.76
K	0.13 / 0.20	0.80 / 0.69	0.85 / 0.64	0.87 / 0.82	0.05/0.87
Mg	0.12 / 0.13	0.42 / 0.27	0.63 / 0.59	0.86 / 0.81	-0.57 / 0.79
Ca	0.15 / 0.18	0.94 / 0.35	1.35 / 0.75	1.52 / 0.97	0.54/1.53

Table 2: Evolution of stabilization energies and atomic charges of alkali and Earth

All results obtained with the primitive cell are reported in Table 2.

i - The first question to consider is the stability of the metallic species embedded in ice bulk. Apart from Calcium, trapping of metallic ions into the perfect crystalline ice is not thermodynamically favorable. It was expected since the perfect crystalline ice structure has the most stable geometry that has no real degree of freedom to accommodate the intrusion of an external perturbation. In this respect there are two values that raise question. The first is the stability of calcium in the perfect crystalline ice structure by  $\sim 0.54$  eV. One may wonder whether the size of the metal could be the answer. The ionic radius of metallic ions ranging in the order  $Mg < Na \sim Ca < K$ , calcium has nearly similar radius as sodium. Then the reason for its favorable trapping cannot be explained by the sizes of the ions. The second is the high repulsion of -0.57 eV for magnesium. Although Mg and Ca are both alkaline earth metals, the two values obtained for their embedding, either much higher or much lower than the non-embedding situation, suggest opposite trends difficult to rationalize. It means that Mg and Ca

would disturb the electronic ice structure much more than the Na and K, which might be understandable, but in an opposite direction, which is not.

In fact, this may simply point to the need for a more improved ice cell model.

ii - The second question to be considered is the shape of the cavities to trap metal atoms in the icy matrix. Two different environments have been studied. First, small cavities with 1 H<sub>2</sub>O molecule missing in the unit cell ( $n=1$ ) for which we have found two different locations. One is inside the bulk whereas the other is on the upper bi-layer, close to the adsorption on the ice surface. For the inclusion ( $n=1$ ) bulk, Na and K are stabilized by  $\sim 1.0$  and  $\sim 0.9$  eV, which is stronger than the ice cohesion of 0.5 eV. The stability of Mg is very close to that of K but drastically different again from that of Ca, which is by far ( $\sim 1.5$  eV) the largest of all.

From Bader charge analysis, it can be seen that Na and K are trapped as positive ions with a charge near +1. Mg and Ca, once inside ice bulk, recover immediately 1 electron from the surrounding ice, so that they exist as positively charged ions with a charge approximately +1, i.e. of the same order of magnitude as Na and K.

In the case of the inclusion ( $n=1$ ) surface, all of the stabilization energies decrease by 0.2 eV with the exception of K for which it stays even. The other important point is the decrease of the charge for all ions. Near the surface, even if the ions are still trapped, positive charges decreases by  $\sim 0.2$  with respect to inclusion in the bulk, and become closer to those found in the adsorption situations discussed below.

iii - The final stage in the transport of the metallic species through the icy crust is their adsorption on the ice surface before their ejection into the exosphere by collisions with energetic particles. We have studied two different sites. One is the adsorption of the metal atoms through the oxygen on the ice surface, the other is the adsorption through the hydrogen of H<sub>2</sub>O pointing out of the icy crust surface. i.e. the final point of metal-ice interaction (Figure 2). Similar to the inclusion cases, calcium is adsorbed better than the others (K, Mg, and Na). With the adsorption over oxygen, we have a systematic stabilization decreases in the range of 0.05 (K) to 0.4 (Ca) eV. These values decrease even more, reaching stabilization energies as low as 0.10 and 0.15 eV in the case of adsorption over H. At the end of the journey in the icy

matrix, metallic species, initially trapped as ions have recovered their electrons and leave the ice as quasi neutral atoms, ejected to the exosphere.

### III.1.2 Improving the model

#### a) Extending the height of the slab to 6 bi-layers

The intriguing results obtained after the preceding calculations concerning the stabilization energies of the alkaline earth Mg and Ca following their inclusion in pure crystalline ice lead to question the pertinence of the parameters used in the 4 bilayers model. The first to check is the thickness of the slab, in other words the number of bi-layers (bL) that has been augmented to 6 bL keeping the basal dimension unchanged.

Only the inclusion situations have been thoroughly checked because the top two bL that are the crucial layers to account for the reorganization of the ice surface have already been optimized in the 4bL treatments of adsorption.

Atom	Inclusion (n=1) (surface)	Inclusion (n=1) (bulk)	Inclusion (n=0)
Na	0.84 / 0.56	1.04 / 0.78	0.00 / 0.78
K	0.84 / 0.67	0.95 / 0.84	-0.09 / 0.87
Mg	0.65 / 0.58	0.93 / 0.73	-0.34 / 0.85
Ca	1.36 / 0.74	1.55 / 0.92	0.14 / 1.58

Table 3: Evolution of stabilization energies and atomic charges of alkali and Earth alkali elements as a function of their position in the ice (Energies in eV/Charges in electron)

All results obtained with the 6bL model are reported in Table 3.

Trapping of metallic ions into the perfect crystalline ice (inclusion n=0) gives similar results to the values obtained with the 4bL model for Na and K (Table 1) with non significant stabilization energies ( $\sim 0.0$  eV), that leaves little chance for an inclusion process. Concerning alkaline earth, Mg inclusion becomes less endothermic while the stabilization energy of Ca decreases to 0.14, compared to 0.54 eV in the 4bL model.

On another side it should be remarked that the charge distribution is not changed significantly by the change of the vertical dimension of the slab. This let us to consider that, if

there is a change due to the size of the cell, it has to be searched for in the effects of the basal (x,y) dimensions.

The trapping of metallic ions in the case of a cavity ( $n=1$ ; bulk) gives stable structures with stabilization energies in the order of  $\sim 1\text{eV}$  for Na, K and Mg. Again, Ca is the most stable ion trapped inside the cavity by  $\sim 1.6\text{ eV}$ . Na and K have a charge close to  $+1$  whereas  $\text{Mg}^{++}$  and  $\text{Ca}^{++}$  immediately recover one electron and become almost singly charged  $\text{Mg}^+$  and  $\text{Ca}^+$ . Compared to the values obtained with the 4bL cell (Table 2), the stabilization energies are only marginally affected.

In the case of the trapping in a cavity inside the upper bL ( $n=1$ ; surface), the stabilization energies decrease for all of the metallic ions by  $\sim 0.2\text{ eV}$ . In a similar manner, the positive charges decrease by 0.2 electrons on all the metallic ions. The values obtained with 6 bi-layers model are all in accordance with those obtained for the 4 bL primitive cell.

Globally, inclusion of the metal ions into the perfect crystal structure is not energetically favorable. Calcium appears as exception but its energy stabilization of  $\sim 0.1\text{ eV}$  is so weak that it is highly questionable.

The two problematic values obtained in the 4bL model for Mg and Ca become more understandable in the frame of the 6 bL cell model. All metallic ions are stable inside a cavity (inclusion ( $n=1$ )) whether it is inside the bulk or near surface. The main difference to be noted is the evolution of the charges between the bulk to the surface. Near the surface, all metal ions have started to regain some part of their electronic density, resulting in a decrease of their positive charges. The last important parameter to check is the cell size by changing the surface of the basal plane.

#### **b) Extending the volume of the 4 bi-layers cell by doubling the basal surface**

An extended cell, with a volume doubled with respect of the primitive 4bL cell, has been used to check the convergence of results. The same procedure like in the previous sections has been applied. Trapping of metallic ions into the perfect crystalline ice and into the cavities formed in different layers (bulk or surface) as well as their adsorption through the two different sites on the ice surface have been checked (Figure 2). All the results obtained can be seen in Table 4.

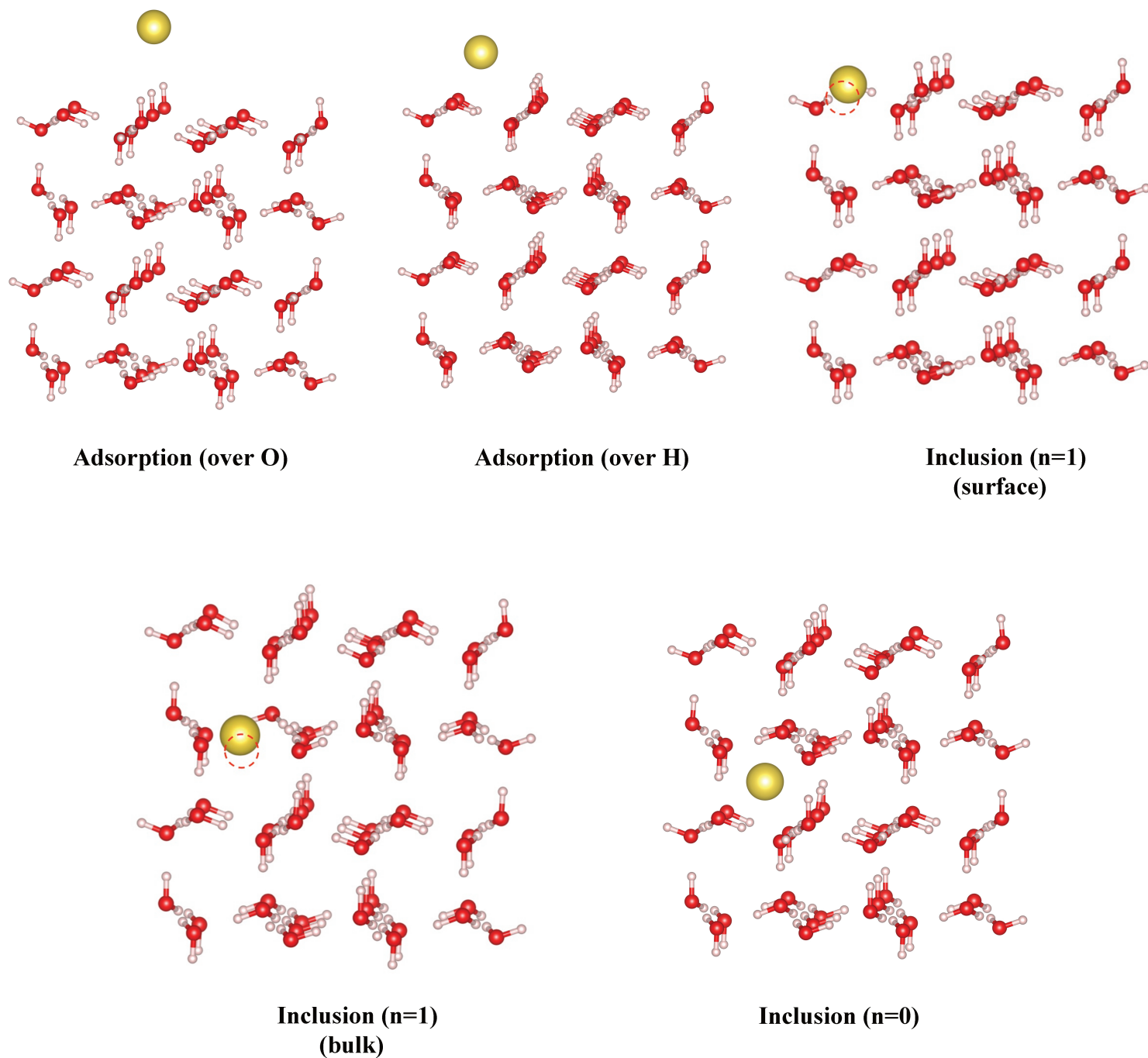


Figure 2: The optimized structures for Na trapped in different type of cavities.

Potassium is the only element whose inclusion is favorable contrary to the primitive 4bL and 6bL models while the calcium inclusion is no longer favorable.

In the case of inclusion of metallic ions into the cavity formed in the ice bulk ( $n=1$ ; bulk), the stabilization energies are much higher compared to the primitive cell or the primitive cell with 6bL. Again calcium has the highest stabilization energy, followed by Na, K and Mg. Nevertheless, compared to other ice models, according to which calcium has stabilization energy around 1.5 eV, the value of a stabilization energy of 3.86 eV associated to a charge of +1.65 is more than doubtful and requires to be checked with a more extended model. The inclusion of metallic ions in the upper layer ( $n=1$ ; surface) gives similar results to the primitive cell with the 6bL model. The most stable ion is still Ca with stabilization energy of 1.44 eV consistent with the preceding models. Na and K have similar energy values around 0.89 eV whereas Mg has the lowest stabilization energy of 0.67 eV. For all metallic ions, positive charge decreases when they are close to the surface.

Atom	Adsorption (over H)	Adsorption (over O)	Inclusion ( $n=1$ ) (surface)	Inclusion ( $n=1$ ) (bulk)	Inclusion ( $n=0$ ) (bulk)
Na	0.10 / 0.20	0.41 / 0.30	0.89 / 0.55	1.35 / 0.88	0.04 / 0.79
K	0.16 / 0.20	0.60 / 0.40	0.86 / 0.55	1.34 / 0.86	0.22 / 0.88
Mg	0.16 / 0.13	0.47 / 0.25	0.67 / 0.56	1.24 / 0.78	-0.39 / 0.66
Ca	0.20 / 0.20	0.98 / 0.30	1.44 / 0.71	3.86 / 1.65	0.07 / 1.33

Table 4: Evolution of stabilization energies and atomic charges of alkali and Earth alkali elements as a function of their position in the ice (Energies in eV/Charges in electrons)

The doubling of the basal surface in the 4bL model allows to check whether the lateral interactions between periodic images on the surface are efficiently avoided. Adsorption of metals to the oxygen of  $H_2O$  molecule on the surface, gives the most stable structure with calcium. Adsorption of metals to the oxygen of  $H_2O$  molecule on the surface, gives the most stable structure with calcium.

To see whether the lateral interactions between metals on the surface with its periodic image are efficiently avoided with the primitive cell, the adsorption cases are studied with double cell. Adsorption of metals to the oxygen of  $H_2O$  molecule on the surface, gives the most stable structure for calcium with  $\sim 1.0$  eV stabilization. Na and Mg have similar adsorption energies around 0.4 eV whereas K has an adsorption energy of  $\sim 0.6$  eV. It can clearly be seen that once the metals are on the surface, their charges decrease to by  $\sim 0.15$  to 0.4 electrons. These values are even lower (0.1 to 0.2 electrons) when adsorption takes place through the hydrogen atom.



As a general remark, inclusion of the metallic ions into the perfect crystalline ice structure is endothermic except K. Metallic ions can be trapped and remain stable for the inclusion in a cavity inside the ice bulk. However within this model, Ca gives unexpectedly stable structures. All ions have positive charges close to +1. When inclusion becomes closer to the surface ( $n=1$ ; surface), the stabilization energy as well as the positive charges decreases. This decrease in charge continues until their adsorption, resulting in almost neutral atoms ready to be ejected by sputtering.

The unexpected results, such as the exothermicity of the trapping of K into the perfect crystalline ice and high stabilization energy value for K inside the cavity within the ice bulk implies that changing one parameter at a time, either the thickness of the slab or the cell size is not efficient enough. For this reason, all the calculations except adsorptions, which are shown to be converged, have been done by using the double cell with 6 bi-layers.

### c) Extending double cell to 6 bi-layers

The erratic results obtained among the 4bL cell, primitive cell with 6 bi-layers and double cell with 4 bi-layers show that the thickness of the slab and the cell size are determining factors at the same time. This requires using a model composed of 6 bi-layers and a double cell size compared to the primitive cell. Within this cell model the same positions as the previous ones are studied: inclusion of the metallic ions into the perfect ice structure, inclusion in the cavity obtained with the removal of 1 H<sub>2</sub>O molecule formed in the bulk or on the upper layer. Since this is the biggest model used in this study, the effect of the cavity size is also studied by forming larger cavities with the removal of 2 H<sub>2</sub>O molecules ( $n=2$ ) or 4 H<sub>2</sub>O molecules ( $n=4$ ) (Figure 3).

All the results obtained are reported in Table 5.

Atom	Inclusion ( $n=1$ )(surface)	Inclusion ( $n=1$ ) (bulk)	Inclusion ( $n=2$ )	Inclusion ( $n=4$ )	Inclusion ( $n=0$ ) (bulk)
Na	0.86 / 0.54	1.02 / 0.78	1.10 / 0.58	1.36 / 0.62	0.06 / 0.86
K	0.86 / 0.55	0.91 / 0.84	1.17 / 0.80	1.58 / 0.84	0.22 / 0.88
Mg	0.68 / 0.56	0.90 / 0.72	0.93 / 0.59	1.12 / 0.54	-0.14 / 0.65
Ca	1.41 / 0.70	1.54 / 0.91	1.71 / 0.83	1.80 / 0.72	0.26 / 1.34

Table 5: Evolution of stabilization energies and atomic charges of alkali and Earth alkali elements as a function of their position in the ice (Energies in eV/Charges in electron)

Trapping of metallic ions in the perfect crystalline ice ( $n=0$ ) is endothermic except for K and its stabilization is also very low comparing to the other environments. These values show that in this particular case both the effect of slab thickness and the cell size are important factors, since some values are closer to the ones obtained with the primitive cell with 6 bi-layers whereas some values are closer to the ones obtained with the 4bL cell with extended basal surface.

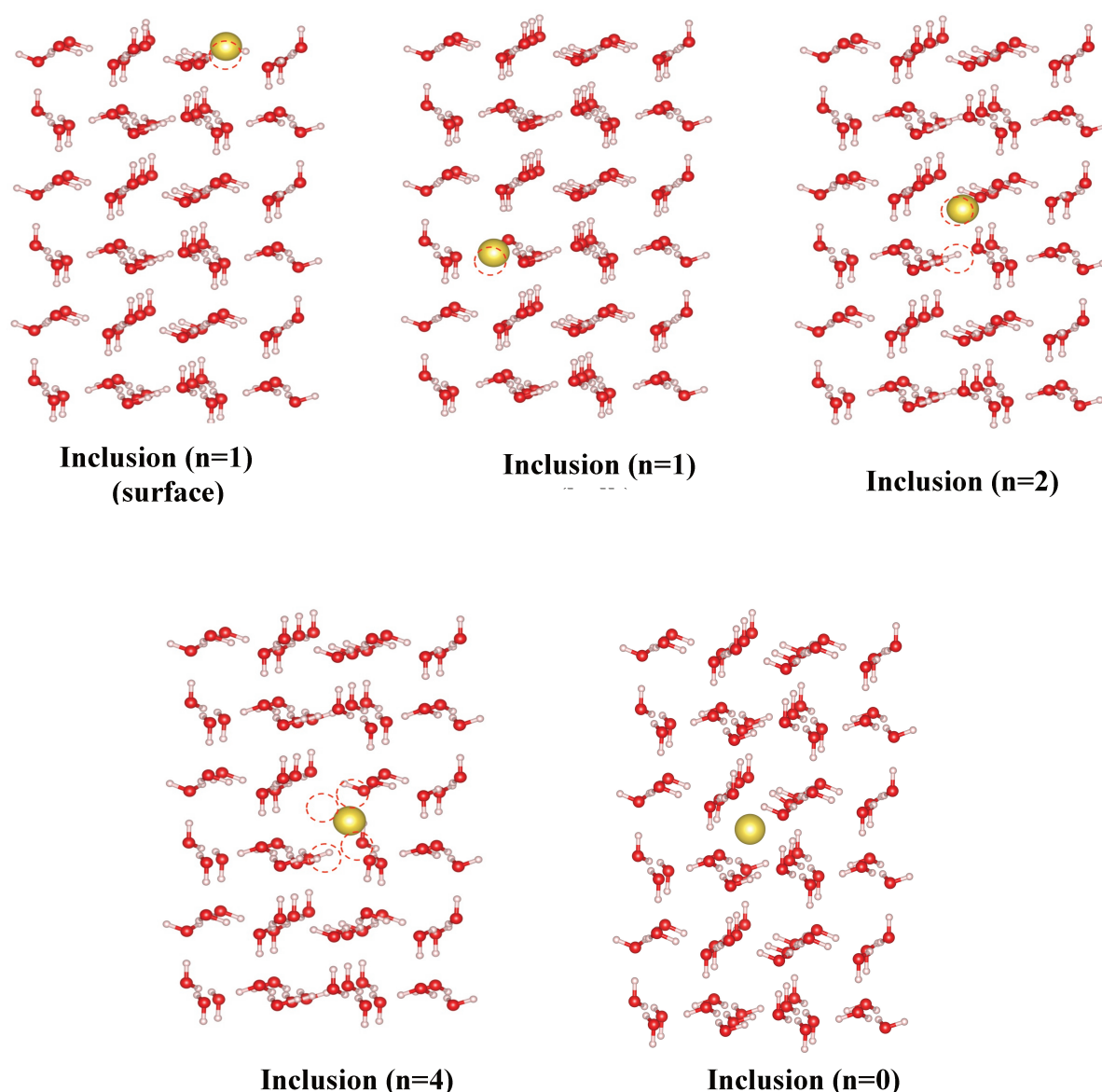


Figure 3: The optimized structures for Na trapped in different type of cavities.

In the case of the inclusion into the small cavity ( $n=1$ ; bulk), metallic ions can be trapped and can stay stable. Ca is the most stable one, followed by Na, K and Mg. Na and K are positively charged with a value near +1 and Ca & Mg, once trapped, immediately regain 1 electron and start to behave like alkali metals Na and K. In this case, comparing these values with the ones obtained from the primitive cell with 6 bL or double cell with 4 bL shows that the effect of slab thickness is more important than the cell horizontal extension since the values are closer to the ones obtained with the primitive cell when extended with 2 bi-layers. Inclusion of ions disturbs the ice structure and letting only the top and bottom bi-layers to be optimized could not describe the situation properly. However, inclusion of ions in a small cavity on the surface gives similar values both for energy and charge for all models including the primitive cell.

Within this double cell with 6 bi-layers model, two other larger cavities ( $n=2$ ; bulk) and ( $n=4$ ; bulk) are also studied. As expected, with more space, ions can be stabilized more easily; hence the stabilization energies are larger for the cavity obtained with the removal of 4  $\text{H}_2\text{O}$  molecules, although the difference in the stabilization energy between different cavities are not so large.

In all types of cavity Ca is the most stable (0.60 eV in the average), followed by K except the inclusion ( $n=1$ ), then Na and Mg. Although the stabilization energies change with the volume of the cavities, the charges of the metallic ions remain roughly unaffected.

#### **IV Conclusion and perspectives**

The scenario that we propose follows the alkali and alkaline earth metals starting from their washing out of the rocky kernel of Europa by the internal ocean in the form of ions, at the early times of Europa's formation. During the cooling period of the satellite, the ice crust formed at the surface of the ocean and trapped the metallic ions allowing them to migrate to the surface by a diapirism mechanism, namely a bottom to top internal convection within the ice crust. Once on the surface in a neutral form they can be ejected in the exosphere by sputtering.

This scenario is supported by “first principle” periodic numerical simulations studying the trapping and progressive neutralization of the initial ions in the ice matrix.

As a general remark, one can say that to describe the trapping of metallic ions properly for each inclusion case, it is necessary to use a large enough unit cell such as a double cell with a 6 bi-layers thickness. For the adsorption, a double cell with a 4 bi-layers is sufficient enough to have consistent results.

The transport process in the icy matrix works roughly similar along the way inside the ice, which can be summarized as follows:

1) A direct inclusion of the metallic ions into the perfect crystalline ice is difficult whereas inclusions into the cavities are easy, which can be considered a usual situation taking into account the assumed porous structure of ices

2) The evolution of charges is the same for all the ions, decreasing when going from the ice bulk to the surface within the ice crust. It should be noted that Mg and Ca, which are released from the solid kernel to the ocean as doubly charged ions, regain immediately one electron when they are trapped in the ice. Then, these Earth-alkali metals behave similarly to the other two singly charged alkali metals.

3) On the final point of interaction with the ice (adsorption over H), they are nearly in their neutral form so it can be said that the release of the metals happens in the form of neutral atoms together with the surface ices.

However, there are some crucial differences between the metallic ions, especially coming from their relative abundances in the liquid ocean. Na and K have very similar behaviors in water ices, with a small difference in their stability in smaller or larger cavity. Na is more stable than K in small cavity ( $n=1$ ) whereas K is more stable in a larger cavity ( $n=4$ ), which might be related to their different ionic radius (larger for K). Since, they show globally similar behaviors in ice, the main difference should come from their initial relative molalities in the ocean water. The ratio of these molalities of the two metals can be estimated reasonably from the geothermal field lake in contact with a rocky kernel, whose analysis gives a value of 30, which is in accordance with the observed value.

Magnesium seems less stable inside the ice compared to the others, which coupled to its much smaller molality in liquid water, implies that it is less susceptible to be observed in Europa's exosphere, according to this scenario. A future observation of it would imply that other processes are at work for explaining magnesium abundance in the exosphere. Calcium, is the most stable one in the ice, well embedded in the icy matrix. With an initial relative abundance one order of magnitude lower than Na, Ca should also be observed in the exosphere but with a smaller abundance.

To conclude, we would like to say that at the beginning this study was aimed at answering the questions related to the origin of Na and K observed in Europa's exosphere, suggesting an endogenous origin. Within the same scenario explaining the relative abundances of Na and K, we found that the opportunity for detection of Ca should be considered seriously for future space missions as those in preparation in international space agencies NASA ESA at horizon 2025, namely JUICE and CLIPPER.

## V References

- Asplund, M., Grevesse, N., Sauval, A. J., & Scott, P. (2009). The chemical composition of the Sun. *Annual Review of Astronomy and Astrophysics*, 47, 481-522.
- Bader, R. F. W., (1990). *Atoms in Molecules: A Quantum Theory*. Oxford, UK: Clarendon Press: .
- Brown, M. E., & Hill, R. E. (1996). Discovery of an extended sodium atmosphere around Europa. *Nature*, 380(6571), 229.
- Brown, M. E. (2001). Potassium in Europa's atmosphere. *Icarus*, 151(2), 190-195.
- Carlson, R. W., Anderson, M. S., Johnson, R. E., Smythe, W. D., Hendrix, A. R., Barth, C. A., ... & Clark, R. N. (1999). Hydrogen peroxide on the surface of Europa. *Science*, 283(5410), 2062-2064.
- De Ronde, C. E., deR Channer, D. M., Faure, K., Bray, C. J., & Spooner, E. T. (1997). Fluid chemistry of Archean seafloor hydrothermal vents: Implications for the composition of circa 3.2 Ga seawater. *Geochimica et Cosmochimica Acta*, 61(19), 4025-4042.
- Ellinger, Y., Pauzat, F., Mousis, O., Guilbert-Lepoutre, A., Leblanc, F., Ali-Dib, M., ... & Doressoundiram, A. (2015). Neutral Na in cometary tails as a remnant of early aqueous alteration. *The Astrophysical Journal Letters*, 801(2), L30.
- Grimme, S. (2006). Semiempirical GGA-type density functional constructed with a long-range dispersion correction. *Journal of Computational Chemistry*, 27(15), 1787-1799.
- Hall, D. T., Strobel, D. F., Feldman, P. D., McGrath, M. A., & Weaver, H. A. (1995). Detection of an oxygen atmosphere on Jupiter's moon Europa. *Nature*, 373(6516), 677-679.
- Henkelman, G., Arnaldsson, A., & Jónsson, H. (2006). A fast and robust algorithm for Bader decomposition of charge density. *Computational Materials Science*, 36(3), 354-360.
- Ip, W. H. (1996). Europa's oxygen exosphere and its magnetospheric interaction. *Icarus*, 120(2), 317-325.



Johnson, R. E., Killen, R. M., Waite, J. H., & Lewis, W. S. (1998). Europa's surface composition and sputter-produced ionosphere. *Geophysical research letters*, 25(17), 3257-3260.

Johnson, R. E. (2013). *Energetic charged-particle interactions with atmospheres and surfaces* (Vol. 19). Berlin, Heidelberg.

Kivelson, M. G., Khurana, K. K., Russell, C. T., Volwerk, M., Walker, R. J., & Zimmer, C. (2000). Galileo magnetometer measurements: A stronger case for a subsurface ocean at Europa. *Science*, 289(5483), 1340-1343.

Kuskov, O. L., & Kronrod, V. A. (2005). Internal structure of Europa and Callisto. *Icarus*, 177(2), 550-569.

Lide, D. R. (1947). *CRC handbook of chemistry and physics*, Internet Version 2007, (87th Edition).

Pappalardo, R. T., Head, J. W., Greeley, R., & Sullivan, R. J. (1998). Geological evidence for solid-state convection in Europa's ice shell. *Nature*, 391(6665), 365.

Pappalardo, R. T., Belton, M. J. S., Breneman, H. H., Carr, M. H., Chapman, C. R., Collins, G. C., ... & Greeley, R. (1999). Does Europa have a subsurface ocean? Evaluation of the geological evidence. *Journal of Geophysical Research: Planets*, 104(E10), 24015-24055.

Paranicas, C., McEntire, R. W., Cheng, A. F., Lagg, A., & Williams, D. J. (2000). Energetic charged particles near Europa. *Journal of Geophysical Research: Space Physics*, 105(A7), 16005-16015.

Perdew, J. P., Burke, K., & Ernzerhof, M. (1996). Generalized gradient approximation made simple. *Physical Review Letters*, 77(18), 3865.

Vogt, S. S., & Keane, M. J. (1993). HIRES: The High Resolution Echelle Spectrometer on the Keck Telescope. *Bulletin of the American Astronomical Society*, 25, 1305.

Zahnle, K., Schenk, P., Levison, H., & Dones, L. (2003). Cratering rates in the outer Solar System. *Icarus*, 163(2), 263-289.

Zhanshi, Z. (2001). Water-rock interaction in the Bakki low-temperature geothermal field, SW-Iceland. The United Nations University, Geothermal Training Programme in Iceland, *Reykjavík University Reports*, 17, 405.

## General Conclusion

The main aim of this study was to answer some problems encountered in planeteology, using ab initio quantum chemistry methods. The results obtained show that ab initio quantum chemistry is a powerful method to study especially difficult cases.

Depending on the environment of interest, a molecular or periodic approach can be employed. On one hand, in the case of the noble gas deficiency problem in Titan's atmosphere, we used a molecular approach for the interaction of noble gases with ions in gaseous phase in PSN. On the other hand, the study of comets composed of icy grains and icy satellites like Europa has required a solid state method.

An innovative aspect of our study was to employ periodical ab initio method to describe trapping mechanisms in water and H<sub>2</sub>S ices. One of the main questions in astrochemistry regarding processes in water ices is whether to model crystalline or amorphous ice structure. Here, we showed that it is possible not only to treat crystalline ice but porous, irregular ice structures with periodic methods by introducing cavities into the perfect crystalline ice. This illustrates that, from a general point of view, computational methods have the advantage of allowing "à la carte" modeling for direct comparison with experiments and observations in various environments.



## **Simulations de processus de séquestration chimique dans le système solaire externe**

### **Résumé :**

Ce projet a pour but de répondre à quelques questions pendantes de planétologie en utilisant des méthodes de chimie quantique. Il recouvre principalement deux études.

La première étude modélise les processus chimiques susceptibles d'expliquer la déplétion en gaz rares observée dans l'atmosphère de Titan par la mission Huygens ; l'étude considère la formation par association radiative, des complexes stables entre Ar, Kr, Xe et  $\text{H}_3^+$  ou les ions protonés, ceci dans la nébuleuse proto-planétaire, avant la formation de Titan en tant qu'objet.

La seconde étude analyse les mécanismes piégeant les volatiles dans les glaces, mécanismes à l'œuvre dans les comètes comme dans la lune Europe. Les scénarios d'une origine primordiale commune de  $\text{O}_2$  et  $\text{S}_2$  observés dans la comète 67P/C-G lors de la mission ROSETTA, ont pu être validés, donnant des rapports d'abondance avec l'eau proches des observations, et proposant une explication pour la corrélation/non corrélation avec l'eau pour les deux espèces. De même, un scénario pour l'origine des éléments mineurs Na et K détectés dans l'exosphère d'Europe, satellite pour lequel l'intérêt a ressurgi en raison des missions à venir, Juice de l'ESA et Europa Clipper de la NASA, a été étudié et s'est révélé valable également pour Mg et Ca pour lesquels des prédictions d'abondance ont été faites.

Du point de vue des simulations numériques, ce travail combine deux approches ab-initio, une approche moléculaire pour la phase gazeuse du premier cas et une approche périodique du solide pour les autres cas.

Mots clés : Chimie théorique, Astrochimie, L'état solide

## **Modeling the chemical trapping processes in the outer solar system**

### **Abstract :**

This project aims at answering some questions in planetology by means of ab-initio quantum chemistry. It can be divided into two main studies. One models the chemical processes likely to explain the noble gases deficiency observed by the Huygens probe in the atmosphere of Titan; it investigates the formation of stable complexes between Ar, Kr, Xe and  $\text{H}_3^+$  or protonated ions by radiative association, in the proto-solar nebula, prior to the formation of Titan. The other analyzes the trapping mechanisms of volatiles in the ice at work in comets as well as in Europa. Scenarios of primordial origin for  $\text{O}_2$  and  $\text{S}_2$ , observed in comet 67P/C-G by the ROSETTA probe, were thus validated, giving abundance ratios with  $\text{H}_2\text{O}$  close to those observed and proposing an explanation for the respective correlation/non-correlation with water of the two species. Also, a scenario for the origin of trace elements Na, K detected in the exosphere of Europa whose interest is revived by anticipating the missions Juice and Europa Clipper, was argued and found available for Mg and Ca to predict relative abundances to be observed.

The computational work combines two ab-initio approaches, molecular calculations in gaseous phase in the first case and periodic solid state calculations in the second.

Keywords : Theoretical chemistry, Astrochemistry, Solid state